Buckling, Flutter, and Postbuckling Optimization of Composite Structures

Omprakash Seresta

Dissertation submitted to the Faculty of the
Virginia Polytechnic Institute and State University
in partial fulfillment of the requirements for the degree of

Doctor of Philosophy
in
Aerospace Engineering

Dr. Zafer Gürdal, Chair
Dr. Doughlas K. Lindner
Dr. Michael W. Hyer
Dr. Mayuresh J. Patil
Dr. Liviu Librescu

Feb 27, 2007
Blacksburg, Virginia

Keywords: Composites, Discrete Optimization, Genetic Algorithms, Global-Local Methodology, Buckling, Flutter, Postbuckling, Blending

Buckling, Flutter, and Postbuckling Optimization of Composite Structures

Omprakash Seresta

ABSTRACT

This research work deals with the design and optimization of a large composite structure. In design of large structural systems, it is customary to divide the problem into many smaller independent/semi-independent local design problems. For example, the wing structure design problem is decomposed into several local panel design problem. The use of composite necessitates the inclusion of ply angles as design variables. These design variables are discrete in nature because of manufacturing constraint. The multilevel approach results into a nonblended solution with no continuity of laminate layups across the panels. The nonblended solution is not desirable because of two reasons. First, the structural integrity of the whole system is questionable. Second, even if there is continuity to some extent, the manufacturing process ends up being costlier.

In this work, we develop a global local design methodology to design blended composite laminates across the whole structural system. The blending constraint is imposed via a guide based approach within the genetic algorithm optimization scheme. Two different blending schemes are investigated, outer and inner blending. The global local approach is implemented for a complex composite wing structure design problem, which is known to have a strong global local coupling. To reduce the computational cost, the originally proposed local one dimensional search is replaced by an intuitive local improvement operator. The local panels design problem arises in global/local wing structure design has a straight edge boundary condition. A postbuckling analysis module is developed for such panels with applied edge displacements. A parametric study of the effects of flexural and inplane stiffnesses on the design of composite laminates for optimal postbuckling performance is done. The design optimization of composite laminates for postbuckling strength is properly formulated with stacking sequence as design variables.

Next, we formulate the stacking sequence design (fiber orientation angle of the layers) of laminated composite flat panels for maximum supersonic flutter speed and maximum thermal buckling capacity. The design is constrained so that the behavior of the panel in the vicinity of the flutter boundary should be limited to stable limit cycle oscillation. A parametric study is carried out to investigate the tradeoff between designs for thermal buckling and flutter.

In an effort to include the postbuckling constraint into the multilevel design optimization of large composite structure, an alternative cheap methodology for predicting load paths in postbuckled structure is presented. This approach being computationally less expensive compared to full scale nonlinear analysis can be used in conjunction with an optimizer for preliminary design of large composite structure with postbuckling constraint. This approach assumes that the postbuckled stiffness of the structure, though reduced considerably, remains linear. The analytical expressions for postbuckled stiffness are given in a form that can be used with any commercially available linear finite element solver. Using the developed

approximate load path prediction scheme, a global local design approach is developed to design large composite structure with blending and local postbuckling constraints. The methodology is demonstrated via a composite wing box design with blended laminates.

Acknowledgements

I express my sincere gratitude, regards and thanks to my supervisor Prof. Zafer Gürdal for his excellent guidance, invaluable suggestions and generous help at all the stages of my research work. His interest and confidence in me was the reason for all the success I have made. I would also like to thank Dr. Mostafa. M. Abdalla (Assistant Professor, Aerospace Structures, Delft University of Technology) for helping with my research throughout the course of my doctoral research. His suggestions and insight were extremely crucial to the research work I have done. A part of the work is also published in TUDelft. I would also like to thank my committee members Dr. Michael W. Hyer, Dr. Douglas K. Lindner, Dr. Mayuresh J. Patil, and Dr. Liviu Librescu for serving in my committee.

I am extremely grateful to my friends for all the encouragement and support I have received from them at all times. I am glad to record my thanks to AOE gradlab administrator Luke Scharf whose kindness and cooperation I remember with gratitude.

Once again, I would like to thank all my classmates and friends - Dr. Joy Mukherjee, Dr. Dhaval P. Makhecha, Dr. Anil Bazaz, Dr. Arvind K. Sharma, Dr. Sameer Mulani, Dr. David B. Adams, Sumit Vasudeva, Bharath Ramesh, Kartik Channkeshava, Ankit Singhal, Dr. V. V. Patel, Shamik Sen, Suman Basu, Pradipta Ranjan Basu Mandal, Arijit Mandal, Hari K. Pyla, Vyas Duggirala, Bijoy Verghese, Shamik Chaudhury, etc for their smile and friendship making my life at Virginia Tech enjoyable and memorable.

Lastly, I would like to thank my parents for their support and love and my childhood friend Debraj Das and Sovanlal Chakraborty for taking care of my parents in my absence.

Omprakash Seresta

Contents

List of Figures

List of Tables

Nomenclature

$\boldsymbol{\Theta}$	Stacking sequence of guide
$\boldsymbol{\theta}^i$	Stacking sequence of i^{th} panel
δ_{all}	Maximum allowed deflection of wing structure
δ_{max}	Maximum deflection of wing structure
$\epsilon_{1,all}, \epsilon_{2,all}, \gamma_{12,all}$	Allowable engineering strains
$\epsilon_x, \epsilon_y, \gamma_{xy}$	Engineering strains
$\epsilon_x^0, \epsilon_y^0, \gamma_{xy}^0$	Mid plane engineering strains
$\kappa_x, \kappa_y, \kappa_{xy}$	Curvature terms
λ	load scaling factor
λ_b^i	Normalized buckling constraint of i^{th} panel
λ_{cr}^i	Buckling factor of i^{th} panel
λ_c^i	Normalized ply contiguity constraint of i^{th} panel
λ_n	Buckling factor under applied biaxial load
λ_{sh}	Shear buckling factor
λ_s^i	Normalized strain constraint of i^{th} panel
ν_{12}	Poisson's ratio
Φ	External virtual work
$\phi^{u/v/w}$	Assumed functions for u/v/w in Rayleigh-Ritz's method
Π	Total potential

A_{ij} Inplane stiffness coefficients

A_{ij}^{PB} Postbuckled stiffness coefficients

a_i, b_i, c_i Unknown coefficients in assumed functions for w, u, and v used in Rayleigh-Ritz method, respectively

C Total constraint violation

D_{ij} Flexural stiffness coefficients

E_1 Young's modulus in direction 1

E_2 Young's modulus in direction 2

f Fitness value

G_{12} Shear modulus

K_{ijkl} Nonlinear stiffness tensor coefficients

K_{il} Stiffness matrix coefficients

K_{il}^g Geometric stiffness matrix coefficients

N_x^i, N_y^i, N_{xy}^i In plane loads acting on i^{th} panel

P Total penalty for ply contiguity violation and unbalanced laminates

t Ply thickness

u, v, w Midplane displacement along x, y, and z axis, respectively

Chapter 1

Introduction

1.1 Introduction

The complete design of any real life structure is a multidisciplinary problem. For example, the design optimization of wing structure involves both structural and aerodynamic design. The aerodynamic design for optimal performance of the wing structure involves shape design. The structural design involves safety and manufacturability. Composites are being increasingly used in industries to replace conventional materials because of its high specific strength and specific weight. In the next section, we present the background of the different design methodologies applied to design optimization of large structures with particular reference to composite structures and the manufacturing issues that needs to be addressed to make the designs viable.

1.2 Composite design and genetic algorithm

Composite structures are manufactured by stacking layers of fibers with different orientation bonded together via a curing process. The advantage of composites compared to conventional materials lies in its ability to tailor the material properties as per the design requirement. The use of laminated composites entails fiber orientation angles as well as the number of layers of the laminates as design variables. Despite the weight savings and the material property tailoring advantages, one factor remains a serious obstacle for widespread use of composite laminates - manufacturing cost. There has been some attempt in the past to formulate the composite laminate design as continuous optimization problem. Schmit *et al.* [2] formulated the design of composite laminates as a continuous optimization problem with ply thickness as design variables. Due to manufacturing constraints, the fiber orientation angles are usually limited to 0, ± 45, and 90 degrees, and the thickness of the layers are kept constant. Thus,

the number of layers and the laminate stacking sequence are discrete design variables. This complicates the design process. The design optimization of composites, as discussed, leads to a combinatorial optimization problem, where the objective is to find an optimum fiber orientation angle of the plies or stacking sequence of the laminate. Nagendra *et al.* [3] investigated stacking sequence optimization of composite laminates with stability constraints using an integer programming method. Another approach to formulate composite laminate design problem is to use lamination parameters as design variables [4]. This formulation reduces the design space considerably. But its difficult to reconstruct the stacking sequence from optimum design.

Genetic algorithms are probabilistic search algorithms based on natural selection to guide the exploration of design space toward a global optimum. Genetic algorithms has been shown to be well suited for stacking sequence design of composite laminates. A comprehensive literature exists on the design and optimization of laminated composites using genetic algorithms. Le Riche *et al.* [5] used genetic algorithm to optimize laminate stacking sequence for buckling load maximization. Several techniques for improving the efficiency of genetic algoritms for composite laminate design have been explored. Kogiso *et al.* [6, 7] studied the advantages of approximation based local improvement and genetic algorithm with memory for composite laminate design with maximum buckling strength. Soremekun *et al.* [8] developed a generalized elitist selection in the context of genetic algorithm for composite laminate design. Recently, Vladimir *et al.* [9, 10] developed an improved genetic algorithm for mixed integer nonlinear programming problems. The improvements suggested are memory as a function of both continuous and discrete design variables [9] and multivariate approximation of the individual function responses in terms of several continuous design variables [10].

The above discussion mainly focuses on design of individual structural elements. The actual structure is made up of thousands of such structural elements. In design of large structural system, we need a better framework taking into consideration not only the safety but manufacturability and cost too. In the next section, we discuss about the different multilevel decomposition techniques applied for design of large structures.

1.3 Multilevel structural optimization

Most of the real life structural designs are complex assemblies of thousands of components. The design of large structure requires design of local details of all the subcomponents. An example is design of fuselage of an aircraft, which is made up of several stiffened panels. Here, the design variables are stiffener spacing or positions, stiffener dimensions, panel thickness, etc. Another example is design of a wing structure configuration. Here, the design variables are ribs or spars or skin panel thickness, skin stiffener spacing and dimensions, etc. Apart from these, in case of composites, these details include stacking sequence of laminate, ply composition (if two or more type of material is used). Many of the response functions used in design optimization require a complete analysis of the structure under the specified design

loads. Full scale analysis of the structure using a detailed finite element models with a large number of degrees of freedom is computationally expensive. When such analysis models are coupled with an optimizer, which necessitates repetitive analysis, the computational cost of the design optimization becomes prohibitively expensive and beyond the scope of the present computational capabilities. In order to reduce the computational effort while maintaining high fidelity analysis, various modeling approaches and improvements to the design methodologies are used.

One approach to reduce the complexity in a large scale design optimization problem is to decompose the problem into several smaller independent/semi-independent optimization problems and a coordination problem to preserve the coupling and/or compatibility among these subproblems. This approach is generally referred to as multilevel optimization. This makes the big problem easily manageable. This enables simultaneous work on different parts of the problem, which significantly reduces the product development time.

Most of the earlier attempts to formulate a large design optimization problem via multilevel optimization were based on fully stressed design (FSD) concept. The FSD technique implies that material is removed from structural components unless minimum thickness constraints are violated or structure is stressed to its maximum for the given failure criterion under specified load condition. This method has been used extensively for aerospace structures by Lansing *et al.* [11], and Giles [12].

Sobieszczanski-Sobieski *et al.* [13] developed a multilevel optimization procedure for design of fuselage structures. The structure is designed in two stages. First, an overall material distribution is found applying FSD technique to an idealized model of the structure. Second, the detailed design of the structural subcomponents is performed by mathematical optimization. Schmit *et al.* [14], correctly pointed out the shortcomings of the approach proposed by Sobieszczanski-Sobieski *et al.* [13]: the use of weight as the objective function at the component level and the use of fully stressed type resizing algorithms at the system level. Schmit *et al.* [14] proposed a modified version of the above approach. Overall proportioning of the structure is achieved at the system level subject to system constraints, while the detailed component designs are carried out separately at component level subject to local constraints. Total structural weight is taken as objective function at the system level and the change in stiffness of the component to be minimized as the component level objective function. Schmit *et al.* [14] unlike Sobieszczanksi-Sobieski *et al.* [13] employed mathematical optimization techniques at both the system and the component level via passing informations from system to component level and vice versa. The minimization of change in stiffness at the component level design aims to weaken the coupling between system and component level problems i.e. to reduce the load redistribution at the system level due to component level optimization. Schmit *et al.* [15] successfully extended the multilevel approach to design of composite structures. However, in their work, the design variables are the thickness of the lamina and the stacking sequence of the laminate is fixed.

The component level objective function used by Schmit *et al.* [14, 15] is square of the

change in stiffness. This implies that at optimum, the derivative vanishes. As noted by Sobieszczanski-Sobieski *et al.* [16], this will result in suboptimum designs and reduced convergence around optimum while employing any gradient based optimization techniques. Sobieszczanski-Sobieski *et al.* [16] proposed a generalized multilevel approach. The decomposition is achieved by separating the structural element optimization problem from the assembled structural optimization problem. Each element optimization problem is minimization of a cumulative measure of the element constraint violation (or component level objective function) subject to specified equality constraints and side constraints (bounds on the design variables). The assembled structural or system level optimization problem is minimization of total weight subject to constraints that also include cumulative measure of element constraint violation for all the elements extrapolated linearly with respect to the element forces and stiffnesses, and side constraints. The equality constraint at subsystem level is imposed to maintain model compatibility between system and subsystem level. The cumulative constraint measure chosen is a Kreisselmeier-Steinhauser function, which is continuous in both feasible and infeasible region. One of the major improvement proposed in the approach, apart from the usage of a continuous objective function at subsystem level optimization, is to use subsystem level information while performing system level optimization. All the multilevel approaches discussed till now are essentially two level approach. Sobieszczanski-Sobieski *et al.* [17] further extends the approach to three level with more focus in analysis details at the third level. The basic underlying principle remains the same as the previous one.

The general multilevel approach is to divide the system into a hierarchy of subsystems. Equality constraints are imposed at each successive level to ensure consistency between levels. In most of the earlier applications these equality constraints were eliminated by reducing the number of design variables. For example, the multilevel design optimization of portal frame considered by Sobieszczanski *et al.* [16] enforces the equality constraints by eliminating variables at the lower level. This is possible only if the relationship between local level (or subsystem level) design variables and global level (or system level) design variables is simple enough to permit such elimination. In complex systems, this may not be possible and these equality constraints may have to be retained in the optimization process. As noted by Thareja *et al.* [18], these equality constraints introduce numerical difficulties, and the numerical solution becomes very sensitive to optimization parameters for a wide range of optimization algorithms.

In the context of composite wing structure design, one of the modeling simplifications is to decouple the effects of the bending and inplane stiffness of the skin laminates. This is reasonable because the total thickness of the skin laminates is very small compared to the overall depth of the wingbox. So, the contribution to overall stiffness of the structure is mainly from the inplane stiffness of the wing structure skin panels, while the bending stiffness mainly contributes to its local buckling performance. The inplane stiffness depends on the number of layers of each type of fiber orientation angle instead of the exact stacking sequence. Hence, the overall design problem can be decomposed into a hierarchical global/

local design problem. The global design problem is to find minimum number of layers of each type of fiber orientation subject to global constraint for all the skin panels. The local design problem is to determine the exact stacking sequence of the panels subject to local constraints. But the local panel design depends on the inplane loads acting on them. These inplane loads are computed from global structural analysis and are functions of all the local panel designs. Any attempt to alter the number of layers at local level will result in global level load redistribution. So, to maintain consistency or compatibility between global and local models it is necessary to keep the number of layers constant while performing local optimization. Thus at the local level, the objective is to generate a stacking sequence given a number of layers with specified orientations, such that the local design is optimized.

Ragon *et al.* [19] developed a global/local method for wing structure design using a response surface methodology. In their work, the local code or local analysis module is replaced by response surface(s). A response surface of minimum weight that satisfies all the local constraints is created a priori with inplane loads, and inplane stiffness coefficients as function parameters. Therefore, while creating the response surface, the designs are constrained to match the specified inplane stiffness coefficient values. The global optimizer interacts with the response surface instead of the local analysis module. At each design iteration, for each panel, the global optimizer passes values of inplane loads, and stiffness coefficients to the response surface module. The response surface returns the minimum weight of the local panel that do not violate any local cosntraints for the specific inplane load and stiffness coefficients. The global optimzer then compares this optimal local panel weight w_l from response surface model with the panel weight w_g calculated using the global design variables and computes the weight constraint g_l as $1 - w_g/w_l$. This weight constraint include the effects of all the local constraints on the local model. If g_l is negative, then the constraint is inactive and the global optimizer improves the design variables to reduce the total weight of the wing structure. If g_l is positive, on the otherhand, then the constraint is violated. The advantage of this methodology lies in the fact that all the computationally expensive work has already been done even before optimization procedure has begun. Ragon *et al.* [19] successfully implemented the above procedure for design of a wing structure made of isotropic material with thickness of membrane elements and cross-sectional area of rod elements as global design variables.

Liu *et al.* [20] extended the approach of Ragon *et al.* [19], for design optimization of composite wing structure. In their work unlike Ragon *et al.* [19], they created a response surface for maximum buckling factor with inplane loads, and number of plies of each fiber orientation as function parameters. The local design variables are the stacking sequence (discrete) of the laminates given the number of plies of each fiber orientation. At the global level optimization, the design variables are the number of layers (continuous) of each type of fiber orientations and the objective is to minimize the total weight of the structure. The buckling constraint margin is computed from the response surface model.

The multilevel techniques discussed above are in particular reference to structural design. Given the nature of similarity between multilevel structural design problem and multidisci-

plinary optimization problem, we present a brief review of the on going research activity in the field of multidisciplinary optimization methods in the next section.

1.4 Multidisciplinary optimization methods

The complete design of any complex engineering system, as mentioned earlier, involves multiple disciplines. For example, the complete design of an aircraft includes aerodynamic, propulsion, structure and control. In multidisciplinary approach, the interaction between multiple disciplines are considered. It is important to notice that any advancements made in multidisciplinary techniques can very easily be applied to multilevel structural optimization because mathematically they deals with decomposition of a system and maintaining consistency between different levels.

The all-in-one is the conventional approach for solving MDO problem. The principal drawbacks are its expense in having to perform a complete multidisciplinary analysis at every stage and its lack of modularity and fit with respect to integrated product systems in industry.

The concurrent subspace optimization (CSSO) method [21, 22, 23] provides multidisciplinary feasibility at each cycle but deals with all of the design variables simultaneously at the system/coordination level. The later approaches to CSSO make use of response surfaces at the system level that is not effective for design spaces of dimensionality over 20.

The collaborative optimization (CO) method [24, 25] and individual discipline feasible (IDF) [26] method dispenses with multidisciplinary compatibility at each system iteration; instead the compatibility is attained as the system optimization process converges. CO has the disciplinary autonomy property. But the problems solved are restricted only to those which have a very small interdisciplinary coupling bandwidth. A large number of coupling variables between the disciplines would proportionally increase the number of system level optimization variables in CO.

The bilevel integrated system synthesis (BLISS) method [27] is an all in one method because a complete system analysis is performed to maintain multidisciplinary compatibility at the beginning of each cycle. It is assumed that system level optimization involves very few design variables that are shared by subspaces or disciplines. Several improvements are suggested like use of gradient information to improve system design and use of response surface [28].

As mentioned earlier, that the multilevel design of large structural systems should also take into account the manufacturability, cost, and structural integrity of the optimum designs. In the next section we review the manufacturing issue - blending that plays an important part in the design optimization of large composite structure.

1.5 Blending

Another problem, apart from global/local model compatibilty, of using a multilevel approach in a large composite structure design is the ply continuity among adjacent panels over the entire structure. This ply continuity among adjacent local panels is referred to as blending. Local loads that dictate the stiffness and strength requirements of the skin panels vary from one location to another. Therefore, the thickness and stacking sequences of the laminates that meet requirements also vary. If the laminate stacking sequence of a panel is entirely different from that of the adjacent panels, this will give rise to discontinuities along the edges. Maintaining ply continuity is an important issue because any attempts to subdivide the wing structure into several local panels and independently design them may lead to incompatible laminate stacking sequences that may not only be structurally unsafe but may also be impossible to manufacture.

In order to prevent laminate discontinuity, Liu *et al.* [29] imposed continuity constraints. They defined two continuity measure - material composition continuity and stacking sequence continuity. A material composition continuity between two panels is defined as fraction of common layers of the thicker laminate. The material composition continuity constraint is imposed at global level design. In their multilevel approach, the global design variables are number of layers of each type of orientations for all the skin panels. Thus, composition continuity measures the numbers of layers of each orientation common between two panels regardless of the stacking sequence because stacking sequence is determined at local level. The stacking sequence continuity between two panels is the fraction of continuous layers of the laminate. Unlike, the composition continuity which is based on the thicker laminate and hence referred in their work as two-sided, the stacking sequence continuity is based on the panel of which continuity is being computed and referred as one-sided. By continuous layers, instead of matching fiber orientation one to one layers, Liu considered that any plies just above or below the current thickness level as continuous if the orientation matched. This definition of *continuous layers* will give rise to layer termination anywhere along the thickness of the laminate.

Soremekun *et al.* [30] used multiple sub-laminates and design variable zone approach to design completely blended composite structures. The blending approach developed by Soremekun *et al.* [30] is a two step optimization procedure. During the first step, each panel in the system of panels is individually designed for minimum weight. During the second step, sub-laminate definitions are reset based on the minimum number of plies required by each panel in step one, and the blending optimization procedure is performed. They implemented and successfully generated blended design for an 18 panel horseshoe configuration arrangement with fixed load. This approach is adhoc and connot be easily applied to more complex design problems.

Adams *et al.* [31] used a distributed genetic algortihm in a parallel processing environment with migration to obtain blended designs. The methodolgy relies on simultaneous evolu-

tion of the stacking sequences of the individual panels mapped to different processors that communicate with one another via migrant individuals. A metric based on Levenstein edit distance is used to evaluate the similarities of the stacking sequence between adjacent panels. Best individual in the independently evolving populations are sent to neighbouring populations in an effort to coerce the evolution of the neigbouring populations so as to minimize the stacking sequence mismatch. Blending is encouraged by comprising each members of the neigbouring populations with the migrant individual(s) and modifying their fitness based on the degree to which they match to the migrant. A scaling factor is used to adjust the degree of pressure imposed on blending of the neigbouring panels. They implemented the above procedure for the problem solved by Soremekun *et al.* [30] and got fully blended solutions.

Recently, Adams *et al.* [32] developed a *guide based* genetic algorithm for the design and optimization of blended composite structures. In a guide based design, the basic laminate stacking sequence (referred to as the *guide*) that is applicable to all the panels is used as a design lay-up, while the individual local panels use only a segment of the guide starting either from the top or from the bottom of the guide. This ensures complete blending at any stage of the design optimization process.

Most of the works done till date on design of composite are mainly on strength and stiffness. Very few efforts have been done to take the advantage of the postbuckling strength of composite laminates. In the next section, we discuss some of the works done in the design optimization of composite laminate for postbuckling strength.

1.6 Postbuckling optimization

Laminated composite plates possess significant postbuckling strength. Though a comprehensive literature exists on the study of postbuckling analysis of composite laminates, very few attempt has been made to include the postbuckling behaviour into the optimization procedure. The obvious difficulty is that the nonlinear postbuckling analyses are computationally expensive.

Shin *et al.* [33] studied the minimum weight design of composite laminates for postbuckling performance. They used maximum strain criterion to predict the laminate failure in postbuckled regime. It was found that the laminate failure criterion predicts failure load reasonably well when compared to the experimental results [34]. The design variables are layer thicknesses with prespecified fiber orientations and assumed to take only discrete values. In their work, they proposed simple and efficient method based on penalty method to achieve discrete valued designs. Perry *et al.* [35] investigated the minimum weight design of stiffened composite panels under uniaxial compression for postbuckling performance. In their work too, the authors used thickness of the layers of a preselected laminate stacking sequence as design variables.

Adali *et al.* [36] proposed a multiobjective formulation to simultaneous take into account

both the buckling and initial postbuckling behaviour of the laminate. Rather than directly maximizing postbuckling strength, they maximized a design index defined as a weighted sum of buckling load, prebuckling stiffness, and initial postbuckling stiffness.

Recently, Diaconu *et al.* [37] studied the optimum design of infinite length composite laminates subject to uniaxial compression. They formulated two optimization problems, minimization of maximum transverse displacement and minimzation of end strain. They used lamination parameters as design variables. As already mentioned that it becomes problematic to find the optimum stacking sequence, particularly when it is known that the postbuckling performance varies widely even with small changes in fiber orientation [36].

As it is evident from the discussion that one of the difficulty in integrating the postbuckling strength in multilevel design optimization of large composite structure is the computationally expensive local postbuckling analysis, another issue is how to compute the load path in the whole structure based on which local level designs are done. In a structure, where some of the components have buckled, a simple idealization of global model is not applicable. To predict the load paths in a structure with buckled components, we need to do full scale nonlinear analysis which is impossible given the current computational resources. We need a global or loads model, which is not only computationally inexpensive, but also accurate enough to be used in design optimization studies.

1.7 Flutter optimization

Apart from local buckling, another chief design consideration for aerospace structures is flutter. Lifting surfaces of aerospace vehicles in supersonic or hypersonic regime exhibit two types of flutter. One is classical low aspect lifting surface flutter and the other is panel flutter. Flutter is defined as the instability associated with increasing amplitudes of oscillation because of the interaction of modes with inertial and aerodynamic coupling. Flutter is a self-sustained oscillation occurring beyond a critical airflow speed in aerospace vehicles. In panel flutter, the dynamic instability occurs when at a specific speed, due to the aerodynamic pressure loads, there is coalescence of two of the structural eigen modes. At this speed, the damping of the system becomes negative which leads to ever increasing oscillation. This aeroelastic instability is of immense concern for aircraft and wing designers as well as for missile designers. Nonlinear effects in aeroelastic systems may be either favorable or unfavorable or a combination of both. For example, when structural stiffness nonlinearity is equivalent to a hardening spring as in the von Kármán plate model, no limit cycle oscillations (LCO) will exist below the flutter boundary determined in the absence of nonlinearity. And above the flutter speed, the nonlinearity will limit the response, a clearly favorable outcome. However, for other nonlinearities such as structural free play or aerodynamic nonlinearities due to flow separation or large shock motion and very high speed, the effect of nonlinearity may be to induce LCO below the nominal flutter speed, but still limit the LCO response to a finite amplitude both below and above the nominal flutter speed. Whether such nonlinear

effects are favorable or not will depend very much on the particular circumstances and parameters involved. Nonetheless it is clear that nonlinear effects often lead to LCO and in their absence the alternative would be catastrophic failure leading to structural failure.

In the recent years with composites increased use as structural elements due to their high specific strength ratio (strength/weight), much research work is carried on to understand the both the linear and nonlinear aeroelastic behavior in this new context. A survey of such studies was given by Dowell [38, 39] and Librescu [40]. Librescu studied the aeroelastic response using a standard linearized formulations [41, 42]. Chatterjee *et al.* [43] studied the effects of shear deformations on flutter of laminated composite plates. Oyibo [44] studied the flutter of orthotropic panels using affine transformations. Birman *et al.* [45] analyzed the supersonic flutter of shear deformable laminated composite plates. In their work, they used the two-dimensional static aerodynamic approximation and a higher order shear deformation theory for the structural plate model. Dixon *et al.* [46] also studied nonlinear flutter of composite panels using finite element methods. Recently Marzocca *et al.* [47] used Volterra approach to predict the aeroelastic response of panels. Aerospace vehicles, such as high-speed aircraft, rockets and spacecraft, are subjected to thermal loads due to aerodynamic and/or solar radiation heating. This results in a temperature distribution and thermal gradient through the thickness of the plate. Therefore, thermal buckling is a significant failure mode governing the design of thin plates used in aerospace structures. Lee *et al.* [48] studied the supersonic flutter analysis of stiffened laminated plates subject to thermal load. Liaw studied the linear [49] and nonlinear [1] supersonic flutter of laminated composite plates under thermal loads using finite element method. Cheng *et al.* [50] studied panel flutter analysis with thermal effects using finite element modal formulation. For the panel flutter problem in presence of thermal loads, the interested reader is referred to a monograph by Bolotin [51].

As mentioned earlier, much work has been carried out to optimally design the stacking sequence of laminate configurations to maximize buckling capacity. A comprehensive literature on the optimization of composite laminates for maximization of buckling load can be found in references [3, 5, 6, 7, 52, 53] and has already been discussed in earlier section. An excellent review on composite laminate optimization is given by Venkataraman *et al.* [54]. However, lesser attempt is made to integrate the advances in aeroelastic concepts within optimization framework. Beiner *et al.* [55] formulated the optimization problem for a shear panel as a minimum weight design with flutter speed constraint. In their work, they formulated weight minimization problem to find the optimum thickness distribution such that the associated flutter speed coincides with that of the reference panel with a uniform thickness. A survey of structural optimization with aeroelastic constraints is given by Haftka [56]. Till date, no attempt is made to simultaneously optimize the stacking sequence of the laminated composite plate for both maximum flutter speed and buckling capacity.

Upto this point, we presented the literature review of structural optimization concepts related to composite structures. The multilevel decomposition techniques, blending issues, optimization of composite panels for postbuckling and flutter is discussed. The literature

review shows that the design problems considered for both postbuckling and flutter are simple structural elements like plates or stiffened plates where the load is assumed to be known apriori. But in actual design, this will come from the global or loads model. In the next section, we discuss the issues associated with the load path prediction in postbuckled structure.

1.8 Load path prediction in postbuckled structure

The most important step in multilevel structural design is to predict the load paths in the structure because based on these internal loads the structural subcomponents are designed. A highly idealized and simplified global model is used to predict the load paths in the structure because of the computational cost involved with full scale analysis of the structure. For example at the preliminary stage of the design of fuselage or wing structure, each panel between the stiffeners or ribs or spars are modeled via a single element to avoid the computational overhead associated with full scale finite element analysis. The aim of the global analysis is to give the internal load distribution. This is the reason the global model is also referred to as loads model. Based on these internal loads, the subcomponents are designed for strain, stability or buckling, and manufacturing constraints. Thus, the research focus in multilevel structural design procedure can be classified in two areas. First, development of loads model with reasonable degrees of freedom for complex structures so that it can be used in optimization studies. Second, development of cheap local model (usually simple structural component like a beam, panel, etc) to be used in local detailings. In the last four decades, the research focus was mainly on developing faster, cheaper, and accurate local models. A comprehensive literature exists on both analysis and design optimization of composite beams, panels, stiffeners, etc against buckling [3, 5, 4, 6, 8, 52], postbuckling [35, 33, 57, 36, 37], failure, etc.

In thin walled structures, one of the most important modes of failure is buckling. After buckling, the load carrying capacity of the structure is reduced because of reduced stiffness. In practice, however, it is customary to allow the secondary load carrying components (like skin panels of fuselage) to go beyond buckling load. The multilevel approach discussed above relies on the idealized loads model to predict the load paths in the structure and hence true only if none of the subcomponents have buckled. Hence, for structural design with structural subcomponents to be loaded beyond buckling load, the loads model must be able to reflect the local changes like reduced stiffness due to some or all buckled components. This, as mentioned earlier, can be done by using a detailed loads model, which is computationally expensive, and beyond scope. Hence, the need for a cheap and sufficiently accurate procedure to predict load paths in postbuckled structure.

Grisham [58] proposed a methodology to incorporate the reduced load carrying capacity of a buckled component by applying prestrains. Grisham's algorithm consists of following steps - compute the internal load distribution using a linear finite element analysis, evaluate the

onset of local buckling based on internal loads calculated in earlier step, apply postbuckling strains to relieve the load that exceed plate capability, redo the whole procedure till convergence. Anderson [59] modified the VICONOPT [60] computer program for design of plate assemblies based on initial buckling to allow buckling. In their work, they reduced the overall stiffness of a buckled plate by a factor of 2. Viljoen *et al.* [61] implemented Grisham's algorithm for design of stiffened thin-walled panels in shear. Collier *et al.* [62] used an ad-hoc approach to account for local postbuckling of skins by forcing the analysis module to disregard already buckled portion of the skin such that it carries no additional load. This is achieved by reducing the effective width of the component. Another approach that is being explored currently is to replace the global loads model of the structure by a response surface [63, 64]. In both the approaches, the design space of the parameters is very small and only axial load is considered. Murphy *et al.* [65] proposed a nonlinear idealization for axially loaded structures only. Their work is based on representing a subsection with a single one dimensional nonlinear spring element in the global model. A number of detailed finite element analysis is performed apriori to generate the spring data. This method also comes into the purview of response surface methods, though it does not uses response surfaces directly to model the global loads model response but only to generate the spring data. Moreover, this methodology cannot be extended very easily to biaxially loaded structures or structures under more complicated loading cases like wing structure under bending load. Recently, Kling *et al.* [66] developed a hybrid subspace analysis procedure for nonlinear static analysis of beam type structures. In this work, the buckling modes and path derivatives have been used as global shape functions to reduce the conventional full finite element system. This approach though reduces the computational cost compared to the full nonlinear analysis but it is still too expensive to be employed as a loads model in a design optimization framework. Also, the proposed methodology has not been extended to plate structures.

All the aforementioned works, except in the field of surrogate approximation, are done for metallic (isotropic) structures only. Till date, no work to quantify the locally buckled information is done in the area of composite structure. Also, Grisham's algorithm is based on prestrains, which will require a mesh unlike the one used in loads model as mentioned earlier. The motivating factor of the current work can be best described by the following words taken verbatim from the original Grisham's paper - *"A generalized method does not yet exist for predicting reliably the postbuckling moduli of plates"*.

The proposed load path prediction scheme though much less expensive compared to full scale nonlinear analysis but together with local postbuckling analysis module, the computational expense adds up to a degree where it is not possible to make optimization runs. We need further sophistication to make it possible to include postbuckling constraints in the design optimization process. In this effect, we discuss the response surface methods in the next section used in design of composite laminates. The discussion/literature review is kept brief remembering the fact that the present work is not related to development of response surface methods but only employs response surface as an alternative to expensive analysis to make the optimization runs possible with the current computational resources at hand.

1.9 Response surface acceleration

In engineering optimization, the simulation model used are usually expensive. Hence, these expensive computational models cannot be integrated to the MDO framework. An alternative is using approximation models. The common approach is to use a linear or quadratic polynomial model created by performing a least square fit to a set of data. These polynomial based modeling methods are referred as response surface models [67]. The popularity of these models are because they provide explicit relationship between response and the independent variables, the method of least square used is relatively simple, inexpensive, and straightforward. Evidence of popularity of polynomial models can be gauged by the number of recent publications in the field of multidisciplinary optimization.

The basic idea of any metamodeling technique is to construct an approximate model using function values at some sampling points, which are typically determined using experimental design methods such as factorial design, latin hypercube, central composite design, or Taguchi orthogonal array. Model fitness is subsequently checked using various statistical methods.

As mentioned earlier, the design of composite laminates is essentially discrete optimization problem. The presence of discrete design variables make it difficult to apply standard metamodeling techniques. However, the lamination parameters suggested by Miki [4] can be used as the design parameters in the response surface construction. The use of lamination parameters has two advantages. First, they reduce the number of design parameters for response model. Second, they do not suffer from multiplicity of local optima. However, because the stacking sequence is discrete in nature, the lamination parameter values jump from one value to another. Todoroki *et al.* [68] suggested a design of experiments for stacking sequence optimization of composite laminates. In their work, lamination parameters are used as design parameter and a D optimality criterion is used to select the sampling points at which response will be evaluated to construct the approximation model. They showed that the use of lamination parameter as function of discrete stacking sequence led to considerable lowering of D optimality criteria. So, it is important to take into account the value that lamination parameters can take while constructing a realistic response surface model.

After summing up the work done till date in design optimization of large composite structure via a multilevel or global/local methodology, we present the motivation and scope of the current work.

1.10 Motivation and scope

The literature survey on multilevel optimization of large composite structures like wing indicates that with the recent development of blending methodologies there exist significant possibilities of improving the stacking sequence continuity of the designs obtained by Liu *et*

al. [29]. Guide based approach applied to design of assembly of composite panels with fixed loads gives excellent results. Since, the loads are fixed there is no reason to worry about global-local model compatibility. But no attempt has been made to develop the methodology for design of structure where global-local coupling cannot be ignored as in the case of a wing structure design.

In this work, in the first part, we focus on developing a guide based module for design of large composite structure. The efficiency of the methodology is demonstrated via design of a composite wing structure configuration subject to local panel buckling constraint and stacking sequence continuity constraint (or blending constraint). The problem of composite wingbox is chosen because of the availability of published work done earlier (Haftka and Liu *et al.* [20, 29]) and also the problem is complex enough. The results obtained by the present methodology are compared with the published ones. In the second part, we develop a postbuckling analysis module for the local panels to investigate the stacking sequence optimization of composite laminates for postbuckling performance. The stacking sequence of the laminate is considered to be chosen from a discrete set following the usual industry practices. The effects of flexural and inplane stiffness coefficients on the postbuckling optimization is investigated. Nest, we study the stacking sequence design of composite laminates for both buckling and supersonic flutter. A pareto study is done to compare the optimal designs for each objective function. Next, we develop a general methodology to predict load paths in postbuckled structure. The proposed load path prediction scheme is extended for more complicated loading cases like bending load and complicated structure like composite wingbox. Finally, we extend the global/local design methodology for design of large composite structures subject to local postbuckling constraint and blending constraint. The aims of the current work are as follows:

1. Develop a guide based approach for a coupled global/local problem as in the case of wing structure design.
2. Investigate the effect of flexural and inplane stiffness coefficients on the design optimization of composite laminates for postbuckling performance.
3. Investigate the trade-off between flutter and buckling optimized designs for composites.
4. Develop a cheap module for load prediction in postbuckled regime that could be used in global analysis.
5. Extend the global/local methodolgy for local postbuckling constraints.

1.11 Organization

The report is organized as follows: Guide based approach to obtain blended designs for strongly coupled global/local problem (chapter 2), postbuckling optimization of composite

laminates (chapter 3), multiobjective flutter and thermal buckling optimization of composite laminates (chapter 4), load path prediction in postbuckled structures (chapter 5), global/ local design with local postbuckling constraint (chapter 6), conclusion and future works (chapter 7), and a brief description of other research works done (chapter 8).

Chapter 2

Design for Blending and Buckling

2.1 Blending problem

The activity of designing laminate stacking sequences across multiple panels with different overall thicknesses so that continuity of the plies is maintained is generally referred to as blending. Blending of laminate stacking sequence is important both from the structural and manufacturing point of view. Blending simplifies the manufacturing process and reduces the cost of lay out and enhances the structural integrity. In the present work, the laminates are assumed to be symmetric about their mid plane. Two simple types of blending are considered - inner blending, where the inner layers of the laminates from the mid plane are continuous, and outer blending, where the outer layers of the laminates are continuous as schematically shown in Fig. 2.1. The need for blended solution complicates the design process. In the next section we discuss the approach to design blended laminates.

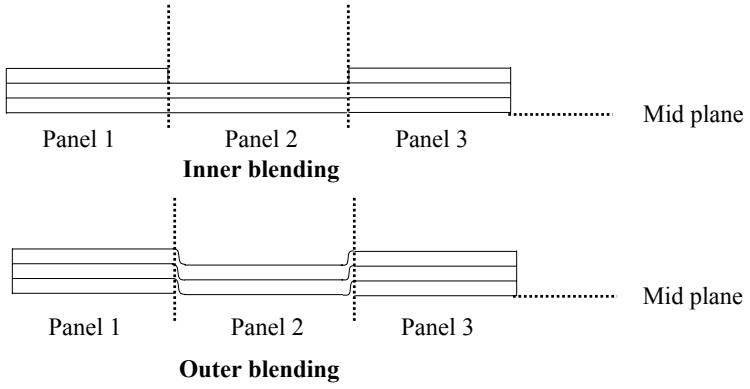

Figure 2.1: Blending schemes.

2.2 Guide based approach

A guide is a basic template laminate stacking sequence that is applicable to all the designated panels. From this guide design, a certain number of contiguous plies are kept to represent a particular panel. This ensures complete blending. If needed, we can also define multiple guides applicable to different sections of a structure. For example, in the case of a wing box design, there is no need of ply continuity between upper and lower skin panels. It is more advantageous to use two different guides with two different requirements instead of using one thick guide for both upper and lower skin panels. In the guide based approach the design variables are the laminate stacking sequence of the guide, and the number of layers to be kept from the guide to represent each of the panels. Depending on whether the outer or inner layers of the guide are taken to represent a panel, the resulting design will be inwardly blended (outer blending, see Fig. 2.1) or outwardly blended (inner blending, see Fig. 2.1), respectively [31, 32]. Lightest possible structure from a guide is obtained by performing one dimensional optimization (stripping plies until the panel thickness is minimum to support the load) at local level (or panel level design).

2.3 Design of composite wingbox

2.3.1 Optimization formulation

The composite wing structure design optimization problem is formulated as a minimum weight design subject to the maximum global deflection, global blending, local strength failure, local panel buckling, and local ply contiguity constraint (successive plies of the same fiber orientation). Laminates with more than four layers of the same fiber orientation are generally assumed to be not practical because of thermal stresses created during curing process, which can lead to matrix cracking. The design variables are the stacking sequence of the guide defined by a vector $\mathbf{\Theta}$ of ply angles chosen from a discrete set of angles, and the number of layers to be kept for each panel n^i, where i is the panel number. The global blending constraint is automatically satisfied by using a guide based design as discussed above. The individual panel stacking sequence $\boldsymbol{\theta}^i$ of the i^{th} panel is defined uniquely as the outer (for outer blending), or inner (for inner blending) n^i plies of the guide stacking sequence $\mathbf{\Theta}$. Therefore, the wing design problem can be stated as:

$$\text{Minimize} \sum_{i}^{N} w^i \left(n^i\right),$$

subject to

1. global constraints

$$\delta_{max}\left(\mathbf{\Theta}, n^1, n^2, \ldots, n^i, \ldots, n^N\right) \leq \delta_{all}$$

2. local constraints

$$\lambda_s^i\left(\boldsymbol{\theta}^i, N_x^i, N_y^i, N_{xy}^i\right) \geq 1.0$$
$$\lambda_b^i\left(\boldsymbol{\theta}^i, N_x^i, N_y^i, N_{xy}^i\right) \geq 1.0$$
$$\lambda_c^i \geq 1.0$$
$$\text{laminate is symmetric and balanced,}$$

where w^i is the weight of the i^{th} panel, N is the total number of panels, n^i is the number of plies in i^{th} panel, $\boldsymbol{\Theta}$ is the stacking sequence of the guide, $\boldsymbol{\theta}^i$ is the stacking sequence of the i^{th} panel, δ_{max} is the maximum deflection, λ_s^i is the normalized strength constraint value of i^{th} panel, λ_b^i is the normalized buckling constraint value of i^{th} panel (see Appendix B), λ_c^i is the ply contiguity constraint value of i^{th} panel, and N_x^i, N_y^i, and N_{xy}^i are the inplane loads acting on the i^{th} panel. The inplane loads N_x^i, N_y^i, N_{xy}^i are function of the stacking sequence of all the panels, i.e., $\boldsymbol{\theta}^1$, $\boldsymbol{\theta}^2$, ..., $\boldsymbol{\theta}^N$. Thus, they depend on the stacking sequence of the guide and the number of layers to be kept from the guide for all the panels. This makes it difficult to completely decompose the problem into a global/local problem.

2.3.2 Guide based genetic algorithm

Genetic algorithms (GA) are commonly used for design optimization problems when the design variables are discrete or the problem under consideration has multiple local minima. A standard genetic algorithm is based on the Darwinian principle of survival of the fittest. They are probabilistic search algorithms based on natural selection to guide the exploration of design space toward a global optimum. The common features of a standard GA are population initialization, parent selection, GA operation (like crossover and mutation), and the selection of successive generations (elitist selection [8]). Each element has many variations, modified to suit a particular problem. GA has been used extensively for composite laminate design with discrete design variables. The suitability of GA for this class of problems is well researched and can be found in Refs [69, 5, 52, 70]. Next, we discuss the laminate representation, the analysis module or fitness evaluation of the designs and local improvement operator, and crossover operator used in the current guide based GA. The GA discussed in the current work is a modification of earlier research work to suit our particular need and we only provide the details to the modifications done. The references are provided at appropriate places.

Laminate encoding

Each laminate stacking sequence (or design or chromosome) must be encoded for use in genetic algorithm. In this work, we used the encoding scheme of McMahon *et al.* [52, 70]. The 0, 45, and 90 degree plies are represented by integers 1, 4, and 7 respectively. Every

occurrence of 4 is alternatively assigned as +45 and minus -45 degree. This representation of ± 45 will restrict the unbalancedness in a laminate to 1 only. The empty ply is represented by integer 0. However, designs with internal empty plies do not have any physical meanings and hence shifted to one side of the laminate chromosome. Till now we discussed a general chromosome structure typically used in composite laminate design. Next, we elaborate the modifications to the above chromosome in a guide based GA. In a guide based GA, we encode the stacking sequence of guide as described above and not of the individual panels. Then, from this guide a certain number of plies are taken to represent a particular panel. A typical individual in a guide based GA is shown in Fig. 2.2. Each individual consists of two parts or strings. The first string is the stacking sequence of the guide and the second string is the number of layers to be retained from the guide for each of the panels that the guide represents. Thus, the second string of the individual is of the same length as the number of panels that the guide represents. From Fig. 2.2, it is evident that each individual contains all the information for every panel of the overall wing structure. The stacking sequence of the first panel is the first n^1 layers of the guide and the second panel has the first n^2 layers of the guide, and so on for each of the successive panels of the wing box.

Initial population

The first part of the individuals (stacking sequence of guide) of the initial population is generated randomly similar to standard genetic algorithm [71]. The second part or string is initially assumed to be equal to the number of plies in the stacking sequence of the guide. Thus, at the start of optimization process, all the local panels are assumed to be of uniform thickness equal to that of the guide.

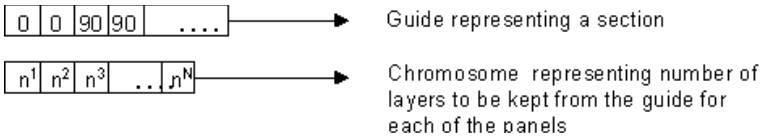

Figure 2.2: A typical individual in guide based GA.

Fitness evaluation

The fitness evaluation of an individual (or a guide design) requires computation of the structural weight as well as the constraint violations or margins, which are obtained via global and local analyses. Based on the number of plies that are to be kept from the guide, the laminate stacking sequence is assigned to all the panels, and a global finite element analysis is performed that gives the inplane loads acting on each of the panels. The maximum deflection constraint is checked and if violated, a penalty is applied to the fitness evaluation. Then

for each panel the local strength constraint and the local buckling constraint is computed (see Appendix B), and the constraint margin (defined as $(\min(\lambda_s, \lambda_b) - 1)$ is calculated. Depending on the constraint margin value, a decision is made either to add a ply (if the constraint margin is negative i.e. panel has failed) or remove a ply (if the constraint margin is positive i.e. panel is safe) while keeping the load for the panel constant. That is, no new expensive global finite element analysis is done to compute the new inplane loads due to change in local stiffness and the local panel analyses are repeated to check the local constraints (Fig. 2.3). The decision to remove a ply is only made if the global deflection constraint is satisfied. If the constraint margin after removing a ply is still positive, then all the calculations pertaining to the local panel (the weight of the panel) are done based on the new number of plies. Otherwise, calculations are performed based on the previous value before removing a ply.

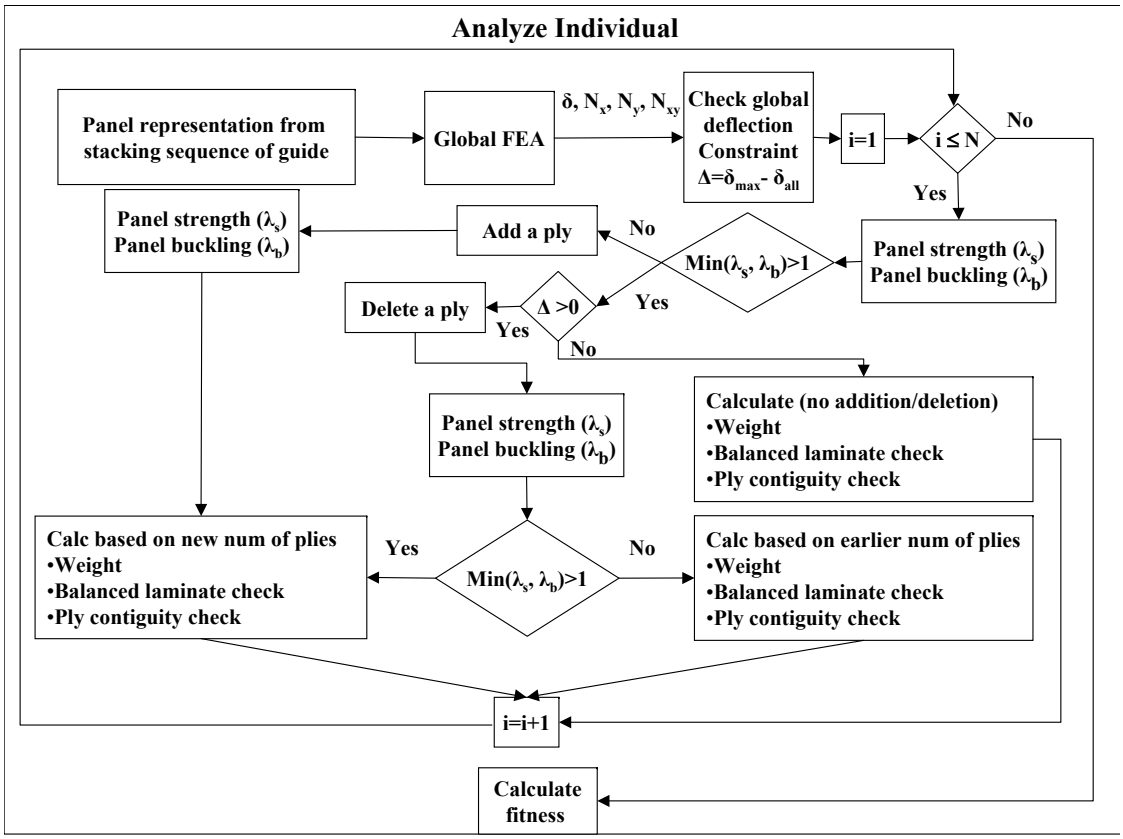

Figure 2.3: Flow chart of guide based GA.

This stripping or adding plies at the local level is referred to as local improvement. The number of layers that is to be kept from the guide for each of local panels due to local improvement is stored for future reference. While improving the current pool of designs at

the local level, the obvious disadvantage of the method is that as soon as the number of layers is changed at the local level, the previously performed global finite element analysis is no longer valid. That is, since a multi-panel wing structure is statically indeterminate in nature, changing the local stiffness of one panel changes the internal load distribution in the wing, possibly affecting the local inplane load of every panel. In order to prevent the local inplane panel loads from jumping severely from one global finite element analysis to another, the local improvement performed at the local level is restricted changing at most one layer per panel. The local improvement discussed here is a variant of one dimensional optimization in Ref. [32] where the plies are deleted until safe minimum thickness laminate is found for the guide. The one dimensional optimization at local level discussed in Ref. [32] is not a good option here because of the changes in the inplane loads as discussed above. After performing local improvement, the new stacking sequence of the panel is checked for the balanced laminate constraint and the ply contiguity constraint. The flow chart of the fitness evaluation or analysis of an individual is shown in Fig. 2.3.

Every individual (or guide design) in the population is assigned a fitness value based on the overall performance of the guide, which is measured by the total weight of the structure (dictated by the number of layers in each panel presented in the second string) and the value of the constraints. If the constraints are satisfied then the fitness value is the total weight of the structure, otherwise, the fitness is the total weight of the structure plus a penalty for the constraint violation. The total constraint violation C for an individual is calculated as the sum of constraint violation for all the panels given by

$$C = \min\left[\left(\frac{\delta_{all}}{\delta_{max}} - 1\right), 0\right] + \sum_{i=1}^{N} \min\left[\left(\lambda_s^i - 1\right), 0\right], \tag{2.1}$$

and the total penalty P for an individual is given by

$$P = \sum_{i=1}^{N} p_u^i + \left(n_{0,max}^i - 4\right) + \left(n_{90,max}^i - 4\right), \tag{2.2}$$

where p_u^i is the penalty for unbalanced laminate, $n_{0,max}^i$ is the maximum number of contiguous (successive) zero degree plies , and $n_{90,max}^i$ is the maximum number of contiguous ninety degree plies in the i^{th} panel. When none of the panels represented by an individual violate the balanced laminate or ply contiguity constraint, the value of P is zero. The fitness f of an individual is computed as

$$f = -W\left(1 + \frac{C^2}{0.005}\right)(P + 1). \tag{2.3}$$

A negative sign is introduced in the fitness evaluation because standard GA traditionally maximizes the objective function.

GA operators

The standard GA operators are used in this work, crossover and mutation. In a standard GA, the crossover operator takes two parent strings, divides them at a crossover point and recombines them into two children strings [71, 8, 52, 70]. In guide based GA, a standard crossover operator is applied to the stacking sequence of the guide or first string in generating the next population of individuals that guide the global design process. However, the number of layers to be kept from the guide is passed on from parent to child from generation to generation without changing them. For example, the GA crossover operation is illustrated in Fig. 2.4. The crossover operator applied to the first string (stacking sequence) is a standard GA one-point crossover operator [71, 8, 52, 70]. The second string that stores number of layers to be kept for each panel is copied from parent 1 to child 1 and so on. Only the local improvement operator described in earlier subsection based on the constraint margin value alters the second string to better the fitness of the individual at the local level. Similarly, in a standard GA, if the mutation criterion is met, then a random position in the chromosome is selected and changed randomly [71, 8, 52, 70]. In guide based GA, we use a standard mutation operator only for the stacking sequence of the guide or first string.

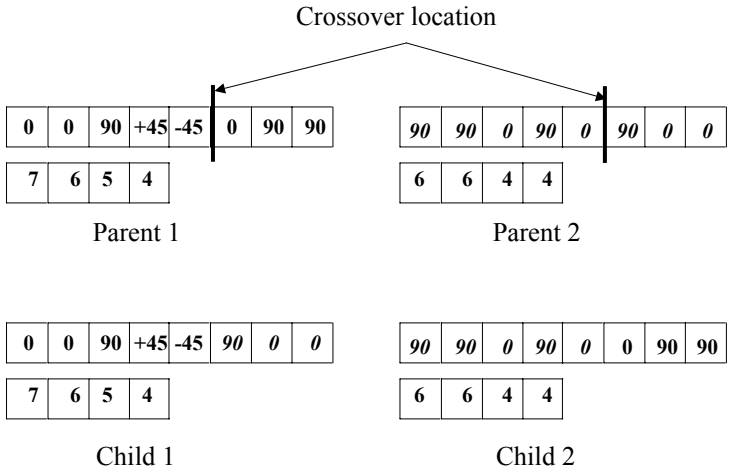

Figure 2.4: Crossover operation in guide based GA.

Selection strategy

The selection strategy used for parent selection in guide based GA is done via a roulette wheel selection process common in the literature [71, 8, 52, 70]. The roulette wheel assigns to each individual of a population a probability of being selected according to its fitness ranking. The probability is biased such that individual with higher fitness has higher probability of

being selected compared to individual with lower fitness. The fraction of roulette wheel occupied by i^{th} best individual in a population of N individuals is precisely given by

$$\text{Fraction of roulette wheel} = \frac{2\,(N+1-i)}{(N^2+N)} \tag{2.4}$$

A standard Fortran90 random number generator is used to provide approximate uniform distributions where random numbers are required to direct evolution.

GA implementation

The present GA work is an adaptation of a pre-existing indigenously developed GA tool at Virginia Tech. The basic GA implementation details are listed in McMahon *et al.* [52, 70]. In order to speed up the computational effort, evaluation of the performance of the individual designs of the populations, which require running the complete finite element wing analysis, is carried out using a node (Beawolf) cluster. A simple master-slave parallel code is implemented for this work [72, 32]. The master process generates and runs the GA code while distributing guide designs to slave processes for analysis in a lock step message-passing phase. The load distribution is calculated statically as an equal division of slave processes into population size with remaining work given arbitrarily to selected nodes with lower rank. For a population size of 400, 25 slave processes were used distributing 16 guides to each process to be analyzed in a given iteration. The parallel code is implemented in Fortran90 using the MPI (message passing interface) library to maintain portability across multiple types of parallel machines. Additional implementation details and recommendations can be found in Ref. [52] from which the parallel implementation is adopted for the current work.

2.3.3 Results

In this section, we present the results for a simple composite wing box design optimization problem originally presented by Liu *et al.* [20, 29]. The wing structure model used is a straight rectangular wing box with the dimensions $139.5'' \times 88.2'' \times 15''$(Fig. 2.5). The top surface and the bottom surface layers are the targeted design panels. The possible ply orientations for the design panels are 0, ± 45, and 90 degrees, while all other panels are fixed to the design $[\pm 45_{11}]_s$ [20, 29]. All the panels are modeled using membrane elements. The root of the wing is fixed and the load is applied at the free end. The total numbers of panels at the top and bottom layer are 9 each. Panel numbering for the upper and lower skin is shown in Fig. 2.6. The composite material is graphite-epoxy: T300/N5208 and the material properties are listed in Table 2.1.

A wing structure in its life cycle is subjected to upward bending during flight due to lift and a relatively smaller magnitude downward bending due to gravity at rest. Realistic wing

designs, therefore, require a complex set of loads and are designed for multiple load cases. Considerations of multiple load cases do not change the essential features of the proposed methodology, and can be accommodated in a straightforward manner. Following Liu *et al.* [20, 29], a single upward loading case is considered. Tip loads at the free end of the wing simulate the upward bending loads. The upward lift force acting is modeled by four concentrated loads of magnitudes $85467lbf$, $42239lbf$, $42239lbf$, and $20235lbf$. The above set of loads induces both upward bending and twisting of the wing box.

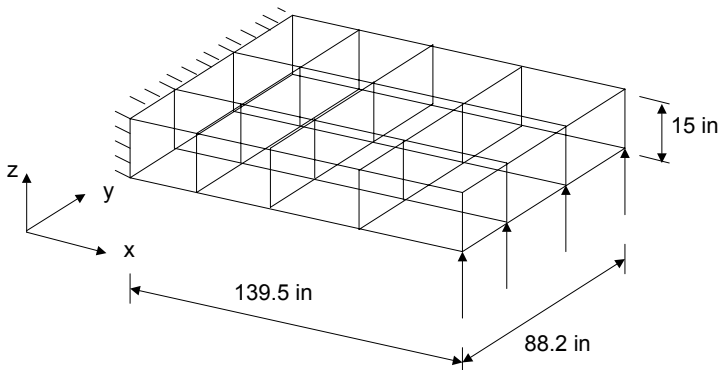

Figure 2.5: Wing structure configuration.

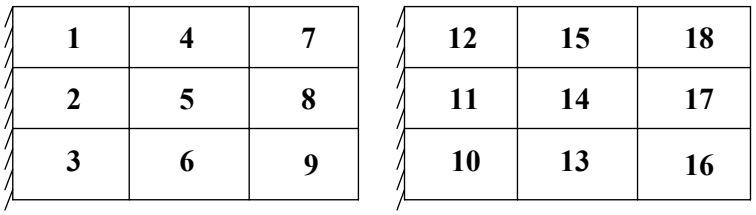

Figure 2.6: Panel numberings in top and bottom skins.

Two different guides are chosen to represent the top and the bottom skin laminates, respectively. GA parameters are reported in Table 2.2. Global finite element analysis is performed using the commercial finite element package GENESIS [73]. An interface module is built to communicate between GENESIS and the locally developed GA code [52] using PERL and Fortran90. The optimal designs reported are obtained after 300 GA generations. Optimal designs for both outer and inner blending are reported.

The upper nine panels are mainly subjected to compressive load and the lower nine panels are under tensile load. Buckling, strength, and ply contiguity constraint is applied to upper nine

panels only. No ply contiguity and buckling constraint is imposed on lower nine panels. At this stage no deflection constraint is imposed on the optimization problem. Next, we compare the stacking sequence continuity of the designs obtained by the proposed methodology (guide based GA) with that of Liu *et al.* [29] (two level design with continuity constraint). A parametric study is performed and a Pareto optimal curve is generated to investigate the effect of global deflection constraint on the total weight of the structure.

Table 2.1: Material properties.

Material properties	Values
Youngs modulus in direction 1, E_1	18.5×10^6 psi
Youngs modulus in direction 2, E_2	1.89×10^6 psi
Shear modulus, G_{12}	0.93×10^6 psi
Poisson's ratio, ν_{12}	0.3
Material density, ρ	0.057 lb/in^3
Ply thickness, t	0.005 in
Allowable strain in 1 direction	0.008
Allowable strain in 2 direction	0.029
Allowable shear strain	0.015

Table 2.2: GA parameters.

GA parameters	Values
Initial population	400
Maximum lenght of chromosome	150/50
Probability of crossover	1.0
Probability of mutation	0.5
Number of elites retained	1
Penalty for unbalanced laminate	2.7

Numerical results

In this section, we present the optimal designs obtained by guide based GA. An important aspect of current approach is local improvement. Since no new global finite element analyses are performed after locally removing or adding a ply, it is important to study the optimization history. A plot of objective function history for both outer and inner blending is shown in Fig. 2.7. The objective function history plot shows that the final result obtained has the minimum weight for the guide and no more local improvement is possible.

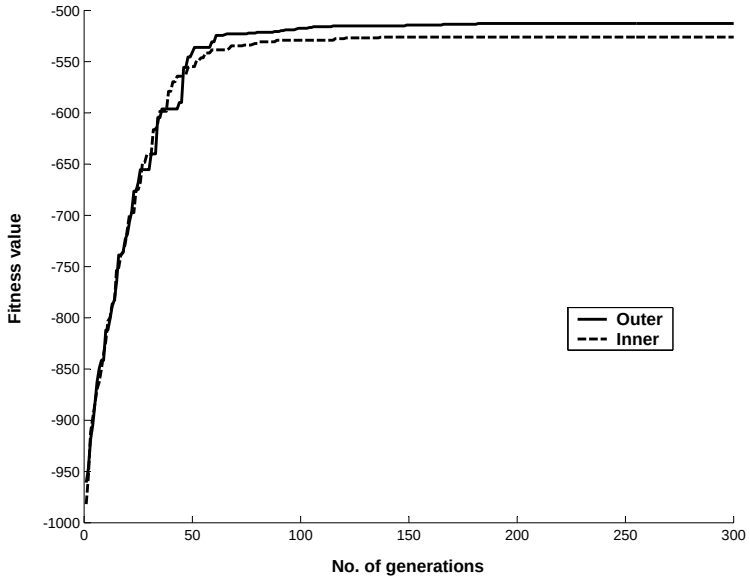

Figure 2.7: Objective function history.

In Table 2.3, the optimal design of all the 18 panels for outer blending is reported. The stacking sequence, constraint margin and the weight of the individual panels are tabulated. We refer the laminate stacking sequence of each panel to the panel thinner than itself. For example, the stacking sequence of panel no. 8 **P8**, refers to stacking sequence of panel no. 7 **P7** which is the immediate thinner panel in terms of thickness. So, **P8** contains **P7** and a few more additional plies. The laminate stacking sequence of the thinnest panel, which in this case is panel no. 7 which actually covers all the panels, is given in details at the bottom of the table and referred to as **P7** (Table 2.3). The above way of reporting the stacking sequence is followed throughout the report. The top skin panels being subjected to biaxial compressive load and shear load due to upward bending and twisting moment fails due to combined biaxial compressive and shear buckling. For that reason, the top skin panels contain all the three possible fiber orientation angles. For each panel, the total number of plies of different orientation angles is also reported. The constraint margins for top skin panels reported in Table 2.3 are that of active buckling constraint margin. Along the span of the wing, the thickness of the laminate increases from tip of the wing to the root of the wing due to bending effect. Along the chord of the wing, the thickness increases from panel 1 (or 4, or 7) to panel 3 (or 6, or 9) due to twisting effect. The bottom skin laminate is subjected to biaxial tensile and shear load due to upward bending and twisting moment with the predominant tensile force along the wing span direction. As explained before only strength constraint is imposed for the bottom skin panels and the constraint margin is reported in Table 2.3. For that reason, the bottom skin panels have only 0 degree plies. Along the span of the wing, the thickness drops considerably from the root of the wing

to the tip of the wing. Also there is gradual thickness variation along the chord of the wing because of differential tensile load induced due to twisting moment. The total weight of the upper nine panels is 445.73 *lbs* and the same for the bottom nine panels is 67.79 *lbs*. The total weight of the wing structure is 513.52 *lbs* and the maximum deflection is 6.03 in.

The results for inner blending are reported in Table 2.4. Most of the qualitative nature of the results for inner blending designs is similar to that of the outer blending designs. The thickness variation follows the same pattern. **P7** and **P3** are the thinnest and the thickest panel in the top skin laminate. Similar to the outer blending results, the top skin laminate is made up of all the three types of possible fiber orientations and the bottom skin laminate is made up of only 0 degree plies. The total weight of the nine top skin panels is 457.42 *lbs* and the total weight of the nine bottom skin panels is 68.57 *lbs*. The total weight of the structure is 525.99 *lbs* which is 2.4% more compared to the outer blending design. The weight increase is predominantly from the increase in weight of the top skin panels. The maximum deflection is 5.86 in.

Comparison between guide based GA and two level design with continuity constraints

A comparison of the results with those obtained by Liu *et al.* [29] follows. In their work, Liu *et al.* [29] defined two continuity measures - composition continuity and stacking sequence continuity. Composition continuity is defined as a measure of number of zero, forty-fives or ninety degree plies that are continuous between two adjacent laminates regardless of exact stacking sequence. Stacking sequence continuity is a measure of number of layers that are continuous between two adjacent laminates. The definition of continuous layer by Liu *et al.* [29] permits layer termination at any point along the thickness of the laminate unlike blending definition where continuous layers means perfect one to one matching from the outer surface (outer blending) or from the mid plane (inner blending). Though the blending definition used in the current work is different, for the purpose of comparison we compute the continuity measures suggested by Liu *et al.* [29] of our inner and outer blending designs. The composition and stacking sequence continuity of the guide based designs are reported in Table 2.5.

The lower bound on the total number of plies is achievable when no continuity constraints are imposed. The lower bound reported by Liu *et al.* [29, 74] is 1296. The corresponding stacking sequence continuity is 56.52 % and composition continuity is 77.79 %. In our formulation, the composition continuity merely suggests the average thickness variation in the wing and as such does not serve any purpose. On the other hand, the formulation by Liu *et al.* [29] uses composition continuity as a tool to improve the stacking sequence continuity. The best design reported by Liu has 1504 plies in total with a stacking sequence continuity of 72.11 % corresponding to a composition continuity of 90.89 %. Guide based GA achieved a stacking sequence continuity of 79.33 % for outer blending design and 80.19 % for inner

Table 2.3: Outer blending designs.

No.	Stacking sequence	No. of plies	Constraint margin	Weight(lbs)
	Top skin panels	0 ± 45 90		445.73
1	$[\mathbf{P9}\ 90\ 0\ 90\ 0\ 45\ 90\ 0_2\ -45\ 0]_s$	34 64 34	0.0068	51.43
2	$[\mathbf{P6}\ 0_3\ 90]_s$	54 64 44	0.0240	63.12
3	$[\mathbf{P2}\ 0\ 90\ 0_3\ 90\ 0_2\ \pm 45\ 90\ 0]_s$	68 68 50	0.0040	72.47
4	$[\mathbf{P8}\ 0_3\ 90\ 45\ 90\ -45]_s$	18 60 24	0.0450	39.74
5	$[\mathbf{P9}\ 90\ 0\ 90\ 0\ 45\ 90\ 0_2\ -45\ 0]_s$	34 64 34	0.0167	51.43
6	$[\mathbf{P1}\ 0\ 90\ 0_2\ 90\ 0_2\ 90\ 0_2\ 90]_s$	48 64 42	0.0330	60.00
7	$[\mathbf{P7}]_s$	08 52 16	0.0302	29.61
8	$[\mathbf{P7}\ 0\ 45\ 90_2\ 0\ -45]_s$	12 56 20	0.0234	34.29
9	$[\mathbf{P4}\ 0\ 90_2\ 0_2]_s$	24 60 28	0.0117	43.64
P7	$\pm 45_3\ 0\ \pm 45\ 45\ 0\ -45\ \pm 45_2$ $0\ 90\ 45\ 90\ -45\ 45\ 90\ -45$ $45\ 90_2\ -45\ \pm 45\ 0\ 45\ 90$ $-45\ 45\ 90\ -45\ 90$			
	Bottom skin panels			67.79
10	$[\mathbf{P13}\ 0_{10}]_s$	56 00 00	0.0141	21.82
11	$[\mathbf{P12}\ 0_3]_s$	24 00 00	0.0478	9.35
12	$[\mathbf{P15}\ 0_3]_s$	18 00 00	0.0512	7.01
13	$[\mathbf{P11}\ 0_6]_s$	36 00 00	0.0292	14.03
14	$[\mathbf{P16}\ 0]_s$	12 00 00	0.1006	4.67
15	$[\mathbf{P16}\ 0]_s$	12 00 00	0.1049	4.67
16	$[\mathbf{P17}\ 0_3]_s$	10 00 00	0.0518	3.90
17	$[\mathbf{P18}\ 0]_s$	04 00 00	0.1484	1.56
18	$[\mathbf{P18}]_s$	02 00 00	0.1759	0.78
P18	0			
	Total			513.52

Table 2.4: Inner blending designs.

No.	Stacking sequence	No. of plies	Constraint margin	Weight(lbs)
	Top skin panels	0 ± 45 90		457.42
1	$[(45\ 90\ -45)_2\ \pm 45\ 90\ \mathbf{P9}]_s$	52 52 30	0.0072	52.21
2	$[45\ 90\ -45\ 90\ \mathbf{P6}]_s$	62 64 38	0.0014	63.90
3	$[90\ \pm 45\ 0\ 45\ 90\ -45\ 0_3\ 90_3\mathbf{P2}]_s$	70 72 48	0.0065	74.03
4	$[\pm 45\ 45\ 0\ -45\ 0\ 90\ 0\ \mathbf{P8}]_s$	48 40 20	0.0244	42.08
5	$[(45\ 90\ -45)_2\ \pm 45\ 90\ \mathbf{P9}]_s$	52 52 30	0.0061	52.21
6	$[90\ \pm 45\ 0\ 45\ 0\ -45\ 0_3\ 90\ \mathbf{P5}]_s$	62 60 34	0.0095	60.78
7	$[\mathbf{P7}]_s$	40 24 16	0.0178	31.17
8	$[\pm 45\ 0\ \pm 45\ 90\ \mathbf{P7}]_s$	42 32 18	0.0400	35.84
9	$[90\ 0_2\ 90\ \mathbf{P4}]_s$	52 40 24	0.0293	45.20
P7	$\pm 45\ 0_3\ 90_2\ 0_2\ \pm 45\ 90\ 45$ $0_2\ 90\ -45\ 45\ 90\ 0\ -45\ 0$ $90\ 0_3\ 45\ 0_3\ 90\ 0_2$ $-45\ 45\ 0\ -45\ 0_2\ 90$			
	Bottom skin panels			67.79
10	$[0_{11}\ \mathbf{P13}]_s$	58 00 00	0.0242	22.60
11	$[0_4\ \mathbf{P15}]_s$	20 00 00	0.0276	7.79
12	$[0_4\ \mathbf{P15}]_s$	20 00 00	0.0480	7.79
13	$[0_8\ \mathbf{P12}]_s$	36 00 00	0.0392	14.03
14	$[0\ \mathbf{P16}]_s$	12 00 00	0.1385	4.67
15	$[0\ \mathbf{P16}]_s$	12 00 00	0.0819	4.67
16	$[0_3\ \mathbf{P18}]_s$	10 00 00	0.0687	3.90
17	$[\mathbf{P18}]_s$	04 00 00	0.2837	1.56
18	$[\mathbf{P18}]_s$	04 00 00	0.5528	1.56
P18	0_2			
	Total			525.99

blending design. The corresponding total numbers of plies are 1318 and 1350, respectively. Compared to the lower bound design obtained by Liu *et al.* [29], there is approximately 30 % increase in stacking sequence continuity whereas the penalty on total number of plies is 1.7 % for outer and 4.2 % for inner blending design. Also compared to the best design obtained by Liu *et al.* [29], outer and inner blending design obtained by guide based GA has 8 % higher stacking sequence continuity with much lesser number of plies. The best design reported by Liu *et al.* [29] has 11.4 % more plies compared to the inner blending design and 14.1 % more plies compared to outer blending design, respectively.

It is important to note that according to the definition by Liu *et al.* [29], any stacking sequence continuity less than 100 % is due to either stacking sequence mismatch or thickness variation or both between two adjacent panels. But in guide based GA, the stacking sequence continuity calculated as per definition by Liu *et al.* [29] is less than 100 % only because of thickness variation and not due to any stacking sequence mismatch. We observed that the results reported by Liu *et al.* [29] have stacking sequence mismatch between the adjacent panels.

Table 2.5: Comparison of total weight and laminate lay-up continuity.

Methodology		Composition continuity (Averaged over all the panels)	Stacking sequence continuity (Upper 9 panels	Total number of plies
Liu *et al.* [29] Two level design		77.79 %	56.52 %	1296
Guide based GA	Outer blending	82.33 %	79.33 % (100 %)	1318
	Inner blending	84.30 %	80.19 % (100 %)	1350

Weight-maximum deflection tradeoff

The optimal design reported for outer blending has a maximum global displacement of 6.03 at the wing tip. We next study the sensitivity of the design to the maximum deflection constraint limit. By varying the deflection constraint limit, a series of design runs are performed and the final weights of the wing structure are determined. The results are presented in Fig. 2.8 in the form of a Pareto tradeoff curve between the wing weight and maximum deflection. The designs are also reported in Table 2.6, Table 2.7, and Table 2.8, for maximum delfection constraint of 5.25 in., 5.50in., and 5.75 in., respectively. Clearly, the requirement of a small wing tip deflection imposes a very substantial penalty on the weight of the wing. On the other hand, if the deflection constraint is larger than a specific value (in

this case it appears to be above 6.03) the panel buckling constraints completely dominate the design and the deflection constraint becomes inactive, Fig. 2.9.

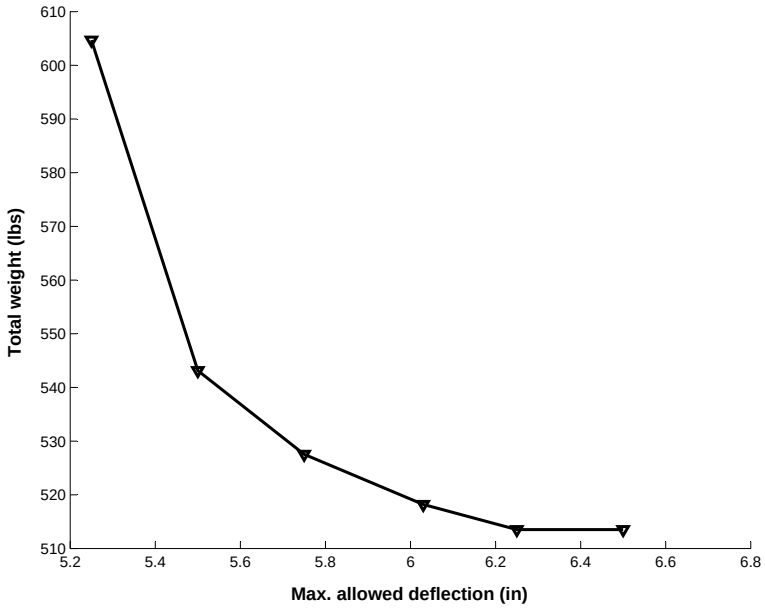

Figure 2.8: Pareto optimal curve.

2.4 Summary

A guide based genetic algorithm approach has been successfully implemented for blended composite wing box structure design. The optimal design obtained is completely blended and balanced. Both the inner and outer blending results are reported and seem to be in good agreement with each other. The design obtained by the present methodology shows considerable improvement compared to earlier published results. The stacking sequence continuity achieved by guide based GA is much higher and also the total weight of the structure is on the lower side. Two different blending schemes are presented. The different stacking sequence for inner and outer blending though of the same weight suggests the presence of multiple optima. This also indicates that feasibility/superiority of the current approach owes much to the presence of several feasible solutions. The result shows that the top skin laminates are thicker compared to the bottom skin laminates. Hence, the use of two different guides for top and bottom skin laminates proved to be advantageous and greatly reduced the computation effort. The current methodology uses only one global finite element analysis for each individual in the population. This reduced the computational effort to a

Table 2.6: Outer blending designs for maximum deflection 5.25 in.

No.	Stacking sequence	No. of plies	Constraint margin	Weight(lbs)
	Top skin panels	0 ± 45 90		445.73
1	$[\mathbf{P5}\ 0\ 90\ 90\ 0\ 0]_s$	78 36 36	0.0823	58.44
2	$[\mathbf{P6}\ 0_2\ \pm 45\ 0\ 45\ 0\ -45\ 90]_s$	88 44 40	0.0248	67.01
3	$[\mathbf{P2}\ 0_2\ 90_2\ \pm 45_2\ 0\ 90]_s$	94 52 46	0.0070	74.81
4	$[\mathbf{P7}]_s$	68 36 30	0.4479	52.21
5	$[\mathbf{P4}\ 0\ 0\ 90]_s$	72 36 32	0.0475	54.55
6	$[\mathbf{P1}\ 90\ 0]_s$	80 36 38	0.0200	60.00
7	$[\mathbf{P7}]_s$	68 36 30	3.2917	52.21
8	$[\mathbf{P7}]_s$	68 36 30	1.8312	52.21
9	$[\mathbf{P7}]_s$	68 36 30	0.6688	52.21
P7	$0\ 45\ 0\ -45\ 90\ 0_2\ 45$ $0\ 90_2\ -45\ \pm 45\ 0_2\ 45\ 90$ $-45\ 90\ 0_4\ 90_2\ 0_2\ 90\ 0_2$ $90\ 45\ 0_3\ -45\ 45\ 0\ -45$ $0_3\ 90_2\ 0\ 90\ 0_2\ 45\ 0$ $-45\ 0_2\ \pm 45\ 0_3\ 90_2\ 0$ $90\ 0\ 45\ 0\ -45$			
	Bottom skin panels			67.79
10	$[\mathbf{P13}\ 0_3\ 45\ 0_2\ -45\ 0_2\ 90\ 0_2]_s$	00 00 00	0.0413	22.60
11	$[\mathbf{P12}\ 0_3]_s$	26 04 00	0.0461	11.69
12	$[\mathbf{P14}\ 0_3]_s$	20 04 00	0.0667	9.35
13	$[\mathbf{P11}\ 0_2]_s$	30 04 00	0.0386	13.25
14	$[\mathbf{P15}\ 0]_s$	14 04 00	0.1008	7.01
15	$[\mathbf{P16}\ 0_2]_s$	12 04 00	0.0862	6.23
16	$[\mathbf{P17}\ \pm 45]_s$	08 04 00	0.0003	4.67
17	$[\mathbf{P18}]_s$	08 00 00	0.6095	3.12
18	$[\mathbf{P18}]_s$	08 00 00	1.3835	3.12
P18	0_4			
	Total			604.69

Table 2.7: Outer blending designs for maximum deflection 5.50 in.

No.	Stacking sequence	No. of plies	Constraint margin	Weight(lbs)
	Top skin panels	0 ± 45 90		445.73
1	$[\mathbf{P5}\ 0_2\ \pm 45]_s$	60 48 36	0.0122	56.10
2	$[\mathbf{P6}\ 90\ 0_3\ 90\ 0_2]_s$	76 48 42	0.0060	64.68
3	$[\mathbf{P2}\ 90\ 0_4\ \pm 45\ 90\ 0_2]_s$	88 52 46	0.0114	72.47
4	$[\mathbf{P9}\ 90\ 45\ 0\ -45]_s$	44 40 34	0.0258	45.97
5	$[\mathbf{P4}\ 0_4\ \pm 45\ 0\ 90\ 0]_s$	56 44 36	0.0180	52.99
6	$[\mathbf{P1}\ 0\ 90\ 0_2]_s$	66 48 38	0.0235	59.22
7	$[\mathbf{P7}]_s$	30 36 20	0.0197	33.51
8	$[\mathbf{P7}\ 90_2\ 0_2]_s$	34 36 24	0.0272	36.62
9	$[\mathbf{P8}\ 90\ 0\ 90\ 0\ 90_2 0_2]_s$	42 36 32	0.0047	42.86
P7	$90\ 0_2\ \pm 45\ 0\ 90\ 0\ 90$ $\pm 45\ 0\ 45\ 90\ 0\ -45\ \pm 45_2$ $45\ 0\ -45\ 45\ 90\ 0_2\ -45$ $45\ 0\ -45\ 90_2\ 0\ 45\ 0$ $90\ 0_2\ 90\ -45\ 90\ 0$			
	Bottom skin panels			67.79
10	$[\mathbf{P13}\ 0_{10}]_s$	50 04 00	0.0139	21.04
11	$[\mathbf{P12}]_s$	22 04 00	0.0354	10.13
12	$[\mathbf{P15}\ 0_4]_s$	22 04 00	0.0625	10.13
13	$[\mathbf{P11}\ 0_4]_s$	30 04 00	0.0256	13.25
14	$[\mathbf{P16}\ 0_2]_s$	12 04 00	0.1084	6.23
15	$[\mathbf{P14}\ 0]_s$	14 04 00	0.0862	7.01
16	$[\mathbf{P17}\ 0_2]_s$	08 04 00	0.0892	4.67
17	$[\mathbf{P18}]_s$	04 04 00	0.3505	3.12
18	$[\mathbf{P18}]_s$	04 04 00	0.5143	3.12
P18	$45\ 0\ -45\ 0$			
	Total			543.13

Table 2.8: Outer blending designs for maximum deflection 5.75 in.

No.	Stacking sequence	No. of plies	Constraint margin	Weight(lbs)
	Top skin panels	0 ± 45 90		445.73
1	$[\mathbf{P5}\ 0_2\ \pm 45]_s$	48 52 22	0.0204	54.55
2	$[\mathbf{P6}\ 0_4\ \pm 45\ 0_2\ 90]_s$	60 56 28	0.0038	63.12
3	$[\mathbf{P2}\ 0_4\ 45\ 0_4\ -45]_s$	76 60 28	0.0085	70.91
4	$[\mathbf{P9}\ 0\ 90_2]_s$	26 48 18	0.0480	43.64
5	$[\mathbf{P4}\ 0_4\ 90\ 0_3\ 90\ 0_2]_s$	44 48 22	0.0101	52.21
6	$[\mathbf{P1}\ 90\ 0\ 90]_s$	50 52 26	0.0012	56.10
7	$[\mathbf{P7}]_s$	10 36 14	0.0048	31.17
8	$[\mathbf{P7}\ 45\ 0_2\ -45\ 0]_s$	16 40 14	0.0017	35.07
9	$[\mathbf{P8}\ 45\ 0_2\ -45\ 45\ 0_2\ -45]_s$	24 48 14	0.0037	41.30
P7	$\pm 45\ 45\ 90\ -45\ \pm 45_4\ 0$ $\pm 45_4\ 0\ 45\ 90\ -45\ 90_2\ \pm 45$ $45\ 90\ -45\ 45\ 0_2\ 90\ -45$ $90\ 0$			
	Bottom skin panels			67.79
10	$[\mathbf{P13}\ 0_{10}]_s$	50 04 00	0.0280	21.04
11	$[\mathbf{P12}]_s$	22 04 00	0.0561	10.13
12	$[\mathbf{P15}\ 0_4]_s$	22 04 00	0.0846	10.13
13	$[\mathbf{P11}\ 0_4]_s$	30 04 00	0.0237	13.25
14	$[\mathbf{P16}\ 0_2]_s$	12 04 00	0.0985	6.23
15	$[\mathbf{P14}\ 0]_s$	14 04 00	0.0789	7.01
16	$[\mathbf{P17}\ 0_2]_s$	08 04 00	0.1015	4.67
17	$[\mathbf{P18}]_s$	04 04 00	0.3289	3.12
18	$[\mathbf{P18}]_s$	04 04 00	0.4699	3.12
P18	$0\ 45\ 0\ -45$			
	Total			527.55

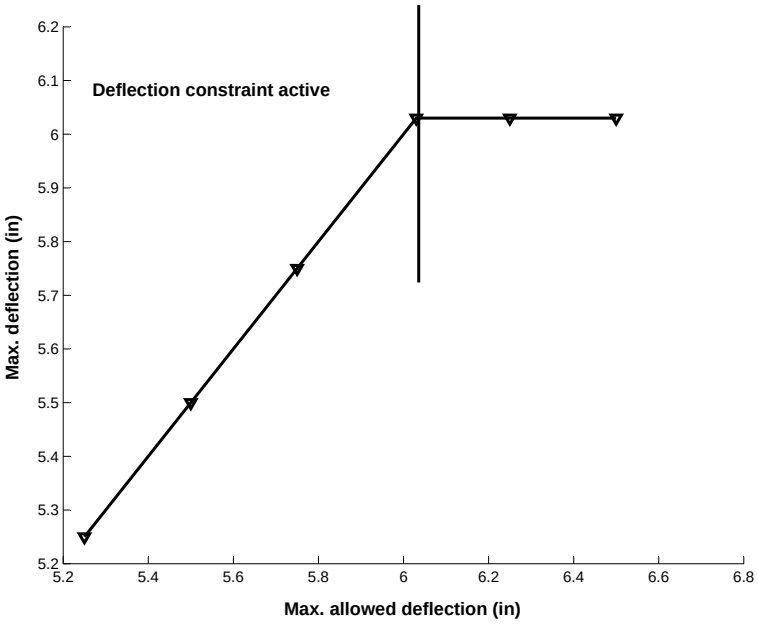

Figure 2.9: Effect of global deflection constraint.

great extent. This is only possible because the number of plies added or deleted at the local level is restricted to one.

Chapter 3

Design for Postbuckling Performance

In this chapter, we formulate the discrete stacking sequence design of simply supported symmetric and balanced flat composite laminates for postbuckling performance. Although the finite element method is a powerful tool for structural analysis, the nonlinear nature of postbuckling response and optimization study which requires repetitive evaluation of the objective function and constraints makes the use of finite element code undesirable due to excessive computational time required. In this work, a Rayleigh-Ritz method in conjunction with normal flow algorithm [75] is used to trace the postbuckling response. In their work, Shin *et al.* [76, 33] found that mode jumping prior to failure in postbuckled plate is important only for lightly loaded very thin plates. Hence, we did not considered mode jumping in the current study. Also it should be noted that the present optimization procedure do not include any randomness in material properties or applied loadings.

3.1 Analysis formulation

3.1.1 Modeling

In this section, we develop the model for relatively large deformation used in local strength evaluation of the panels. Assuming that the plate is thin, such that the Kirchhoff hypothesis is valid, the strain in terms of midplane strain (superscript 0) are given as [77, 78],

$$\epsilon_x = \epsilon_x^0 + z\kappa_x,\ \epsilon_y = \epsilon_y^0 + z\kappa_y,\ \text{and}\ \gamma_{xy} = \gamma_{xy}^0 + z\kappa_{xy}. \tag{3.1}$$

In the moderately large rotation case, according to the von Kármán model, the mid plane strains and the curvature terms are given in terms of mid plane displacements u, v, and, w

along x, y, and, z axes respectively as [77, 78],

$$\begin{aligned}\epsilon_x^0 &= u_{,x} + \frac{1}{2}w_{,x}^2;\ \epsilon_y^0 = v_{,y} + \frac{1}{2}w_{,y}^2;\ \gamma_{xy}^0 = u_{,y} + v_{,x} + w_{,x}w_{,y},\ \text{and} \\ \kappa_x &= -w_{,xx};\ \kappa_y = -w_{,yy};\ \kappa_{xy} = -2w_{,xy}, \end{aligned} \tag{3.2}$$

where a comma with a variable following it in the subscript indicates space derivative with respect to the variable following.

The total potential, using the above expression for strain in Eq. (3.2), of a $\underline{a}\times\underline{b}$ symmetric and a balanced laminate is given by [77, 78]

$$\begin{aligned}\Pi(u,v,w) &= \frac{1}{2}\int_0^{\underline{a}}\int_0^{\underline{b}} [A_{11}\left(\epsilon_x^0\right)^2 + 2A_{12}\epsilon_x^0\epsilon_y^0 + A_{22}\left(\epsilon_y^0\right)^2 + A_{66}\left(\gamma_{xy}^0\right)^2 + \\ &\quad D_{11}\kappa_x^2 + 2D_{12}\kappa_x\kappa_y + D_{22}\kappa_y^2 + D_{66}\kappa_{xy}^2]dxdy, \end{aligned} \tag{3.3}$$

where the inplane stiffness coefficients - A_{11}, A_{12}, A_{22}, and A_{66}, and the flexural stiffness coefficients - D_{11}, D_{12}, D_{22}, and D_{66} are given in terms of engineering constants of the materials,and the laminate stacking sequence [77]. Following the Rayleigh-Ritz procedure, the following displacement functions are assumed,

$$\begin{aligned} w(x,y) &= \sum_{i=1}^{N} a_i\phi_i^w, \\ u(x,y) &= -\frac{\lambda u_0 x}{\underline{a}} + \sum_{i=1}^{2N} b_i\phi_i^u,\ \text{and} \\ v(x,y) &= -\frac{\lambda v_0 y}{\underline{b}} + \sum_{i=1}^{2N} c_i\phi_i^v. \end{aligned} \tag{3.4}$$

λ is the load displacement scaling factor and depending on the choice of $\phi_i^u, \phi i^v,$ and ϕ_i^w various boundary conditions are satisfied. In the above formulation, we assume a edge displacement loaded panels because of its simplicity in implementation and more accurate representation of boundary conditions discussed next. Moreover, any local loads can be converted into equivalent edge displacement loading using material constitutive law. In a global/local decomposition of a composite wing structure it is assumed that the local panels are simply supported and the effects of the surrounding is usually neglected. However these panels are not alone and exists as a structural unit. Along the edges, each individual panel is bonded with spars, ribs and other adjacent panel. This represents a very complex boundary condition. In the current work, we assume a linearly varying deformable straight edges simply supported boundary condition. This is justified in the sense that the spars, ribs, and adjacent panels will give resistance to the straight edges from deforming too much. The

boundary condition can be summed up as,

$$\begin{aligned}
\text{At } x &= 0, u(0,y) = 0, v(0,y) = -\frac{\lambda v_0 y}{\underline{b}}, \text{ and } w(0,y) = 0 \\
\text{At } x &= \underline{a}, u(\underline{a},y) = -u_0, v(\underline{a},y) = -\frac{\lambda v_0 y}{\underline{b}}, \text{ and } w(\underline{a},y) = 0 \\
\text{At } y &= 0, v(x,0) = 0, u(x,0) = -\frac{\lambda u_0 x}{\underline{a}}, \text{ and } w(x,0) = 0 \\
\text{At } y &= \underline{b}, v(x,\underline{b}) = -v_0, u(x,\underline{b}) = -\frac{\lambda u_0 x}{\underline{a}}, \text{ and } w(x,\underline{b}) = 0.
\end{aligned} \tag{3.5}$$

We assumed a double sine series for $\phi_i^u, \phi i^v,$ and ϕ_i^w as

$$\phi_i^{u/v/w} = \text{Sin}\frac{m\pi x}{\underline{a}}\text{Sin}\frac{n\pi y}{\underline{b}}, \tag{3.6}$$

where m, and n are integer (m and n is the number of half sine waves in x and y direction respectively). We further assume that the maximum value taken by m and n is equal and all the possible combinations are included. Therefore, $m = 1, 2, \ldots, \sqrt{N}$ and $n = 1, 2, \ldots, \sqrt{N}$.

By using the stationarity priciple conditions of total potential and minimizing with respect to the ritz coefficients $a_i, b_i,$ andc_i, we obtain the general equilibrium equation for a symmetric and balanced laminate (see Appendix C for further details) as

$$\begin{aligned}
-g_l^u + K_{il}^{ub} b_i + K_{il}^{uc} c_i + K_{ijl}^{uaa} a_i a_j = 0, \\
-g_l^v + K_{il}^{vb} b_i + K_{il}^{vc} c_i + K_{ijl}^{vaa} a_i a_j = 0, \\
K_{il} a_i - \lambda \bar{K}_{il}^g a_i + K_{ikl}^{wba} b_i a_k + K_{ikl}^{wca} c_i a_k + K_{ijkl}^{waaa} a_i a_j a_k = 0.
\end{aligned} \tag{3.7}$$

The first two equations are linear in ritz coeffcients corresponding to inplane displacement. Thus, the above three can be reduced to a single nonlinear equation, by eliminating the b_i, and c_i coefficients from the last equations. For the details of this condensation procedure, the reader is referred to Appendix C. The final nonlinear equation obtained after condensation is

$$\left[K_{il} - \lambda K_{il}^g\right] a_i + K_{ijkl}^{NL} a_i a_j a_k = 0. \tag{3.8}$$

3.1.2 Postbuckling analysis

The postbuckling equilibrium path is traced using a normal flow algorithm [75]. Eq. (3.8) can be written as,

$$F_l(a_i, \lambda) = K_{il} a_i - \lambda K_{il}^g a_i + K_{ikjl}^{NL} a_i a_j a_k = 0, \text{ or } \boldsymbol{F}(\boldsymbol{a}, \lambda) = \boldsymbol{0}. \tag{3.9}$$

In the normal flow algorithm, successive Newton Raphson iterates converge to the equilibrium solution along a path which is normal (in an symptotic sense) to the so called Davidenko

flow. The Davidenko flow can be described by considering a small perturbation, δ, to the above nonlinear system of equations:

$$\boldsymbol{F}\left(\boldsymbol{a},\lambda\right)=\boldsymbol{\delta}. \tag{3.10}$$

As the parameter varies, small changes will occur in the solution curve of Eq. (3.10). The system of curves generated by varying $\boldsymbol{\delta}$ is referred to as Davidenko flow. The system of equations given by Eq. (3.10) is solved via a Newton Raphson method. The Newton Raphson iterate is given by expanding in Taylor series around the present equilibrium point and neglecting the higher order terms as,

$$D\boldsymbol{F}\boldsymbol{c}=-\boldsymbol{F}\left(\boldsymbol{a}_n,\lambda_n\right), \tag{3.11}$$

where $\boldsymbol{c}^{=}\left[\boldsymbol{\Delta a},\Delta\lambda\right]^T$; and $D\boldsymbol{F}=\left[\frac{\partial\boldsymbol{F}}{\partial\boldsymbol{a}}\frac{\partial\boldsymbol{F}}{\partial\lambda}\right]$. The next point in the equilibrium path is given as: $\boldsymbol{a}_{n+1}=\boldsymbol{a}_n+\boldsymbol{\Delta a}$, and $\lambda_{n+1}=\lambda_n+\Delta\lambda$. The system of equation given by Eq. (3.11) is $m\times(m+1)$ undetermined system. We augment the system by,

$$\boldsymbol{u}.\boldsymbol{c}=0, \tag{3.12}$$

where $\boldsymbol{u}$ is the kernel of $D\boldsymbol{F}$.

3.1.3 Failure analysis

The failure prediction in postbuckled regime is important in the view that the plate has a definite curvature and a detailed analysis is required. In the current work, because of its simplicity and relative success in predicting the failure loads of test panels by , we used a maximum strain criterion [34]. According to the maximum strain criterion, failure is assumed to occur when any of the strains referred to the material axes exceeds its allowable value. As such, failure is assumed to occur in i^{th} panel when,

$$\lambda_s^i=\frac{1}{f}\max\left(\frac{\epsilon_{1,all}}{\epsilon_{1,max}^i},\frac{\epsilon_{2,all}}{\epsilon_{2,max}^i},\frac{\gamma_{12,all}}{\gamma_{12,max}^i}\right)\geq 1.0, \tag{3.13}$$

where $\epsilon_{1,max}^i$, $\epsilon_{2,max}^2$, and $\gamma_{12,max}^i$ is the maximum strain along the material axes (referred as 1, and 2) in the i^{th} panel. The maximum strains in terms of ϵ_x^i, ϵ_y^i, and γ_{xy}^i, are given as

$$\begin{aligned}
\epsilon_{1,max}^i &= \max\left(\epsilon_{x,j}^i\mathrm{Cos}^2\theta_j+\epsilon_{y,j}^i\mathrm{Sin}^2\theta_j+2\gamma_{xy,j}^i\mathrm{Cos}\theta_j\mathrm{Sin}\theta_j\right)\forall j=1,n^i,\\
\epsilon_{2,max}^i &= \max\left(\epsilon_{x,j}^i\mathrm{Sin}^2\theta_j+\epsilon_{y,j}^i\mathrm{Cos}^2\theta_j-2\gamma_{xy,j}^i\mathrm{Cos}\theta_j\mathrm{Sin}\theta_j\right)\forall j=1,n^i,\text{ and}\\
\gamma_{12,max}^i &= \max\left(-\epsilon_{x,j}^i\mathrm{Cos}\theta_j\mathrm{Sin}\theta_j+\epsilon_{y,j}^i\mathrm{Cos}\theta_j\mathrm{Sin}\theta_j+\gamma_{xy,j}^i\left(\mathrm{Cos}^2\theta_j-\mathrm{Sin}^2\theta_j\right)\right)\forall j=1,n^i.
\end{aligned} \tag{3.14}$$

In the postbuckling regime, the plate has a finite curvature and strains are no longer constant over the panel. The strains $\epsilon_{x,j}^i$, $\epsilon_{y,j}^i$, and $\gamma_{xy,j}^i$ in the j^{th} layer of i^{th} panel is computed at

the top and bottom surfaces taking into account the bending curvature given in Eq. (3.1). To locate the maximum strain over the panel, a Simplex search method (an in-built fuction fminsearch available in MATLAB) is used. To avoid getting stuck at local minima, the search is repeated with different initial points. We used nine different initial points, one at the center, four corner nodes, and four mid points of the edges of the plates. The locations chosen are based on the previous experience while attemping to optimize a composite panel for maximum postbuckling strength [57].

The choice of step size used for tracing the nonlinear response is important. If we use too large a step size then it is difficult to compute the exact failure load since the strains calculated at the failure load may well exceed the allowable limit by considerable margin. On the other hand, if we use too small a step size then the analyses becomes computationally expensive. Instead we use a variable step size. We start with a large step size and the step size is decreased by a factor of two with successive iterations. However, to avoid the step size becoming too small, a lower limit on step size is specified.

3.2 Optimization formulation

In this work, for the purpose of comparison we consider two objectives - maximization of buckling parameter and maximization of failure parameter. A number of practical engineering constraints are imposed to obtain realistic designs. First, we restrict the lamination to symmetric balanced laminates. The symmetry condition of laminate is taken care of implicitly by using only half of the laminate stacking sequence as design variables. The balanced condition of the laminate is imposed explicitly by penalizing designs violating the constraint. The second practical condition is the ply contiguity constraint. When the numbers of contiguous plies of the same orientation are large, composite laminates are known to experience matrix cracking. Therefore, ply contiguity constraint [3] is imposed so that no more than a certain number of plies of same fiber orientation angles are allowed successively. In the current formulation, no more than four plies of 0 (n_{c0}) or 90 (n_{c90}) degree fiber orientation angles are allowed successively. For ± 45 degree plies, the ply contiguity constraint is satisfied automatically. The design variable is the stacking sequence of the laminate Θ.
Depending on the optimization objective, we have the following optimization problems,

3.2.1 Maximization of buckling parameter

The optimization problem is formulated as,
Maximize $\lambda_{cr}(\Theta)$
subject to:

1. $n_{c0} \leq 4$

2. $n_{c90} \leq 4$

3. Laminate is symmetric and balanced

3.2.2 Maximization of failure parameter

The laminate is loaded beyond the critical or first bifurcation point. The objective of the design optimization problem is to maximize the failure parameter.
Maximize $\lambda^F(\Theta)$
subject to:

1. $n_{c0} \leq 4$

2. $n_{c90} \leq 4$

3. Laminate is symmetric and balanced

Several different optimization algorithms can be applied to above formulations. Among them, integer programming and genetic algorithms have been widely applied to solve discrete design variable problem. Previous works by different authors indicated the suitability of genetic algorithm for stacking sequence design of composite laminate [3, 5, 6, 52, 8]. In this work, a standard genetic algorithm (without any modification as described in chapter 2) is used as an optimizer. The common features of a standard GA are population initialization, parent selection, crossover, mutation, and the selection of successive generations. Each element has many variations, modified to suit a particular problem. A Fortran 90 GA framework that was designed in an earlier research effort specifically for composite laminate design is used in the current work [52]. This framework consists of a GA module, encapsulating GA data structures, and a package of GA operators like crossover and mutation. The module along with the package of operators constitutes a standard GA. An integer alphabet is used to code ply genes (as described in chapter 2). The implementation details of the GA module and GA packages can be found in the paper by McMahon et al. [52] and also discussed briefly in chapter 2.

3.3 Results and discussions

Results are obtained for a square 10″×10″and a rectangular 20″×10″graphite-epoxy: T300/N5208 composite plate. The total thickness of the laminate is 0.08 in. Two different laminates are chosen, one has 16 plies in total with ply thickness 0.005 in and other has 32 plies in total with ply thickness 0.0025 in. The material properties and the GA parameters are given in Table 3.1 and 3.2 respectively. In an earlier study [33], it was found that the Rayleigh-Ritz

analysis gives excellent accuracy as compared to finite element analysis for number of terms $m/n = 6$ or $N = 36$, and adequate accuracy for $m/n = 2$ or $N = 4$. In this work, we chose to use $m/n = 2$ or $N = 4$ because of the use of GA as optimization platform to reduce the computational cost. The optimum designs obtained for different cases of applied edge displacement loading ratio are tabulated in Table 3.3, 3.4, 3.5, and 3.6. All the designs reported are obtained after 50 GA iterations. The normalized effective inplane stiffness E_x, and E_y [77] of the optimum designs are also reported. The N_x, and N_y values reported are the averaged values computed along the displaced edges. The superscript "B"refers to buckling and "F"refers to failure. In all the tables, the objective function is reported in bold. The tensile forces are shown negative.

In Table 3.3, the optimal designs of stacking sequence of a 16 ply square laminates are reported. Four different applied edge loading conditions are considered: $u_0/v_0 = 0.001/0$ (uniaxial), $u_0/v_0 = 0.001/0.001$ (loading ratio 1), $u_0/v_0 = 0.001/0.667 \times 10^{-3}$ (loading ratio 1.5), and $u_0/v_0 = 0.001/0.0005$ (loading ratio 2). For uniaxial loading case, the failure parameter and the buckling parameter of failure-optimized design is 1.3 and 0.44 times that of the buckling-optimized design, respectively. For loading ratio 1, the failure parameter and the buckling parameter of failure-optimized design is 1.43 and 0.61 times that of the buckling-optimized design, respectively. For loading ratio 1.5, the failure parameter and buckling parameter of the failure-optimized design is 1.42 and 0.6 times that of the buckling-optimized design, respectively. Similarly for loading ratio 2, the failure parameter and the buckling parameter of the failure-optimized design is 1.5 and 0.56 times that of the buckling-optimized design, respectively. We note that the failure-optimized goes deeper into postbuckling regime compared to buckling-optimized. On the other hand, the buckling performance of the failure-optimized design is poorer than buckling-optimized design.

As already discussed that the failure-optimized designs have higher failure parameter compared to buckling-optimized designs, it is important to study how it affects the average loads along the displaced edges at failure. It is seen that the loads at failure along the primary load-path direction i.e. x axis (or N_x) is much larger for failure-optimized designs compared to buckling optimized designs (see Table 3.3). For example, the average N_x value for loading ratio 1, 1.5, and 2, are 620.30 lb/in, 924.38 lb/in, and 1082.4 lb/in respectively. This is true for all the load cases considered. The value of N_x at failure increases as the loading ratio is increased and is maximum for the uniaxial loading case, which is 1378.7 lb/in. The N_x/N_y ratio of failure-optimized design for loading ratio 1, 1.5, and 2 is 1.0, 3.0, and 11.6, respectively. It is clear that the ratio is not constant and is strongly dependent unlike buckling-optimized design where the N_x/N_y ratio for loading ratio 1, 1.5, and 2 is 1.0, 1.05, and 1.33, respectively.

Next we study the optimum stacking sequence obtained for the 16 ply square laminate design. It is seen that the failure-optimized design converges to cross-ply laminate (see Table 3.3). This is true for all the load cases. Also, we observe that the effective inplane stiffness of the failure-optimized designs are equal which means the number of 0 and 90 degree plies are same. It is seen that the failure-optimized designs have higher inplane stiffness compared to

buckling-optimized designs for all the loading cases.

As discussed before that the optimum stacking sequence of the failure-optimized designs converges to cross-ply laminate and do not changes with loading ratio, we study the effect of increasing the number of layers and thus expanding the design space on the optimal designs. In this effort, we discretize the total thickness of the laminate into a 32 ply problem, thus keeping the basic optimization problem same. Only two loading cases with ratio 1 and 2 are examined (see Table 3.4). It is seen that both the failure-optimized and buckling-optimized design converge to more or less the same objective function value i.e., failure and buckling parameter value. This is true for both the loading cases. For example, the failure parameter of failure-optimized design for loading ratio 1 and 2 converged to 20.38 and 25.88, respectively. This is close to the value obtained in 16 ply problem i.e., 20.38 and 25.78, respectively. It is seen that the failure-optimum designs once again converges to cross-ply laminate like earlier but the number of 0 and 90 degree layers may or may not be equal depending on loading ratio. For example, the E_x/E_y ratio of failure-optimzed design for loading ratio 1 and 2 is 1.0 and 1.23, respectively unlike in the 16 ply problem where the ratio was 1.0 for both the loading cases. We note that the optimum stacking sequence is different from 16 ply problem because of ply contiguity constraint, though the ultimate failure performance is same.

The above discussions are related to a square laminate design. Next, we study the design of a rectangular plate with aspect ratio 2. The optimal designs for a 16 and 32 ply rectangular laminate problem are reported in Table 3.5 and 3.6, respectively. Two biaxial loading cases with ratio 1 and 2 are considered. It is seen that the failure-optimized designs consistently have better postbuckling performance than buckling-optimized designs and poorer buckling performance like in the square laminate design problem. For example, the failure parameter of failure-optimized design for loading ratio 1 is 26.16 as opposed to 15.88 of buckling-optimized design while the buckling parameter is 0.7 times that of the buckling-optimized design.

In square laminate design, it was observed that the failure-optimized designs had a primary load path direction along x axis and the buckling-optimized designs had average loads distributed evenly. On the contrary, in rectangular laminate design, it is seen that the above trend reverses. Now the buckling-optimized design has a primary load path along x axis and failure-optimized designs have evenly distributed loads in both direction. The N_x/N_y ratio of failure-optimzed design for loading ratio 1 and 2 is 0.8 and 1.03, respectively. On the otherhand, the same ratio of buckling-optimized design for loading ratio 1 and 2 is 3.33 and 4.76, respectively. It is seen that the failure load ratio do not depends on loading ratio as strongly as it was earlier.

Next, we study the optimum stacking sequences of failure-optimized designs of rectangular laminate. It is seen that the optimum stacking sequence of failure-optimized design is primarily consists of 0 and 90 degree plies. This is true also for square laminate designs as discussed earlier. From Table 3.5, it is clear that the inplane stiffness distribution of

Table 3.1: Material properties.

Material properties	Values
Youngs modulus in direction 1, E_1	18.5×10^6 psi
Youngs modulus in direction 2, E_2	1.6×10^6 psi
Shear modulus, G_{12}	0.832×10^6 psi
Poisson's ratio, ν_{12}	0.35
Ply thickness, t	0.005/0.0025 in
Allowable strain	0.004

buckling-optimized and failure-optimized design is opposite of each other. For example, the E_x/E_y ratio of failure optimized design for loading ratio 1 and 2 is 0.62 as opposed to 3.18 of buckling-optimized design and 0.36 as opposed to 1.61, respectively. It is observed that the ratio decreases with increase in loading ratio. On the contrary, in square laminate design the E_x/E_y ratio remained close to 1 with increasing loading ratio.

Finally, we discuss the effect of increasing the number of layers on the optimal designs of rectangular laminates. Like earlier, we discretize the total thickness into a 32 ply problem. It is seen that the optimum designs converge to the same failure parameter. The stacking sequence primarily consists of 0 and 90 degree plies as in the 16 ply problem. The stacking sequences are different because of ply contiguity constraint but the postbuckling and buckling performance are more or less same. The same observation was also found in 16 and 32 ply square laminate design problem.

3.4 Summary

In this chapter, we formulated the optimal design of edge displacement loaded composite laminated plates for postbuckling strength with discrete stacking sequence of the laminate as design variable. The results are compared with buckling optimized designs. The results show that considerable improvement in failure performance is achieved. The failure-optimized designs, unlike buckling-optimized designs, primarily consists of zero and ninety degree plies i.e. cross-ply laminate. The effect of loading ratio on the optimal design is significantly less for both square and rectangular plates. The effect of aspect ratio of the plate is considerable as compared to edge displacement loading ratio. A parametric study is done to recognize the influence of effective inplane stiffnesses on the failure optimized designs. The study shows that for symmetric problems i.e. square panel with symmetric biaxial loading failure optimized designs consistently have higher effective inplane stiffness. Hence, it is possible to design laminates with better postbuckling performance by including the effective inplane stiffness in the optimization formulation. This will ensue considerable time saving because it will not need any expensive postbuckling analysis. However, this simplified assumption is not found to be true for rectangular panel or non-symmetric loading.

Table 3.2: GA parameters.

GA parameters	Values
Initial population	20
Probability of crossover	1.0
Probability of mutation	0.5
Number of elites retained	1

Table 3.3: Optimal designs for 16 ply square laminate problem.

Obj.	v_0/u_0 $\times 10^{-3}$	λ_{cr}	N_x^B (lb/in)	N_y^B (lb/in)	λ^F	N_x^F (lb/in)	N_y^F (lb/in)	Optimum Designs	E_x	E_y
Buckling	0/1	**2.78**	87.13	56.84	19.75	449.05	−22.90	$[(45\ 90\ -45\ 90)_2]_s$	0.183	0.183
Failure	0/1	1.22	98.82	5.5	**25.41**	1378.7	−571.4	$[(0\ 90)_4]_s$	0.547	0.547
Buckling	0.5/1	**1.42**	77.21	92.84	17.16	430.13	322.55	$[\pm 45_3\ 90_2]_s$	0.200	0.370
Failure	0.5/1	0.80	67.72	36.61	**25.78**	1082.4	93.51	$[(0\ 90)_4]_s$	0.547	0.547
Buckling	0.67/1	**1.23**	73.41	96.63	17.08	430.80	409.65	$[\pm 45_s\ 90_2]_s$	0.200	0.370
Failure	0.67/1	0.73	61.50	42.83	**24.25**	924.38	303.86	$[(0\ 90)_4]_s$	0.547	0.547
Buckling	1/1	**1.0**	85.55	85.55	14.28	431.66	431.66	$[\pm 45_4]_s$	0.156	0.156
Failure	1/1	0.61	52.16	52.16	**20.38**	620.30	620.30	$[(0\ 90)_4]_s$	0.547	0.547

Table 3.4: Optimal designs for 32 ply square laminate problem.

Obj.	v_0/u_0 $\times 10^{-3}$	λ_{cr}	N_x^B (lb/in)	N_y^B (lb/in)	λ^F	N_x^F (lb/in)	N_y^F (lb/in)	Optimum Designs	E_x	E_y
Buckling	0/1	**3.1**	95.00	38.63	21.15	523.17	−130.69	$[45\ 90\ -45\ 45\ 90_4\ 0\ 90_2\ -45\ 90_4]_s$	0.198	0.750
Failure	0/1	1.52	97.45	6.87	**25.51**	1202.37	−537.92	$[90_2\ 0\ 90_2\ 0_3\ 90\ 0\ 90_2\ 0\ 90_3]_s$	0.432	0.662
Buckling	0.5/1	**1.44**	59.48	100.7	19.0	407.86	372.04	$[\pm 45_3\ 45\ 90_4\ -45\ 90_4]_s$	0.183	0.583
Failure	0.5/1	0.78	72.24	32.08	**25.88**	1158.92	58.08	$[90\ 0\ 90_3\ 0_2\ 90_2\ 0_3\ 90\ 0_3]_s$	0.605	0.490
Buckling	1/1	**1.0**	85.55	85.55	14.28	431.66	431.66	$[\pm 45_8]_s$	0.156	0.156
Failure	1/1	0.61	52.16	52.16	**20.38**	620.30	620.30	$[90\ 0\ 90_3\ 0_2\ 90\ 0_2\ 90_2\ 0_2\ 90\ 0]_s$	0.547	0.547
Buckling	2/1	**0.71**	97.13	68.68	9.04	342.62	424.50	$[\pm 45_4\ 45\ 0_4\ -45\ 0_2]_s$	0.476	0.196
Failure	2/1	0.43	46.63	57.70	**12.80**	185.80	910.06	$[0_3\ 90\ 0_3\ 90_2\ 0_4\ 90_3]_s$	0.662	0.432

Table 3.5: Optimal designs for 16 ply rectangular laminate problem.

Obj.	v_0/u_0 $\times 10^{-3}$	λ_{cr}	N_x^B (lb/in)	N_y^B (lb/in)	λ^F	N_x^F (lb/in)	N_y^F (lb/in)	Optimum Designs	E_x	E_y
Buckling	0.5/1	**1.42**	73.63	49.18	25.38	944.45	198.38	$[90_2 \ \pm 45 \ 0_4]_s$	0.592	0.368
Failure	0.5/1	1.18	30.29	70.38	**32.1**	622.20	605.82	$[90_4 \ 0 \ 45 \ 90 - 45]_s$	0.255	0.699
Buckling	1/1	**0.89**	62.24	36.77	15.88	584.51	175.45	$[\pm 45_2 \ 0_4]_s$	0.583	0.183
Failure	1/1	0.62	25.30	60.26	**26.16**	650.59	808.60	$[90_2 \ (0 \ 90)_2 \ \pm 45]_s$	0.368	0.592

Table 3.6: Optimal designs for 32 ply rectangular laminate problem.

Obj.	v_0/u_0 $\times 10^{-3}$	λ_{cr}	N_x^B (lb/in)	N_y^B (lb/in)	λ^F	N_x^F (lb/in)	N_y^F (lb/in)	Optimum Designs	E_x	E_y
Buckling	0/1	**7.07**	78.07	44.02	42.00	399.06	−24.55	$[90\ 45\ 90_3\ -45\ 90_4\ 45\ 90\ -45\ 90_3]_s$	0.141	0.794
Failure	0/1	4.84	93.36	10.96	**49.91**	818.03	−304.84	$[90\ 0\ 90_4\ 0\ 90_4\ 0\ 90_4]_s$	0.259	0.834
Buckling	0.5/1	**1.36**	69.65	46.52	23.64	879.43	185.28	$[45\ 90_4\ -45\ 45\ 0_4\ -45\ 0_4]_s$	0.592	0.368
Failure	0.5/1	1.06	27.44	63.77	**33.94**	673.21	634.19	$[90_3\ 0\ 90_2\ 0\ 90_4\ 45\ 0\ 90\ -45\ 90]_s$	0.287	0.742
Buckling	1/1	**0.85**	54.60	44.38	17.49	631.88	258.09	$[90_2\ \pm 45_2\ 0_2\ 45\ 0_4\ -45\ 0_2]_s$	0.600	0.276
Failure	1/1	0.44	18.78	39.47	**26.19**	690.93	738.2	$[0\ 90\ 0_2\ 90_2\ 0_3\ 90_3\ 45\ 90\ -45\ 90]_s$	0.459	0.573
Buckling	2/1	**0.50**	40.39	48.11	11.35	370.87	362.06	$[90_2\ \pm 45_2\ 0_2\ 45\ 0_3\ -45\ 0_3]_s$	0.600	0.276
Failure	2/1	0.36	26.36	32.82	**12.11**	326.72	373.35	$[90\ 0_3\ 45\ 90\ 0_4\ 90\ 0_2\ -45\ 0_2]_s$	0.742	0.287

Chapter 4

Design for Flutter

4.1 Problem formulation

A laminated plate of dimension $\underline{a} \times \underline{b}$ in supersonic flow U_∞ (along x axis only) is considered (Fig. 4.1). The plate is subjected to uniform temperature variation ΔT. Two modes of failure of the plate is considered, thermal buckling and supersonic flutter.

The linear flutter Mach number M_L is the value of the free stream M_∞ for which the equilibrium position of the laminate becomes unstable. To be more precise, at the critical Mach number a pair of eigenvalues of the system crosses the imaginary axis. In the mathematics literature, this phenomenon is referred to as Hopf bifurcation. The determination of the critical Mach number depends on the knowledge of the small deflection response of the structure and as such is governed by a linear system of equations. If the free stream Mach number M_∞ is increased beyond the critical value, due to the presence of structural nonlinearity stiffness equivalent to a hardening spring of the von Kármán plate model, the panel exhibits self sustained vibrations referred to as limit cycle oscillations or LCO. In the post-flutter regime, the amplitude of the limit cycle oscillation depends on how far the Mach number is increased beyond the critical value. This type of behavior characterizes stable flutter also known as supercritical Hopf bifurcation. When the flutter is not stable, also known as subcritical Hopf bifurcation, the post flutter response itself is unstable and the system response can be characterized through time simulations. The amplitude-Mach number relation is controlled by the structural and aerodynamic nonlinearities of the system. Librescu et al. [79] examined the implications of structural and aerodynamic nonlinearities on the determination of stable/unstable LCO and the character of flutter critical boundary. In their work, the behaviour in the vicinity of the flutter boundary has been characterized via a Lyapunov based approach. It was shown that at high flight mach numbers, cubic aerodynamic nonlinearities contribute invariably toward the catastrophic character of the flutter boundary (unstable LCO) whereas the quadratic aerodynamic and structural nonlinearities

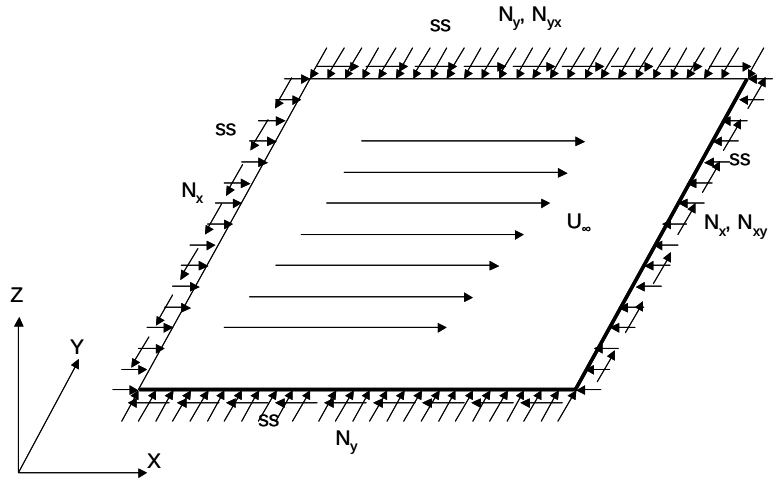

Figure 4.1: Plate with coordinate axes, inplane loads, and boundary conditions.

contributing to its benign nature (stable LCO). This implies that with the increase of the supersonic/hypersonic flight speed, the flutter boundary becomes catastrophic, irrespective of the presence of structural and quadratic aerodynamic nonlinearities.

It is, thus, desirable to design laminates with stable post-flutter response. It is also important that the post flutter response remains bounded to avoid excessive loading that might lead to failure. For this purpose a nonlinear flutter speed is usually defined as the Mach number at which the amplitude of the response reaches a predefined value,

$$M_{NL} = M_L + \delta M, \tag{4.1}$$

where δM is the contribution of structural and aerodynamic nonlinearities.

In the present work, the value of δM is calculated based on a perturbation method. Since, the perturbation method is valid only locally near the Hopf bifurcation, the value of the nonlinear flutter Mach number is only approximate. On the other hand, the use of a perturbation method is advantageous in the sense that a value for δM can be calculated even for unstable flutter. The laminate shows stable bifurcation if δM is positive while a negative value indicates unstable flutter.

For buckling analysis, the laminate is subjected to uniform temperature variation $\lambda^T \Delta T$. λ^T_{cr} is the buckling factor for which the laminate buckles. The linear (suffix L) or nonlinear (suffix NL) aerodynamic pressure parameter $\lambda_{L/NL}$ is defined as, $\lambda_{L/NL} = \frac{2q_\infty}{\sqrt{M^2_{L/NL}-1}}$, where q_∞ is the aerodynamic pressure. The laminate is optimized to maximize $\lambda_{L/NL}$ (linear or nonlinear aerodynamic pressure parameter), and λ^T_{cr} (thermal buckling factor). The laminate is made up of N plies with orientations restricted, for manufacturability, to 0, ± 45, and 90 degrees. Each ply has a constant thickness t and plies are made up of the same material. Thus the total thickness of the laminate is $h = Nt$. The laminate is assumed to be symmetric and

balanced. Hence, only the half-laminate stacking sequence need to be considered for the design. The vector of design variables (fiber orientations) is denoted as $\boldsymbol{\Theta}$. Next the analysis model is developed for moderately large deformation using von Kármán plate theory.

4.2 Analysis formulation

4.2.1 Modeling

In this subsection, we present a short description of the development of the equations of motion. The flow velocity direction is along x-direction as shown in Fig. 4.1. The plate is simply supported and subjected to uniform temperature variation ΔT. Since the laminate is assumed to be symmetric, no thermal moments generate. The equation of motions of the plate is given by Hamilton's principle as [80],

$$\int \delta \left(T - U + W \right) dt = 0, \tag{4.2}$$

where T, U, and W are the kinetic energy, internal strain energy, and work done by external load respectively. Using von Kármán plate theory for moderately large deformation of thin plates, the expressions for T and U can be derived in terms of mid plane displacements: $u(x, y, t)$, $v(x, y, t)$, and $w(x, y, t)$. The total external work done comprises of work done by aerodynamic load and work done by thermal load. The work done by the aerodynamic load is calculated using third order piston theory. For more details of calculation, the readers are referred to Appendix D.

Since it is difficult to find an analytical solution, and keeping in view that the primary focus of the work is on design optimization, we adopt a Rayleigh-Ritz method for the purpose of numerical solution. Following the Rayleigh-Ritz procedure, we assume the following displacement fields,

$$w(x,y,t) = \sum_{i=1}^{n} a_i(t)\phi_i^w(x,y),\ u(x,y,t) = \sum_{i=1}^{2n} b_i(t)\phi_i^u(x,y),\ \text{and } v(x,y,t) = \sum_{i=1}^{2n} c_i(t)\phi_i^v(x,y). \tag{4.3}$$

The functions ϕ_i^w, ϕ_i^u, and ϕ_i^w are chosen such that they satisfy all the specified boundary conditions. The following boundary conditions are assumed:

$$w/u/v(x,0,t) = w/u/v(x,\underline{b},t) = w/u/v(0,y,t) = w/u/v(\underline{a},y,t) = 0. \tag{4.4}$$

The number of assumed modes for u, and v is twice that of lateral displacement in w. This is done to ensure that the inplane equilibrium is adequately satisfied. Substituting the expression for assumed solutions in the expression of T, U, and W, we get simplified

expressions in terms of unknown ritz coefficients a_i, b_i, and c_i. Using Hamilton's principle and minimizing with respect to ritz coefficients, the system of equations reduce to the form

$$\begin{aligned} -g_l^u + K_{il}^{ub} b_i + K_{il}^{uc} c_i + K_{ijl}^{ua} a_i a_j &= 0 \quad \forall \delta b_l = 0 \; (4.5) \\ -g_l^b + K_{il}^{vb} b_i + K_{il}^{vc} c_i + K_{ijl}^{va} a_i a_j &= 0 \quad \forall \delta c_l = 0 \; (4.6) \\ M_{il}\ddot{a}_i + \bar{K}_{il}^{s} a_i - \bar{K}_{il}^{g} a_i + K_{ikl}^{wba} b_i a_k + K_{ikl}^{wca} c_i a_k + \bar{K}_{ijkl}^{waa} a_i a_j a_k + Q_l &= 0 \quad \forall \delta a_l = 0, (4.7) \end{aligned}$$

where Q_l (the aerodynamic contribution associated with third order piston theory) is given by

$$\begin{aligned} Q_l &= K_{il}^{(1)} a_i + K_{il}^{(2)} \dot{a}_i + K_{ijl}^{(3)} a_i a_j + K_{ijl}^{(4)} a_i \dot{a}_j + K_{ijl}^{(5)} \dot{a}_i \dot{a}_j + \\ & \quad K_{ijkl}^{(6)} a_i a_j a_k + K_{ijkl}^{(7)} a_i a_j \dot{a}_k + K_{ijkl}^{(8)} a_i \dot{a}_j \dot{a}_k + K_{ijkl}^{(9)} \dot{a}_i \dot{a}_j \dot{a}_k. \end{aligned} \tag{4.8}$$

The terms mentioned in above equations are given in Appendix D. The first two Eqs. (4.5), and (4.6) are linear in the Ritz's coefficient corresponding to inplane displacements u and v. Thus, the above three Eqs. (4.5), (4.6), and (4.7) can be reduced into a single equation by eliminating the b_i, and c_i coefficient from the Eq. (4.7) using Eqs. (4.5) and (4.6). For details of this condensation process the reader is referred to Appendix C. The final set of nonlinear panel motion equations governing the plate behavior is given by,

$$M_{il}\ddot{a}_i + K_{il} a_i + K_{ijkl} a_i a_j a_k + Q_l = 0. \tag{4.9}$$

In the current work, we assumed simply supported boundary conditions for the out of plane displacements and immovable boundary conditions for the inplane displacements. These boundary conditions are representative of panels in aerospace applications. The boundary conditions can be easily satisfied by assuming ϕ_i in Eq. (4.3) for all the displacement components as,

$$\phi_i = sin\frac{\underline{m}\pi x}{\underline{a}} sin\frac{\underline{n}\pi y}{\underline{b}}, \tag{4.10}$$

where $\underline{m}$ and $\underline{n}$ are integers, $i = \sqrt{n}(\underline{m} - 1) + \underline{n}$, and n is number of terms in the assumed functions. Thus, $\underline{m}$ and $\underline{n}$ varies from 1, 2, ..., $\sqrt{n}$.

4.2.2 Flutter analysis

The linear panel flutter analysis requires only the linear terms in Eq. (4.9). Neglecting the higher order terms, Q_l consists of two parts- aerodynamic stiffness $K^{(1)}$ and aerodynamic damping $K^{(2)}$. Similarly by neglecting structural nonlinearities, the resultant system of equations reduce to the form

$$[\boldsymbol{M}]\{\ddot{\boldsymbol{a}}\} + \left[\boldsymbol{K}^{(2)}\right]\{\dot{\boldsymbol{a}}\} + \left[\boldsymbol{K} + \boldsymbol{K}^{(1)}\right]\{\boldsymbol{a}\} = 0. \tag{4.11}$$

The state space equation is given by

$$\left\{ \begin{array}{c} \dot{\boldsymbol{a}} \\ \ddot{\boldsymbol{a}} \end{array} \right\} = \left[\begin{array}{cc} [\boldsymbol{0}] & [\boldsymbol{I}] \\ -[\boldsymbol{M}]^{-1}\left[\boldsymbol{K}+\boldsymbol{K}^{(1)}\right] & -[\boldsymbol{M}]^{-1}\left[\boldsymbol{K}^{(2)}\right] \end{array} \right] \left\{ \begin{array}{c} \boldsymbol{a} \\ \dot{\boldsymbol{a}} \end{array} \right\}. \tag{4.12}$$

By varying the flow speed, eigenvalue analysis of the state space equation is performed. The flow speed for which the damping ratio becomes zero is the linear flutter speed.

In aeroelastic problems, unlike structural geometric nonlinearities which are usually stabilizing in nature, the aerodynamic nonlinearities can be destabilizing. Although structural damping can be added, the behaviour of the system will not change. In order to investigate the stability of the post flutter response, and also to approximate the nonlinear flutter speed, we reduce the equations of motion (Eq. (4.9)) to the normal form of the Hopf bifurcation [81] in the vicinity of the flutter point. The reduction process can be carried out using either center manifold reduction [81], or more conveniently using the method of multiple scales [82]. Following the method of multiple scales [82](with scales $T_0, T_1, T_2, ...$), and using complex variable notation, the state space equation at the flutter point can be written as,

$$\left(\omega^2\left[\boldsymbol{M}\right] - i\omega\left[\boldsymbol{K}^{(2)}\right] - \left[\boldsymbol{K}+\boldsymbol{K}^{(1)}\right]\right)\{\boldsymbol{r}\} = 0. \tag{4.13}$$

At flutter i.e., $\omega = \omega_f$, the corresponding left and right eigenvectors are given by $\{\boldsymbol{l}\}$ and $\{\boldsymbol{r}\}$, respectively. The eigenvectors are normalized such that

$$\{l\}^T\left[2i\omega_f\left[\boldsymbol{M}\right] + \left[\boldsymbol{K}^{(2)}\right]\right]\{\boldsymbol{r}\} = 1. \tag{4.14}$$

Hence, the complete flutter mode (upto second order terms) is given by

$$w = \sum_{j=1}^{n}\left(qr_j\phi_j^w e^{i\omega_f T_0} + \bar{q}\bar{r}_j\phi_j^w e^{-i\omega_f T_0}\right), \tag{4.15}$$

where $\bar{r}$ is complex conjugate of right eigen vector r. The eigenvectors are further normalized such that the maximum deflection is equal to the total laminate thickness. The normal form of the Hopf bifurcation is given as,

$$\dot{q} = A_f q\delta U_\infty + B_f q(q\bar{q}). \tag{4.16}$$

For a maximum amplitude of unity, which means $w_{max}/h = 1$, the nonlinear contribution to the flutter speed δU_∞ is computed as

$$Re\left(A_f\right)\delta U_\infty + Re\left(B_f\right) = 0, \tag{4.17}$$

where

$$A_f = -\{l\}^T\left[\frac{\partial K^{(1)}}{\partial U_\infty}\right]\{r\}, \tag{4.18}$$

and

$$\begin{aligned} B_f &= -K^{NL}_{ijkl}\left(r_i\bar{r}_j r_k + \bar{r}_i r_j r_k + r_i r_j \bar{r}_k\right) l_l - K^{(4)}_{ijkl}\left(r_i\bar{r}_j r_k + \bar{r}_i r_j r_k + r_i r_j \bar{r}_k\right) l_l - \\ & j\omega_f K^{(5)}_{ijkl}\left(r_i\bar{r}_j r_k + \bar{r}_i r_j r_k - r_i r_j \bar{r}_k\right) l_l + \omega_f^2 K^{(6)}_{ijkl}\left(-r_i\bar{r}_j r_k + \bar{r}_i r_j r_k - r_i r_j \bar{r}_k\right) l_l + \\ & j\omega_f^3 K^{(7)}_{ijkl}\left(-r_i\bar{r}_j r_k - \bar{r}_i r_j r_k - r_i r_j \bar{r}_k\right) l_l. \end{aligned} \tag{4.19}$$

The nonlinear contribution to mach no at flutter speed, δM is given as $\frac{\delta U_\infty}{a_\infty}$. The aerodynamic pressure parameter is given as

$$\lambda_{L/NL} = \frac{2q_\infty}{\sqrt{M^2_{L/NL} - 1}} \tag{4.20}$$

4.2.3 Thermal buckling analysis

The standard buckling equation is obtained by neglecting the nonlinear terms, aerodynamic stifness and time dependent terms in Eq. (4.7) as follows

$$\left(\bar{K}^s_{il} - \lambda^T \bar{K}^g_{il}\right) a_i = 0. \tag{4.21}$$

The nontrivial solution of Eq. (4.21) gives the buckling factor λ^T_{cr} computed as the lowest eigen value of the above system of equation. The corresponding eigen vector gives the buckling mode of the laminated plate.

4.3 Optimization formulation

The multi-objective design optimization problem is usually formulated in two ways. One is weighted sum of the two or more objectives [83]. Another approach is to add the second objective as the constraint and change the constraint margin to generate a pareto front [83]. In this work, we followed the second approach. The objective is to maximize the aerodynamic parameter (linear and nonlinear). The second objective i.e. thermal buckling factor is added as a constraint. Other constraints are ply contiguity constraint, symmetricity, and balanced condition of the laminate. The design variables are the fiber orientation angles of the layers chosen from a discrete set of 0, ±45, and 90 degrees. The optimization problem is stated as

$$\text{Maximize } \lambda_{L/NL}(\boldsymbol{\Theta})$$

subject to :

$$\delta M \geq 0$$

$$\lambda_{cr}^{T}(\mathbf{\Theta}) \geq \lambda_{all}^{T}$$
$$n_{c0} \leq 4$$
$$n_{c90} \leq 4$$
laminate is symmetric and balanced,

where $\lambda_{L/NL}$ is the aerodynamic pressure parameter, δM is the contribution due to strcutural and aerodynamic nonlinearities, $\mathbf{\Theta}$ is the stacking sequence of the laminate, λ_{cr}^{T} is the thermal buckling factor, and λ_{all}^{T} is the allowable thermal buckling factor. By varying the value of λ_{all}^{T}, a Pareto tradeoff curve is to be generated.

The symmetric condition of the laminate is taken care of implicitly because only half laminate stacking sequence is used as design variables. The balanced condition of the laminate is taken care of by imposing a penalty on designs violating the constraint. The ply contiguity constraint [3] is imposed so that no more than a certain number of plies of same fiber orientation angles are allowed successively. In the current formulation, designs with more than four successive 0 (n_{c0}) or 90 (n_{c90}) degree plies are penalized. For ± 45 degree plies, the ply contiguity constraint is satisfied automatically.

The standard genetic algorithm (GA) discussed earlier in chapter 2 and 3 is employed as an optimizer because of the presence of discrete design variables [3, 5, 6, 7, 52, 53].

4.4 Results

To evaluate the validity of the solution procedure, a series of linear, and nonlinear flutter analyses are performed and compared. In all examples, the number of terms in the assumed displacement is $\underline{m} = \underline{n} = 4$. For these values the error in the analysis was found to be of acceptable accuracy for preliminary design purposes. To verify the analysis, some of the cases analyzed in Liaw [1] are reproduced.

The example rectangular plate studied is assumed as simply supported with length $\underline{a} = 100$ in, and width $\underline{b} = 50$ in. The laminate configuration is $[\theta/-\theta/-\theta/\theta]$ with thickness of each lamina equal to 0.25 in. The material is boron/epoxy with the following properties: $E_1 = 10.0$ mpsi, $E_2 = 1.0$ mpsi, $G_{12} = 0.33$ mpsi, $\nu_{12} = 0.3$, $\rho = 0.145 \times 10^{-3}$ lb $-$ sec^{2}in^{-4}, $\alpha_1 = 1.0 \times 10^{-6}$ in in^{-1}/°F, and $\alpha_2 = 2.0 \times 10^{-6}$ in in^{-1}/°F. The following value of air density and speed of sound at sea-level is used: $\rho_\infty = 1.208 \times 10^{-6}$ lb $-$ sec^{2}in^{-4}, and $a_\infty = 12990$ in/sec. In Table 4.1, a comparison of results with Liaw [1] is presented for $w_{max}/h = 0.25$. It is seen that the difference between the results for linear analysis is well below 2 percent. In accordance with Liaw [1], only structural nonlinearity is considered for the purpose of comparison of nonlinear panel flutter analysis. The discrepancy in nonlinear analysis is about 10%. For cases $\frac{1}{\lambda_{cr}^{T}} \leq 0.5$ and $w_{max}/h \leq 0.25$, the quality of our approximate analysis is deemed representative enough of the panel behavior and can be used for optimization.

4.4.1 Stacking sequence optimization

The stacking sequence design optimization problem is investigated for four cases of laminated plates with aspect ratio 0.5, 1, 2, and 3. All plates have a side length of 50 in. normal to the flow direction except the first one, where the side length is 100 in. All plates are subject to a uniform temperature differential equal to 100F^{o}. The GA parameters used for the optimization run are: number of individuals in a population = 20, probability of crossover = 1.0, probability of mutation = 0.05, number of elites retained in the population = 1, and number of iterations = 50. The total number of plies in each laminate is equal to 20 and ply thickness is 0.05 in. In all the tabulated results, the corresponding objective function is in bold.

The optimum laminate configurations for plate with aspect ratio 0.5 for linear and nonlinear panel flutter are given in Table 4.2 and Table 4.3. The first row lists the design optimized for maximum flutter speed, while the last row lists the design optimized for maximum thermal buckling load. The intermediate results are obtained by optimizing the panel for maximum flutter speed and a minimum thermal buckling constraint as discussed in section 4.3.

The flutter optimized deign, using linear flutter analysis has a linear flutter parameter λ_L of 1621.327 and a critical thermal buckling ratio λ_{cr}^T of 3.473. The buckling optimized design has a linear flutter parameter λ_L of 1213.992 and a thermal buckling parameter λ_{cr}^T of 3.691. Thus, over the pareto front the linear flutter pressure varies approximately within 25% of its maximum value, the nonlinear flutter speed varies within approximately 27%, while the thermal buckling load varies within approximately 6% of its maximum value. For the flutter optimized designs using nonlinear flutter analysis (Table 4.3), the range of nonlinear flutter parameter is 30%, and of linear flutter parameter is 24% and of thermal buckling is 3%. These results indicate a much stronger sensitivity of flutter performance compared to thermal buckling. The maximum difference in the nonlinear flutter parameter between designs optimized for linear and nonlinear analysis is approximately 4%. The corresponding maximum difference in the linear flutter parameter is approximately 1%. The optimal stacking sequences for linear and nonlinear flutter analysis are similar but not identical.

The optimum laminate configuration for a panel of aspect ratio 1 for linear and nonlinear panel flutter analysis are given in Table 4.4, and Table 4.5. Unlike the previous case, here thermal buckling and flutter performance show a much stronger competition. The range of thermal buckling parameter and flutter speed are both approximately 20% of their respective maxima. The strong trade-off in design can be attributed to the difference in tailoring requirements of the bending stiffness for flutter and thermal buckling. For example, the difference in designs when λ_{all}^T is increased from 4.2 to 4.4 in Table 4.4. Here, in both cases the number of 0, ± 45, and 90 plies is same implying the inplane stiffness coefficients A_{ij} are identical. The difference in stacking sequence implies a change in bending stiffness coefficients D_{ij}. The difference in bending stiffness is reflected in the increase of buckling capacity by 3.6%, and decrease in λ_L by 1.1%. The trade-off between critical aerodynamic pressure and buckling capacity is almost linear as shown in Fig. 4.2. The optimal designs or

laminate lay ups obtained for linear and nonlinear panel flutter analysis is different in some cases. But this difference, as mentioned in the previous case, is not significant in the sense that the flutter parameter values are close, the difference being less than 2%.

For plate with aspect ratio 2, the optimum laminate configuration is given in Table 4.6. Also in this case, we observed that the optimum designs obtained using linear and nonlinear flutter analysis are exactly identical. This does not necessarily imply that the objective function contours for linear and nonlinear are identical, and could be the result of the discrete nature of the design problem. The trade-off between critical aerodynamic pressure parameter and buckling capacity is no longer linear as shown in Fig. 4.3. Initially the pareto curve is very flat suggesting insensitiveness to increased buckling constraint, but after a certain point the aerodynamic pressure parameter decreases rapidly. The range of flutter and thermal buckling parameters is approximately 60% and 25% of their respective maximum values.

The optimal laminate configuration for plate with aspect ratio 3 is given in Table 4.7, and Table 4.8. The optimal designs for linear panel flutter and nonlinear panel flutter are different, particularly for case $\lambda^T_{all} = 2.6$ and 3.0. For all the other cases, the difference is either very small or not present at all. From Fig. 4.4, we see that the trade-off follows the same pattern found in the case of aspect ratio 2. The range of thermal buckling and flutter parameters with respect to their maximum values is also similar.

4.5 Summary

In this chapter, we formulated the laminate configuration optimization of flat composite panels for both maximum flutter speed (flutter aerodynamic pressure parameter) and maximum thermal buckling capacity with stability constraint on the postflutter response. The panel equations of motion are developed using third order piston theory including structural geometric nonlinearities. A semi-analytical method of solution is adopted, and a perturbation approach is used to compute the flutter stability constraint and approximate the nonlinear flutter speed. The tradeoff between thermal buckling load and aerodynamic pressure parameter is investigated, and the effect of aspect ratio of the plate is also studied. It is observed that there exists an almost linear trade off between aerodynamic pressure parameter and thermal buckling capacity of square panels. For rectangular plates, this is no longer true, and the trade off is nonlinear. Also, we compared the optimum designs obtained using linear and nonlinear flutter analysis. For the example problems considered, the optimal stacking sequences are found to be weakly dependent on the consideration of nonlinearity in prediciting the flutter speed. It is concluded that while linear flutter analysis significantly underestimates flutter speed as compared to nonlinear calculations, for panel optimization purposes, linear flutter analysis should be sufficient.

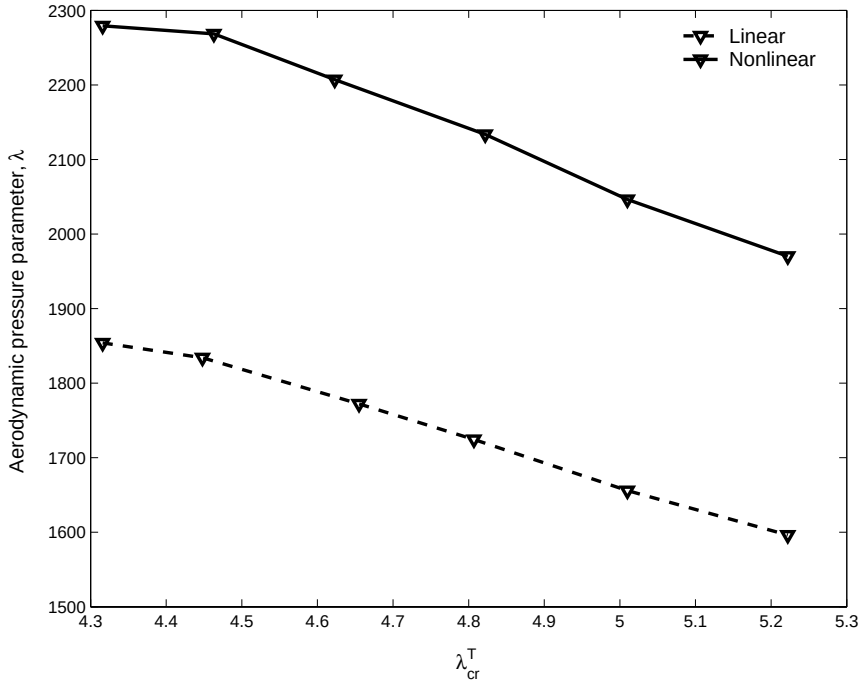

Figure 4.2: Trade off between aerodynamic pressure parameter and buckling capacity for aspect ratio 1.

Table 4.1: Comparison of results with Liaw [1].

Stacking sequence	$\frac{1}{\lambda^T_{cr}}$	λ_L	λ_L (Liaw [1])	Error (%)	λ_{NL}	λ_{NL} (Liaw [1])	Error (%)
[0/0/0/0]	0.0	342.4	342.0	0.12	387.5	350.0	10.7
[0/0/0/0]	0.5	279.0	280.0	0.36	325.1	300.0	8.4
[90/90/90/90]	0.0	96.2	95.0	1.3	109.6	100.0	9.6
[90/90/90/90]	0.5	59.4	60.0	1.0	75.6	70.0	8.0

Table 4.2: Optimum laminate configuration for aspect ratio 0.5 and linear flutter analysis.

λ^T_{all}	Stacking sequence	λ^T_{cr}	$\lambda_{\mathbf{L}}$	λ_{NL}
0.0	$[0_2/\pm 45/0/\pm 45_2/90]_s$	3.473	**1621.327**	1888.805
3.4	$[0_2/\pm 45/0/\pm 45_2/90]_s$	3.473	**1621.327**	1888.805
3.6	$[0_2/\pm 45/0/45/90/-45/90_2]_s$	3.647	**1604.430**	1857.178
-	$[0_2/45/0/-45/45/90/-45/90_2]_s$	**3.691**	1213.992	1374.868

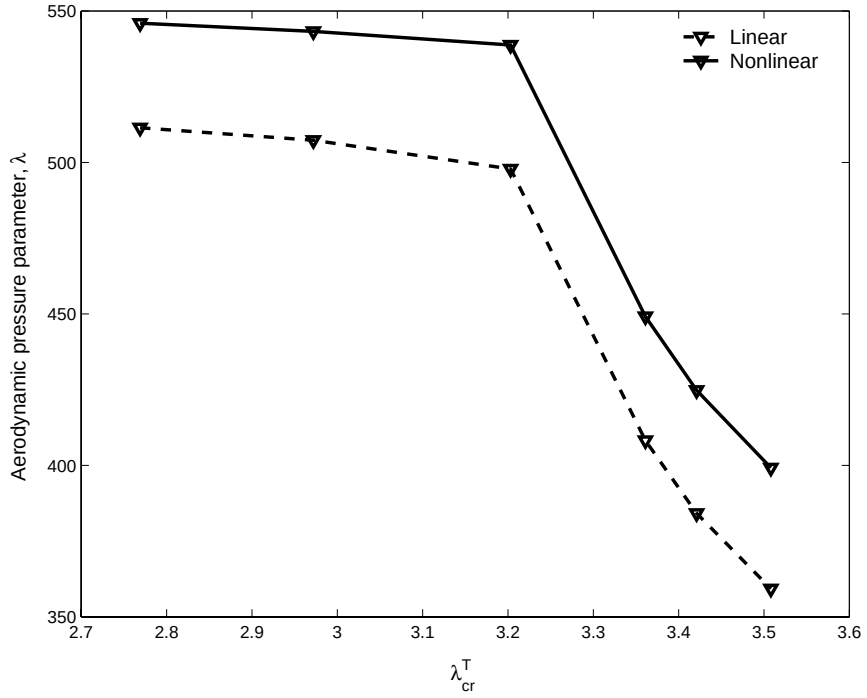

Figure 4.3: Trade off between aerodynamic pressure parameter and buckling capacity for aspect ratio 2.

Table 4.3: Optimum laminate configuration for aspect ratio 0.5 and nonlinear flutter analysis.

λ^T_{all}	Stacking sequence	λ^T_{cr}	λ_L	$\lambda_{\mathbf{NL}}$
0.0	$[0_2/45/0/-45/90_2/\pm 45/90]_s$	3.579	1601.026	**1961.074**
3.4	$[0_2/45/0/-45/90_2/\pm 45/90]_s$	3.579	1601.026	**1961.074**
3.6	$[0_2/\pm 45/0/45/90/-45/90_2]_s$	3.647	1604.430	**1857.178**
-	$[0_2/45/0/-45/45/90/-45/90_2]_s$	**3.691**	1213.992	1374.868

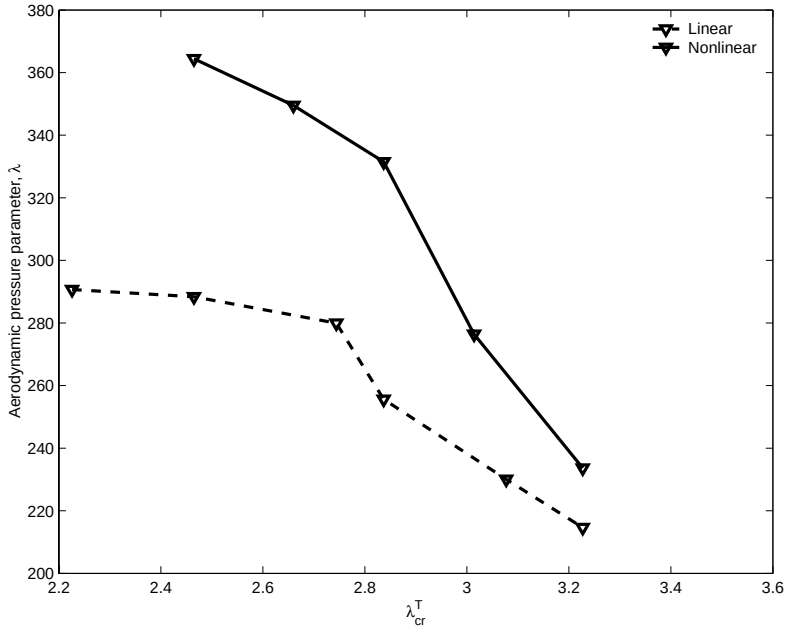

Figure 4.4: Trade off between aerodynamic pressure parameter and buckling capacity for aspect ratio 3.

Table 4.4: Optimum laminate configuration for aspect ratio 1 and linear flutter analysis.

λ^T_{all}	Stacking sequence	λ^T_{cr}	$\lambda_{\mathbf{L}}$	λ_{NL}
0.0	$[0_2/\pm 45/45/0/-45/\pm 45/90]_s$	4.316	**1853.969**	2279.193
4.2	$[0_2/\pm 45/45/0/-45/\pm 45/90]_s$	4.316	**1853.969**	2279.193
4.4	$[0_2/\pm 45_3/0/90]_s$	4.448	**1834.094**	2266.484
4.6	$[0/\pm 45/0/\pm 45_2/90_2]_s$	4.655	**1772.250**	2167.307
4.8	$[0/\pm 45_2/0/\pm 45/90_2]_s$	4.807	**1724.517**	2106.043
5.0	$[\pm 45/0/\pm 45/0/45/0/-45/90]_s$	5.010	**1655.882**	2046.280
5.2	$[\pm 45_2/0_2/\pm 45/90_2]_s$	5.222	**1596.280**	1939.052
-	$[\pm 45_5]_s$	**5.582**	1499.747	1772.491

Table 4.5: Optimum laminate configuration for aspect ratio 1 and nonlinear flutter analysis.

λ_{all}^T	Stacking sequence	λ_{cr}^T	λ_L	$\lambda_{\mathbf{NL}}$
0.0	$[0_2/\pm 45/45/0/-45/\pm 45/90]_s$	4.316	1853.969	**2279.193**
4.2	$[0_2/\pm 45/45/0/-45/\pm 45/90]_s$	4.316	1853.969	**2279.193**
4.4	$[0/\pm 45/0_2/\pm 45_2/90]_s$	4.463	1833.482	**2268.518**
4.6	$[0/\pm 45/0/\pm 45/45/0/-45/0]_s$	4.623	1764.415	**2207.086**
4.8	$[\pm 45/0_2/\pm 45/0/\pm 45/90]_s$	4.822	1722.188	**2133.604**
5.0	$[\pm 45/0/\pm 45/0/45/0/-45/90]_s$	5.010	1655.882	**2046.280**
5.2	$[\pm 45_2/0_2/\pm 45/0/90]_s$	5.222	1595.529	**1970.232**
-	$[\pm 45_5]_s$	**5.582**	1499.747	1772.491

Table 4.6: Optimum laminate configuration for aspect ratio 2 and both linear and nonlinear flutter analysis.

λ_{all}^T	Stacking sequence	λ_{cr}^T	$\lambda_{\mathbf{L}}$	λ_{NL}
0.0	$[\pm 45_4/90_2]$	2.769	**511.463**	545.969
2.6	$[\pm 45_4/90_2]$	2.769	**511.463**	545.969
2.8	$[\pm 45_5]_s$	2.959	**507.313**	542.569
3.2	$[\pm 45_4/0_2]_s$	3.203	**497.839**	538.777
3.3	$[\pm 45/90/\pm 45/45/0/-45/0_2]_s$	3.361	**408.249**	449.158
3.4	$[45/90/-45/\pm 45/45/0/-45/0_2]_s$	3.421	**384.222**	424.820
3.5	$[90/\pm 45_2/45/0/-45/0_2]_s$	3.508	**359.302**	399.224
-	$[90_2/45/90/-45/45/0/-45/0_2]_s$	**3.691**	201.180	237.240

Table 4.7: Optimum laminate configuration for aspect ratio 3 and linear flutter analysis.

λ_{all}^T	Stacking sequence	λ_{cr}^T	$\lambda_{\mathbf{L}}$	λ_{NL}
0.0	$[\pm 45_3/0/\pm 45/90]_s$	2.226	**290.663**	360.671
2.2	$[\pm 45_3/0/\pm 45/90]_s$	2.226	**290.663**	360.671
2.4	$[\pm 45_3/0/45/0/-45]_s$	2.465	**288.399**	364.445
2.6	$[\pm 45_3/0_4]_s$	2.744	**279.962**	299.416
2.8	$[\pm 45/45/90/-45/\pm 45/0_3]_s$	2.837	**255.632**	331.516
3.0	$[45/90/-45/\pm 45_2/0_3]_s$	3.077	**230.037**	249.210
3.2	$[90/\pm 45_3/0_3]_s$	3.227	**214.629**	233.645
-	$[90_2/45/90/-45/45/0/-45/0_2]_s$	**3.690**	118.007	136.252

Table 4.8: Optimum laminate configuration for aspect ratio 3 and nonlinear flutter analysis.

λ_{all}^{T}	Stacking sequence	λ_{cr}^{T}	λ_{L}	$\lambda_{\mathbf{NL}}$
0.0	$[0_2/\pm 45/45/0/-45/\pm 45/90]_s$	2.465	288.399	**364.445**
2.4	$[0_2/\pm 45_3/0/90]_s$	2.465	288.399	**364.445**
2.6	$[\pm 45_2/45/90/-45/0_3]_s$	2.660	271.987	**349.509**
2.8	$[\pm 45/45/90/-45/\pm 45/0_3]_s$	2.837	255.632	**331.516**
3.0	$[90/\pm 45_2/45/90/-45/0_2]_s$	3.014	211.841	**276.399**
3.2	$[90/\pm 45_3/0_3]_s$	3.227	214.629	**233.645**
-	$[90_2/45/90/-45/45/0/-45/0_2]_s$	**3.690**	118.007	136.252

Chapter 5

Approximate Load Path Prediction

5.1 Introduction

The most important step in structural design is to predict the load paths in the structure because based on these internal loads the structural subcomponents are designed. A highly idealized and simplified global model is used to predict the load paths in the structure. For example at the preliminary stage of the design of fuselage or wing structure, each panel between the stiffeners or ribs or spars are modelled via a single element to avoid the computational overhead associated with full scale finite element analysis. The aim of the global analysis is to give the internal load distribution. Based on these internal loads, the subcomponents are designed against strain, stability or buckling, and manufacturing constraints. This works well in the linear static behaviour. In practice, however, it is customary to allow the secondary load carrying components (like skin panels of fuselage) to go beyond critical load where the linear analysis is no longer true. So, a linear global finite element analysis is not accurate enough to predict the load paths where some or all of the subcomponents have buckled. Murphy *et al* [65] proposed a nonlinear idealization for axially loaded structures only. The strategy is based on representing a subsection with a single one dimensional nonlinear spring element in the global model. The spring data is generated by performing a detailed finite element analysis of the subsections. The proposed methodology cannot be extended very easily to biaxially loaded structures or structures under bending load. Other proposed methodologies are discussed in detail in chapter 1.

5.2 Reduced stiffness modeling

The displacement functions in Eq. 3.5 can be restated as,

$$\begin{aligned} w(x,y) &= \sum_{i=1}^{N} a_i \phi_i^w, \\ u(x,y) &= -\lambda e_{x0} x - \lambda \frac{g_{xy0}}{2} y + \sum_{i=1}^{2N} b_i \phi_i^u, \text{ and} \\ v(x,y) &= -\lambda e_{y0} y - \lambda \frac{g_{xy0}}{2} x + \sum_{i=1}^{2N} c_i \phi_i^v. \end{aligned} \tag{5.1}$$

λ is the load displacement scaling factor. Note that e_{x0} is the applied displacement loading and not mid plane strains which is denoted by a superscript 0 and in absence of g_{xy0}, it is equal to $u_0/\underline{a}$. Then the tensors in Eq. 3.8 and Eq. 3.8 can be expressed as,

$$g_l^u = g_l^{ux} e_{x0} + g_l^{uy} e_{y0} + g_l^{uxy} g_{xy0} \tag{5.2}$$

$$g_l^v = g_l^{vx} e_{x0} + g_l^{vy} e_{y0} + g_l^{vxy} g_{xy0} \tag{5.3}$$

$$\bar{K}_{il}^g = \bar{K}_{il}^{gx} e_{x0} + \bar{K}_{il}^{gy} e_{y0} + \bar{K}_{il}^{gxy} g_{xy0} \tag{5.4}$$

$$K_{il}^g = K_{il}^{gx} e_{x0} + K_{il}^{gy} e_{y0} + K_{il}^{gxy} g_{xy0}. \tag{5.5}$$

The external virtual work is defined as,

$$\Phi = \int_0^S \left(N_s \delta u_s + N_n \delta u_n \right) ds \tag{5.6}$$

where s is the contour direction taken along the contour of the plate in counter clockwise direction, and n is the outward normal direction to the contour defined by s. S is the total length or perimeter of the contour. N_s is the load along tangential direction s and N_n is load along normal direction n. After taking into considerations the boundary conditions and

subsituting the different expressions, we get the following form,

$$\begin{aligned}\Phi = & \left[\underline{a}\int_0^{\underline{b}} N_x\left(\underline{a},y\right)dy - \int_0^{\underline{a}} N_{xy}\left(x,0\right)xdx + \int_0^{\underline{a}} N_{xy}\left(x,\underline{b}\right)xdx\right]\left(-e_{x0}\right)\\ & \left[\underline{b}\int_0^{\underline{a}} N_y\left(x,\underline{b}\right)dx - \int_0^{\underline{b}} N_{xy}\left(0,y\right)ydy + \int_0^{\underline{b}} N_{xy}\left(\underline{a},y\right)ydy\right]\left(-e_{y0}\right)\\ & \left[\frac{1}{2}\int_0^{\underline{b}} N_x\left(\underline{a},y\right)ydy + \frac{1}{2}\int_0^{\underline{a}} N_y\left(x,\underline{b}\right)xdx\right.\\ & \left. + \frac{\underline{a}}{2}\int_0^{\underline{b}} N_{xy}\left(\underline{a},y\right)dy + \frac{\underline{b}}{2}\int_0^{\underline{a}} N_{xy}\left(x,\underline{b}\right)dx\right]\left(-g_{xy0}\right)\\ = & \left[N_{xavg}\left(-e_{x0}\right) + N_{yavg}\left(-e_{y0}\right) + N_{xyavg}\left(-g_{xy0}\right)\right]\left(\underline{ab}\right).\end{aligned} \tag{5.7}$$

The inplane stiffness coefficients can be predicted by the following expressions.

$$\begin{aligned}A_{11} &= \frac{DN_{xavg}}{De_{x0}}; A_{12} = \frac{DN_{xavg}}{De_{y0}}\\ A_{21} &= \frac{DN_{yavg}}{De_{x0}}; A_{22} = \frac{DN_{yavg}}{De_{y0}}\\ A_{66} &= \frac{DN_{xyavg}}{Dg_{xy0}}.\end{aligned} \tag{5.8}$$

Since at bifurcation point derivative does not exist, we employ a perturbation technique to compute the postbuckled inplane stiffness coefficients. The nonlinear equilibrium equation Eq. 3.8 depends on the following input parameters e_{x0}, e_{y0}, g_{xy0}, and a_i. The parameters e_{x0}, e_{y0}, g_{xy0}, and a_i is expanded as follows,

$$e_{x0} = e_{x0}^{(0)} + \epsilon^2 e_{x0}^{(2)} + \ldots \tag{5.9}$$

$$e_{y0} = e_{y0}^{(0)} + \epsilon^2 e_{y0}^{(2)} + \ldots \tag{5.10}$$

$$g_{xy0} = g_{xy0}^{(0)} + \epsilon^2 g_{xy0}^{(2)} + \ldots \tag{5.11}$$

$$a_i = \epsilon a_i^{(1)} + \epsilon^3 a_i^{(3)} + \ldots \tag{5.12}$$

Note that the zeroth term in the above expressions correspond to prebuckling state and hence $a_i^{(0)} = \{0\}$. Also $a_i^{(1)}$ corresponds to buckling state and hence inplane terms $e_{x0}^{(1)}$ vanishes and in the postbuckling region only third order nonlinearity corresponding to a_i exists. This can be easily verified by substituting the complete expansion and equating the corresponding ϵ terms. Substituting the above expressions in Eg. 3.8, and comparing the coefficients of

ϵ gives the linear buckling eigen value problem from where we can determine the critical values $e^{(0)}_{x0}$, $e^{(0)}_{y0}$, $g^{(0)}_{xy0}$, and the buckling mode $a^{(1)}_i$. Comparing the coefficients of ϵ^3, we get the following equation,

$$K_{il}a^{(3)}_i - K^{gx}_{il}a^{(3)}_i e^{(0)}_{x0} - K^{gy}_{il}a^{(3)}_i e^{(0)}_{y0} - K^{gxy}_{il}a^{(3)}_i g^{(0)}_{xy0} = K^{gx}_{il}a^{(1)}_i e^{(2)}_{x0} + K^{gy}_{il}a^{(1)}_i e^{(2)}_{y0} + K^{gxy}_{il}a^{(1)}_i g^{(2)}_{xy0} + K^{NL}_{ijkl}a^{(1)}_i a^{(1)}_j a^{(1)}_k \tag{5.13}$$

The solvability condition requires,

$$K^{gx}_{il}a^{(1)}_i a^{(1)L}_l e^{(2)}_{x0} + K^{gy}_{il}a^{(1)}_i a^{(1)L}_l e^{(2)}_{y0} + K^{gxy}_{il}a^{(1)}_i a^{(1)L}_l g^{(2)}_{xy0} + K^{NL}_{ijkl}a^{(1)}_i a^{(1)}_j a^{(1)}_k a^{(1)L}_l = 0, \tag{5.14}$$

where $a^{(1)L}_l$ is the corresponding left eigen vector at bifurcation point. From the above equation, we get the following set of solutions,

$$e^{(2)}_{x0} = \frac{K^{NL}_{ijkl}a^{(1)}_i a^{(1)}_j a^{(1)}_k a^{(1)L}_l}{K^{gx}_{il}a^{(1)}_i a^{(1)L}_l} \quad e^{(2)}_{y0} = 0 \quad g^{(2)}_{xy0} = 0 \tag{5.15}$$

$$e^{(2)}_{x0} = 0 \quad e^{(2)}_{y0} = \frac{K^{NL}_{ijkl}a^{(1)}_i a^{(1)}_j a^{(1)}_k a^{(1)L}_l}{K^{gy}_{il}a^{(1)}_i a^{(1)L}_l} \quad g^{(2)}_{xy0} = 0 \tag{5.16}$$

$$e^{(2)}_{x0} = 0 \quad e^{(2)}_{y0} = 0 \quad g^{(2)}_{xy0} = \frac{K^{NL}_{ijkl}a^{(1)}_i a^{(1)}_j a^{(1)}_k a^{(1)L}_l}{K^{gxy}_{il}a^{(1)}_i a^{(1)L}_l}. \tag{5.17}$$

Similarly, N_{xavg}, N_{yavg}, and N_{xyavg} is expanded in terms of ϵ as,

$$N_{xavg} = N^{(0)}_{xavg} + \epsilon^2 N^{(2)}_{xavg} + \ldots \tag{5.18}$$

$$N_{yavg} = N^{(0)}_{yavg} + \epsilon^2 N^{(2)}_{yavg} + \ldots \tag{5.19}$$

$$N_{xyavg} = N^{(0)}_{xyavg} + \epsilon^2 N^{(2)}_{xyavg} + \ldots \tag{5.20}$$

Now, the approximate postbuckled stiffness can be computed by taking the appropriate denominator to get the following expressions,

$$\begin{aligned} A^{PB}_{11} &= \frac{N^{(2)}_{xavg}}{e^{(2)}_{x0}}; A^{PB}_{12} = \frac{N^{(2)}_{xavg}}{e^{(2)}_{y0}}; \\ A^{PB}_{21} &= \frac{N^{(2)}_{yavg}}{e^{(2)}_{x0}}; A^{PB}_{22} = \frac{N^{(2)}_{yavg}}{e^{(2)}_{y0}}; \\ A^{PB}_{66} &= \frac{N^{(2)}_{xyavg}}{g^{(2)}_{xy0}}. \end{aligned} \tag{5.21}$$

5.3 Load path prediction scheme

In this section, we present an approach to predict the load path in an assembled structure progressively as the some of the structural components starts buckling. The load path prediction scheme consists of the following steps. The strains due to the applied load (full value always) after k panels are buckled are denoted asΔ increments. Total strains up to load level corresponding to the buckling of the k-th panel are denoted without a Δ.

$$K = \Delta e_{x0}^{k} K^{gx} + \Delta e_{y0}^{k} K^{gy} + \Delta g_{xy0}^{k} K^{gxy} \tag{5.22}$$

$$K_b = K - e_{x0}^{k} K^{gx} - e_{y0}^{k} K^{gy} - g_{xy0}^{k} K^{gxy} \tag{5.23}$$

$$K_b \cdot a = \Delta\lambda K^{g} \cdot a \tag{5.24}$$

The minimum value of the buckling factor is the incremental load factor:

$$\Delta\lambda^{k} = \min \Delta\lambda \tag{5.25}$$

$$\lambda^{k+1} = \lambda^{k} + \Delta\lambda^{k} \tag{5.26}$$

$$e_{x0}^{k+1} = e_{x0}^{k} + \Delta\lambda^{k} \Delta e_{x0}^{k} \tag{5.27}$$

The load path prediction scheme, as described above, consists of the following three steps. First, compute the buckling sequence corresponding to internal load distribution and local models. Stop iteration if the lowest buckling factor is greater than 1 because none of the panels are buckled before the desired load carrying capacity is reached. Rest of the procedure is applicable only if the lowest buckling factor is less than 1. Second, reduce the stiffness of the panel with lowest buckling factor. Compute the new buckling sequence corresponding to new internal load distribution. Third, continue second step until all the panels have buckled or desired load level is achieved, whichever happens earlier.

5.4 Results

In this section, we present the results obtained for three different problems: single panel problem subjected to edge displacement compression, two panel problem under axial compression, and four panel (top skin) wing structure configuration under bending load.

5.4.1 One panel problem

A simply supported one panel composite structure of $10'' \times 10''$is considered. The laminate lay-ups and the edge displacement loading condistions are reported in Table 5.1. The total edge displacement at the displaced edges i.e. at $x = \underline{a}$ and $y = \underline{b}$ is given by u_0 and v_0 (see Table 5.1). The material properties are: $E_1 = 18.5 \times 10^6$ psi, $E_2 = 1.6 \times 10^6$ psi, $G_{12} = 0.832 \times 10^6$ psi, $\nu_{12} = 0.35$, and ply thickness $t = 0.005$ in. In the Rayleigh-Ritz method, we used $N = 9$ ($m = 1, \ldots, 3$ and $n = 1, \ldots, 3$) to predict postbuckled stiffness under the prescribed loading and boundary conditions. The full nonlinear analysis is also done with $N = 9$. In some cases it is observed that the postbuckled stiffness coefficients A_{12} and A_{21} are not exactly the same. Hence, we averaged them and the corresponding responses are reported in bold in Table 5.1. The N_x and N_y reported in Table 5.1 is the average load computed along the displaced edges as follows,

$$N_x = \frac{1}{\underline{b}} \int_0^{\underline{b}} N_x(\underline{a}, y)\, dy, \text{ and} \tag{5.28}$$

$$N_y = \frac{1}{\underline{a}} \int_0^{\underline{a}} N_y(x, \underline{b})\, dx. \tag{5.29}$$

From Table 5.1, we observe that for almost all the laminate stacking sequences and edge displacement loading conditions considered, the proposed approximate methodology predicts the primary load paths within reasonable margins. λ^F is the applied load scaling factor. In all the cases, the edge displacement applied is more than 10 times that of the critical (or buckling) factor λ_{cr}. The maximum relative error in average load prediction in x direction (i.e. N_x) is 10 percent. In some cases of N_y prediction, the relative error is very large. It is observed that as the average load along the edges approaches zero, the error increases as in the case of laminate lay-up $[(0\ 90)_4]_s$ with edge displacement loading ratio 2. But it can argued that whenever such case arises; they are not the primary load path direction and is redundant in the design process as more critical load cases will be identified out of thousands of load cases for which the structure is being designed. Also it is noted that the discrepancy due to non-symmetry of postbuckled stiffness A_{12} and A_{21} are negligible and can be very safely averaged while using it with any commercial finite element software.

5.4.2 Two panel problem

A two panel composite structure is considered. Each panel P1 and P2 has a dimension $10'' \times 10''$. The boundary conditions and the edge displacement loading conditions are shown in Figure 5.2. The laminate stacking sequence for panel P1 and P2 are $[(0\ 90)_8]_s$ and $[(0\ 90)_4]_s$ respectively. The material properties are: $E_1 = 18.5 \times 10^6$ psi, $E_2 = 1.6 \times 10^6$ psi, $G_{12} =$

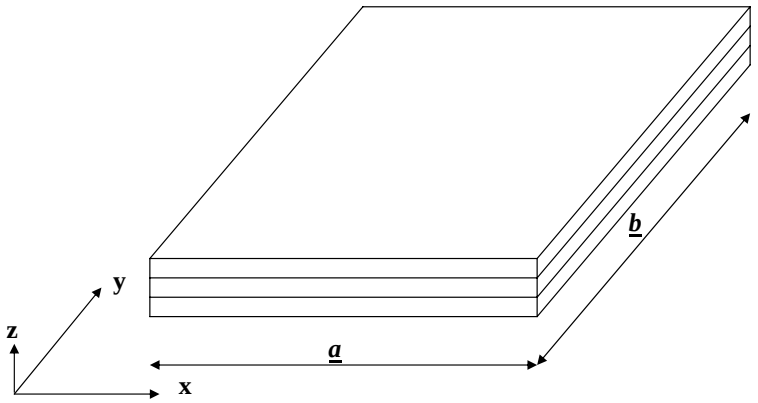

Figure 5.1: Flat composite panel.

Table 5.1: Comparison of full and approx analysis.

Laminate Lay-up	u_0/v_0 $\times 10^{-3}$	λ_{cr}	λ^F	Full analysis N_x	Full analysis N_y	Approx. N_x	Approx. N_y
$[(45\ 90\ -45\ 90)_2]_s$	1/0	2.78	19.93	405.29	-30.11	436.97	-38.41
						436.97	**-31.83**
$[(0\ 90)_4]_s$	1/0	1.22	13.96	711.51	-294.51	767.58	-303.61
$[\pm 45_4]_s$	1/1	1.0	12.12	317.54	317.54	290.81	290.81
$[(0\ 90)_4]_s$	1/1	0.61	8.29	244.80	239.07	268.96	268.96
$[\pm 45_3\ 90_2]_s$	1.5/1	0.82	9.65	312.62	302.42	323.55	316.17
						321.37	**319.42**
$[(0\ 90)_4]_s$	1.5/1	0.49	7.02	382.07	119.1	417.31	147.98
$[\pm 45_3\ 90_2]_s$	2/1	0.71	8.18	350.32	254.34	364.46	269.64
						362.62	**273.32**
$[(0\ 90)_4]_s$	2/1	0.40	6.13	481.29	30.92	529.68	59.31

0.832×10^6 psi, $\nu_{12} = 0.35$ and ply thickness $t = 0.005$ in. In the Rayleigh-Ritz method, we used $N = 25$ ($m = 1, 2, \ldots, 5$ and $n = 1, 2, \ldots, 5$) to predict postbuckled stiffness of the laminates with the prescribed loading and boundary conditions as described earlier. For the purpose of comparison both the full nonlinear finite element analysis and the proposed approximate model is reported in Table 5.2. Both linear and nonlinear analysis is done using commercial finite element software NASTRAN [84] with 100 CQUAD4 [84] elements for each panels.

The buckling factor and postbuckled stiffness of P1 and P2 is computed assuming it to be simply supported with the boundary conditions given in Figure 5.1 with edge displacement loading ratio 1 and 0.5 respectively. These assumptions closely resemble the local boundary conditions. The load prediction scheme is compared with full nonlinear analysis at 5 different stages of loading, reported in Table 5.2. In Case 1, only P2 has buckled. The maximum relative error in edge load prediction for P2 is 26 percent. The same for P1 is 15 percent. It is noted that the maximum error for P1 occurs at the edge which it shares with buckled P2 panel. In Case 2, once again, only P2 has buckled. It is noted that the error has not increased linearly as it should have been if it was due to error in postbuckled stiffness. This indicates that a substantial percentage of the error is due to error in buckling factor. It is understandable because buckling factors are computed using an idealized boundary condition. For example at R1 and L2, there should be slope continuity which the local model cannot capture. In Case 3, both P1 and P2 has buckled but the loading condition is such that P1 is very near to its buckling load. We can see that the error in load prediction for P1 (barring R1) is still within 1.35 percent. At R1, the error is 11.4 percent. For P1, the maximum error has dropped to 17.66 percent. It is observed that the error is actually reducing with increased loading. This is because the nonlinear equilibrium path obtained by full nonlinear analysis is a curve with reducing slope unlike the approximate predicted curve which is a straight line. As we increase the loading, the error reduces till the two curves intersect each other and then the error will start growing. In Case 4, both P1 and P2 has buckled. The total loading is 1.5 times that of buckling load for P1 and 8 times that of buckling load of P2. The maximum error for P1 is 16.47 percent and has occured at R1. The maximum error for P2 is 23.4 percent and has occured at L2. In Case 5, the total loading for P1 is 3.1 times that of it buckling load and for P2 is 16.4 times that of its buckling load. The maximum error in P1 is 21.21 percent and in P2 is 15.82 percent. In general for all the cases, it has been found that the approximate scheme gives reasonably good results and the maximum error is around 20 percent.

5.4.3 Wing structure problem

8 panel winbox

A simple rectangular, untapered composite wing structure 139.5″×88.2″×15″as shown in Figure 5.3 is considered. The wingbox is fixed at the root and upward load is applied at the

Table 5.2: Load path prediction for two panel problem.

P1: $u_0/v_0 = 0.001/0.002$; $\lambda_{cr} = 1.62$ P2: $u_0/v_0 = 0.002/0.002$; $\lambda_{cr} = 0.304$

Case 1: $u_0 = -0.002$, $v_0 = -0.002$

Analysis	L1(N_x)	B1(N_y)	T1(N_y)	R2(N_x)	L2(N_x)	B2(N_y)	T2(N_y)	R2(N_x)
Full NL	122.97	326.87	326.87	96.45	86.06	127.83	127.83	70.45
Approx	117.25	329.23	327.43	81.85	67.61	100.4	99.87	52.1
Rel. error	4.65	-0.72	-0.17	15.13	21.44	21.46	21.87	26.05

Case 2: $u_0 = -0.0025$, $v_0 = -0.0025$

Analysis	L1(N_x)	B1(N_y)	T1(N_y)	R2(N_x)	L2(N_x)	B2(N_y)	T2(N_y)	R2(N_x)
Full NL	146.24	406.41	402.51	118.0	96.06	145.93	143.99	73.96
Approx	143.24	410.59	412.19	97.57	77.31	117.87	118.49	58.32
Rel. error	2.05	-1.03	-2.4	17.31	19.52	19.23	17.71	21.15

Case 3: $u_0 = -0.0033$, $v_0 = -0.0033$

Analysis	L1(N_x)	B1(N_y)	T1(N_y)	R2(N_x)	L2(N_x)	B2(N_y)	T2(N_y)	R2(N_x)
Full NL	179.54	526.29	523.19	133.45	108.94	172.40	170.86	78.59
Approx	181.97	533.40	528.65	118.22	94.01	146.94	145.28	64.71
Rel. error	-1.35	-1.35	-1.04	11.4	13.7	14.77	14.97	17.66

Case 4: $u_0 = -0.005$, $v_0 = -0.005$

Analysis	L1(N_x)	B1(N_y)	T1(N_y)	R2(N_x)	L2(N_x)	B2(N_y)	T2(N_y)	R2(N_x)
Full NL	216.3	714.36	714.36	145.93	127.33	228.03	228.03	84.58
Approx	185.46	670.83	668.21	121.89	97.53	214.58	213.99	69.82
Rel. error	14.26	6.09	6.46	16.47	23.4	5.9	6.16	17.45

Case 5: $u_0 = -0.01$, $v_0 = -0.01$

Analysis	L1(N_x)	B1(N_y)	T1(N_y)	R2(N_x)	L2(N_x)	B2(N_y)	T2(N_y)	R2(N_x)
Full NL	254.3	1117.2	1117.2	172.05	128.22	402.53	402.53	82.21
Approx	200.40	1073.3	1070.2	137.25	107.94	414.67	413.85	81.76
Rel. error	21.21	3.93	4.21	20.22	15.82	3.01	2.81	0.55

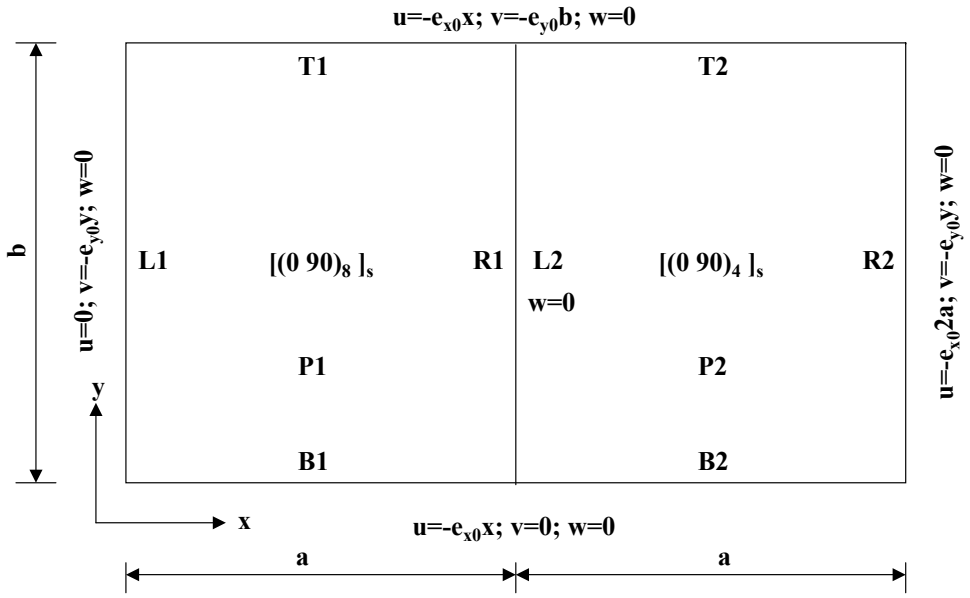

Figure 5.2: Two panel composite structure with boundary and edge displacement loading conditions.

free end. The bending load applied will result in compression in the top skin panels P1, P2, P3, and P4. P1 and P2 are root panels and P3 and P4 are the panels at the free end. The laminate configuration for the skin panels (both top and bottom) is $[(0\ 90)_8]_s$ and for the rib and spar panels is $[(0\ 90)_{16}]_s$. The total load applied at the free end is 5500 lbf which is distributed uniformly among all the nodes in the finite element model at the free edge. Each skin panels in the finite element model is modeled by 25 CQUAD4 elements and all the spar or rib panels are modeled by 10 CQUAD4 elements. The material properties are: $E_1 = 18.5 \times 10^6$ psi, $E_2 = 1.6 \times 10^6$ psi, $G_{12} = 0.832 \times 10^6$ psi, $\nu_1 2 = 0.35$, and ply thickness $t = 0.005$ in. In the Rayleigh-Ritz method, we used $N = 25$ to predict postbuckled stiffness of the laminates with the prescribed loading and boundary conditions as described earlier.

The predicted loads are compared with full nonlinear analysis in Table 5.3. Under the given loading condition only P1 and P2 has buckled. It is known that the inplane load will increase in the panel with the bending moment or as we go towards the root of the wingbox. It is very difficult to compute the buckling load for such a complicated loading condition. In this work, we computed the buckling load assuming the edge load on the panel which is at the far end from the root of the wingbox. We noted that the maximum error in N_x prediction for buckled P1 and P2 panel is 10 percent. The N_y prediction is very bad. But as explained earlier, they are close to zero and hence most probably be eliminated from the critical design load cases. The maximum error for unbuckled P3 and P4 is 1.48 percent. The current scheme predicts the load paths within reasonable margin for a complicated structure like wingbox subjected to bending load.

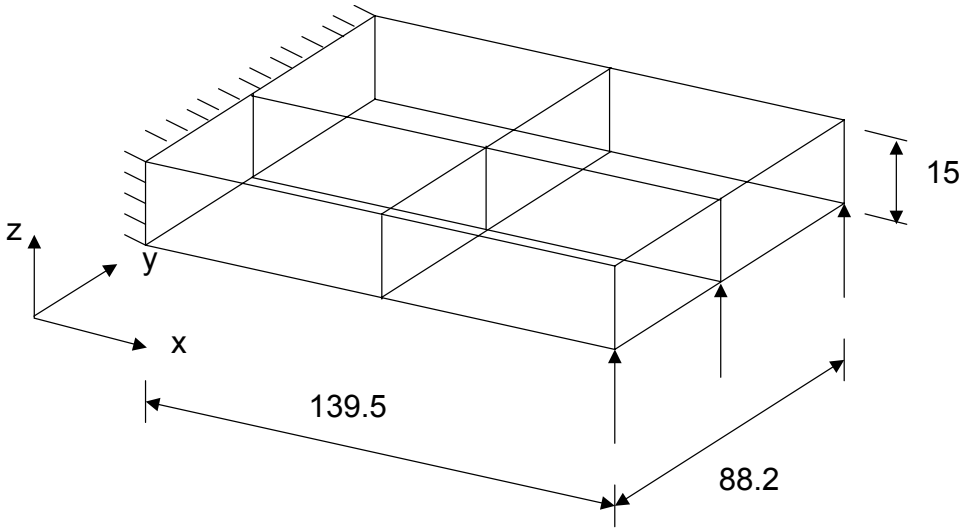

Figure 5.3: A composite wing structure under bending load.

Table 5.3: Wing structure problem.

Panel 1 (P1)	L(N_x)	B(N_y)	T(N_y)	R(N_x)
Full NL	404.44	9.55	-4.35	246.69
Approx	363.01	-16.68	-37.94	227.21
Rel. error	-10.24			-7.90
Panel 2 (P2)				
Full NL	404.44	-4.35	9.55	246.69
Approx	363.01	-37.94	-16.68	227.21
Rel. error	-10.24			-7.90
Panel 3 (P3)				
Full NL	206.00	-4.03	-7.44	22.27
Approx	205.28	-0.40	-2.08	22.60
Rel. error	-0.35			1.48
Panel 4 (P4)				
Full NL	206.00	-7.44	-4.03	22.27
Approx	205.28	-2.08	-0.40	22.60
Rel. error	-0.35			1.48

48 panel wingbox

In this example, we solve a large tapered rectangular composite wingbox $160' \times 30' \times 4'$ (root) $/2.4'$ (free). The composite wingbox is divided into 24 upper skin panels and 24 bottom skin panels (same as in the previous problem) by longitudinal spars and transverse ribs. All top and bottom skin panels are $20' \times 10'$ in dimension. Each of the top and bottom skin panels is modeled using 200 CQUAD4 elements for nonlinear finite element analysis using NASTRAN. The total number of elements in the model is 13120. The root of the wing is fixed. A total of 3100 lb upward load is applied at the free end uniformly distributed among nodes at the top edge of the free end. In approximate analysis and linear analysis, the number of elements per panel is one. So, the present methodology considerably reduces the degrees of freedom. The wingbox panels are divided into three regions: root, intermediate, and free-end ones. All panels in the region within $60'$ from the fixed edge are referred as root panels. All the top skin root panels (numbered 1 to 9 in Table 5.4) are made of $[(0\ 90)_{40}]_s$, bottom skin root panels are made of $[(0\ 90)_{25}]_s$, spar root panels are made of $[(0\ 90)_{50}]_s$, and rib root panels are made of $[(0\ 90)_{50}]_s$. All in the panels in the region between $60' - 120'$ from the fixed edge are referred as intermediate panels. The top skin intermediate panels (numbered 10 to 18) are made of $[(0\ 90)_{20}]_s$, bottom skin intermediate panels are made of $[(0\ 90)_{15}]_s$, spar intermediate panels are made of $[(0\ 90)_{50}]_s$, and rib intermediate panels are made of $[(0\ 90)_{50}]_s$. All the panels in the region between $120' - 160'$ are referred as free-end panels. The top skin free-end panels (numbered 19 to 24) are made of $[(0\ 90)_{10}]_s$, bottom skin free end panels are made of $[(0\ 90)_5]_s$, spar free-end panels are made of $[(0\ 90)_{50}]_s$, and rib free-end panels are made of $[(0\ 90)_{50}]_s$. The material properties are same as the earlier example.

For the purpose of comparison, we present the load paths in the structure for full nonlinear analysis, approximate analysis with predetermined buckling sequence, linear analysis, and approximate analysis without predetermined buckling sequence in Table 5.4. The stress resultants reported are taken at the mid section of each panels. From the full nonlinear and linear analysis, we see that panel 19, 20, and 21 has buckled under the load and linear analysis over predicts the stress resultants. Compared to linear analysis, approximate analysis performs better. However, the nonlinear analysis clearly shows that panel 10-18 has not buckled but the approximate analysis based on the local analysis deems them to have buckled. This is because the local model based on which the buckling analysis is done assumes the panel to be simply supported which is not true. The spar and rib panel in this model are too thick to allow free rotation of edges but this is necessary to avoid the buckling of spars and ribs under the load. But one has to remember that the proposed approach is only for preliminary design optimization. And since based on local model, the panel buckles earlier, the design will be always conservative in nature. It can also be seen that approximate analysis with predetermined buckling sequence is also in good agreement with the case when one recomputes the buckling sequence at every iterations. This is because in the present example the panels are uniaxially loaded.

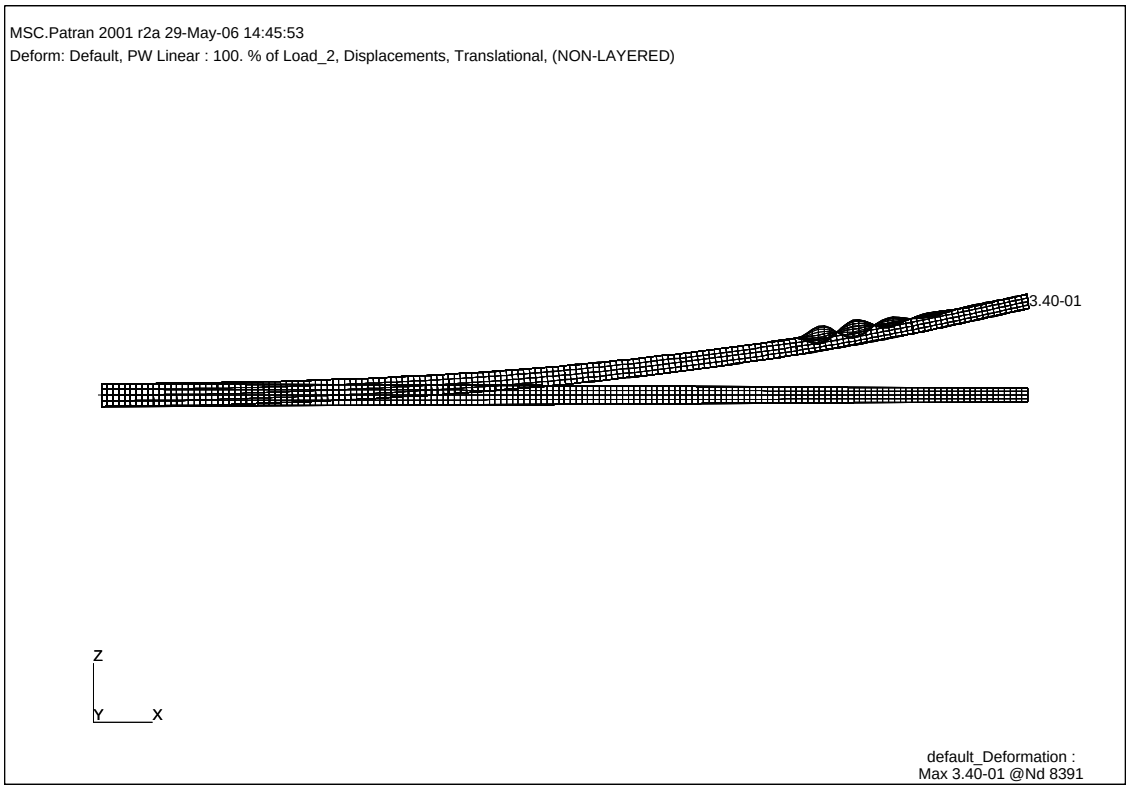

Figure 5.4: Deformed wingbox configuration under total applied load.

Table 5.4: Load path prediction in a 48 panel postbuckled composite structure.

Panel No.	Full NL N_x(lb/ft)	App PDBS N_x(lb/ft)	Linear N_x(lb/ft)	App N_x(lb/ft)
1	3724.1	3733.6	3734.3	3733.6
2	3707.8	3712.8	3711.4	3712.7
3	3724.1	3733.6	3734.3	3733.6
4	3415.4	3420.2	3419.5	3420.1
5	3400.1	3408.7	3411.0	3408.8
6	3415.3	3420.2	3419.5	3420.1
7	3059.4	3099.3	3080.0	3098.5
8	3026.5	2997.2	3037.3	2998.8
9	3059.5	3099.3	3080.0	3098.5
10	2446.6	2211.9	2445.1	2220.2
11	2456.6	2252.2	2463.8	2259.5
12	2446.3	2211.9	2445.1	2220.2
13	2037.0	1860.6	2044.3	1867.7
14	2032.4	1874.3	2044.9	1880.2
15	2036.9	1860.6	2044.3	1867.7
16	1539.0	1493.3	1578.1	1490.2
17	1515.9	1440.2	1556.9	1439.1
18	1539.0	1493.3	1578.1	1490.2
19	757.01	784.74	954.71	784.67
20	782.95	794.89	945.37	794.46
21	757.01	784.74	954.71	784.67
22	309.76	292.72	346.15	286.48
23	306.10	277.14	323.63	271.91
24	306.38	292.71	346.15	286.48

PDBS is pre determined buckling sequence.

5.5 Summary

In this chapter, we presented a new methodolgy to predict load paths in postbuckled composite structures. The proposed scheme is similar to progressive buckling where with application of load as soon as any local component buckles, the stiffness of that component is replaced by postbuckled stiffness for any load above its own buckling capacity. An analytical method is presented to compute the postbuckled stiffness. The expressions are derived for a simply supported composite panel with sliding edges. This type of boundary condition occurs in stiffened panel in fuselage or wing structure configurations. The proposed scheme is demonstrated via three different problems. First, a single panel problem subjected to edge displacement both uniaxial and biaxial is solved. The result shows that the proposed scheme predicts the load in either direction very well provided their ratio is not too large. We also observe that sometimes the reduced stiffness coefficient matrix is not symmetric but the difference is very small and can be reasonably averaged for application along with commercial finite element packages. Second, a two panel problem subjected to biaxial edge displacement is solved. In this case, also the load paths are predicted with reasonable confidence. The importance of local models used in predicting either buckling factor or postbuckled stiffness is addressed. Third, a four panel composite wing structure subjected to bending load is solved. It is found that the current methodology predicts load path with reasonable confidence. In all the three example problems, we observed that the current scheme performs very well in predicting major load path. If the ratio of loads in either direction is too large, though the prediction of major load path (dominant load direction magnitudewise) is consistently good, the same is not true for minor load path (non dominant load direction magnitudewise). Based on the example problems solved, it is concluded that the proposed methodology can be applied as a loads model in multilevel design of large structure at the preliminary stages. In an effort to show the advantages of the proposed scheme in large structure, we solved a large composite wingbox problem. This example showed that as the problem becomes larger, the computational time savings via the proposed scheme also gets better. Also, we present a systematic approach to pass on the local information to global model without the need to refine the finite element model and thus saving a significant computational time and cost.

Chapter 6

Design for Blending and Postbuckling

In chapter 2, the local constraint on the panels are buckling and strength. We already know that the laminated composite plates possess significant postbuckling strength. It is imperative that with increasing manufacturing cost and drive to make the structure fuel efficient by reducing the total weight of the structure, many secondary components are allowed to go beyond the buckling load. A comprehensive literature on nonlinear postbuckling analysis of laminated composite plates can be found in references [85, 86, 87]. Though, a comprehensive literature on optimal design of laminates for buckling exists (see references [5, 3, 6, 7, 52, 30]), very less focus is given in integrating the postbuckling performance of the laminates in the design optimization framework. This is because of computationally expensive nature of postbuckling analysis. Perry *et al.* [35] and Shin *et al.* [76] studied optimum design of laminates in postbuckling regime with ply thickness as design variables for a preselected stacking sequence. Adali *et al.* [36] proposed a multiobjective formulation to take into account prebuckling, buckling and initial postbuckling behaviour. Diaconu *et al.* [37] studied the optimum design of infinite length laminated composite plates subjected to compression using normal displacement and strain as objective function. In chapter 3 [72], we studied the optimal design of laminated composite plates for a general biaxial edge displacement loads in the postbuckling regime with stacking sequence as discrete design variables. It is noted that most of the design and optimization of composite laminates for postbuckling performance is restricted to design of simple panel or multi-bay stiffened panel structure. This work focuses on developing a general methodology to design large composite structures with locally postbuckled panels using stacking sequence of laminates as discrete design variables. There are two difficulties. First, the global model or loads model used to compute load paths in the structure has to take into account the postbuckled components of the structure. This will require a full scale nonlinear analysis of the structure which is beyond the scope. Second, even the local postbuckling analyses are expensive enough to be used in an optimization framework, which requires numerous evaluations. In this work, we used the iterative approach to predict the approximate load paths in the structure following the methodology described in chapter 5. The expensive local postbuckling analysis is done

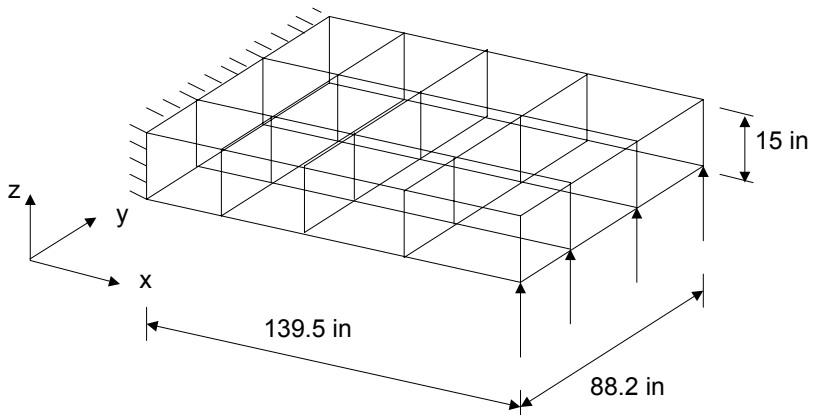

Figure 6.1: Composite wing structure.

via a response surface method. The guide based genetic algorithm approach with local improvement operator developed in chapter 2 is employed to obtain globally blended designs. The same composite wing structure design problem is chosen to demonstrate the methodology because of the complexity of the design problem, availability of published results, and earlier experience. The objective function is minimization of total weight of the structure. The design variables are the stacking sequence of the guide and the number of layers in each panel.

6.1 Problem formulation

6.1.1 Composite wingbox design problem

The same composite wing box example used in chapter 2 is considered. Fig. (6.1) shows the wing structure with the dimensions. The top and bottom surface panels are the targeted design panels. All the other sections are fixed to $[\pm 45_{11}]_s$. The root of the wing is fixed and the load is applied at the free end. The total number of panels at the top and bottom surface layers is 9 each. The upward lift force acting is modeled by four concentrated loads of magnitudes 85467 lbf, 42239 lbf, 42239 lbf, and 20235 lbf [72] as in the design example for chapter 2.

The objective is to minimize the total weight of the structure subjected to local postbuckling and blending constraint. The laminate is assumed to be balanced and symmetric. A ply contiguity constraint is imposed to restrict successive plies of same fiber orientation more than 4 [3]. In design procedure, because of the difficulty in incorporating micromechanical details, macroscopic failure criteria are often used [34]. In this work, the laminates are

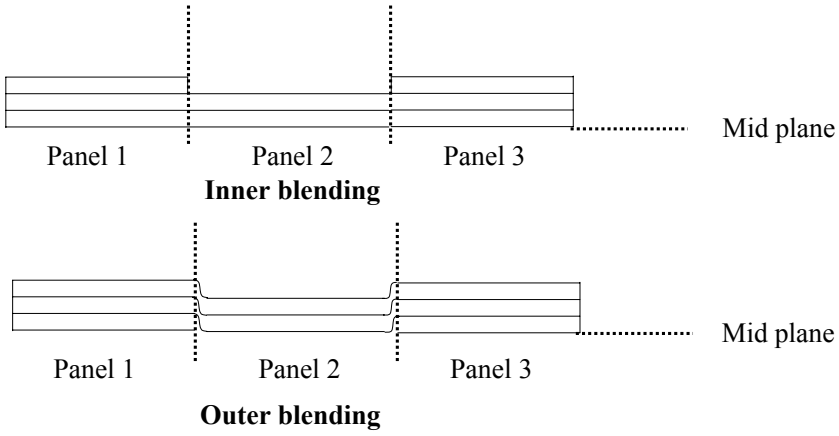

Figure 6.2: Inner and outer blending schemes.

assumed to have failed if the maximum strain in the domain reaches allowable limits.

6.1.2 Blending problem

As mentioned earlier, blended design is the one where there is ply continuity across multiple panels. The blending definitions are the same as in chapter 2 and shown in Fig. 6.2.

Guide based approach

The guide based approach described in chapter 2 is used to impose blending [72]). Lightest possible design from a guide is obtained by performing a one dimensional optimization at local level or stripping plies at panel level design until the panel thickness is minimum to safety criteria imposed.

6.2 Optimization formulation

The optimization problem is formulated as minimization of total weight of the wing structure subjected to local postbuckling and blending constraint. As explained chapter 2, the blending constraint is imposed globally via a guide based approach. Other constraints are maximum deflection constraint, ply contiguity constraint, symmetricity, and balanced condition of the laminate. The design variables are the fiber orientation angles of the ply chosen from a discrete set of 0, ± 45, and 90 degrees and the number of layers to be kept from the guide for each panel. The optimization problem is stated as

$$\text{Minimize} \sum_{i=1}^{N} w^i \left(n^i\right)$$

subject to :

$$\lambda_s^i \left(\mathbf{\Theta}^i, N_x^i, N_y^i, N_{xy}^i\right) \geq 1.0$$
$$\lambda_c^i \geq 1.0$$
$$\text{laminate is symmetric and balanced,}$$

where w^i is the weight of the i^{th} panel, N is the total number of panels, n^i is the number of plies in i^{th} panel, $\mathbf{\Theta}$ is the stacking sequence of the guide, $\mathbf{\Theta}^i$ is the stacking of the i^{th} panel, λ_s^i is the normalized strength constraint in the postbuckled regime associated with i^{th} panel, λ_c^i is the ply contiguity constraint value of i^{th} panel, and $N_x^i, N_y^i, \text{and} N_{xy}^i$ are the inplane loads acting on the i^{th} panel.

The symmetric condition of the laminate is taken care of implicitly because only half laminate stacking sequence is used as design variables. The balanced condition of the laminate is taken care of by imposing a penalty on designs violating the constraint. In the current formulation, no more than four plies of 0 or 90 degree fiber orientation angles are allowed successively. For ± 45 degree plies, the ply contiguity constraint is satisfied automatically.

6.2.1 Guide based genetic algorithm

The guide based genetic algorithm used in the this work is the same as the one used in chapter 2 with some modifications. Since, the basic underlying principle is already discussed, in this section, we present a brief description of the modfications done to avoid the numerical difficulties associated with design optimization of large composite structures with local postbuckling constraint.

For each panel, the local strength constraint is computed, and the constraint margin (defined as $(\lambda_s - 1.0)$ is calculated. A safety margin of 0.2 is applied to avoid the numerical difficulties associated with local improvement operator as solution converges. This is important because as the solution converges, the basic assumption that the load paths do not change significantly on deleting or adding plies is no longer true. Infact while doing numerical experiment, we faced such numerical difficulties where genetic algorithm goes into the infeasible domain. Depending on the constraint margin value, a decision is made either to add a ply (if the constraint margin is less than safety margin) or remove a ply (if the constraint margin is greater than safety margin) while keeping the load for the panel constant. That is, no new expensive global finite element analysis is done to compute the new inplane loads due to change in local stiffness and the local panel analyses are repeated to check the local constraints. If the constraint margin after removing a ply is still positive, then all the calculations pertaining to the local panel (primarily the weight of the panel) are done based

on the new number of plies. Otherwise, calculations are performed based on the previous value before removing a ply.

Every individual (or guide design) in the population is assigned a fitness value based on the overall performance of the guide, which is measured by the total weight of the structure (dictated by the number of layers in each panel presented in the second string) and the value of the constraints. If the constraints are satisfied then the fitness value is the total weight of the structure, otherwise, the fitness is the total weight of the structure plus a penalty for the constraint violation. The total constraint violation C for an individual is calculated as the sum of constraint violation for all the panels given by

$$C = \min\left[\left(\frac{\delta_{all}}{\delta_{max}} - 1\right), 0\right] + \sum_{i=1}^{N} \min\left[\left(\lambda_s^i - 1.2\right), 0\right], \tag{6.1}$$

and the total penalty P for an individual is given by

$$P = \sum_{i=1}^{N} p_u^i + \left(n_{0,max}^i - 4\right) + \left(n_{90,max}^i - 4\right), \tag{6.2}$$

where p_u^i is the penalty for unbalanced laminate, $n_{0,max}^i$ is the maximum number of contiguous (successive) zero degree plies , and $n_{90,max}^i$ is the maximum number of contiguous ninety degree plies in the i^{th} panel. When none of the panels represented by an individual violate the balanced laminate or ply contiguity constraint, the value of P is zero. The fitness f of an individual is computed as

$$f = -W\left(1 + \frac{C^2}{0.0005}\right)(P + 1). \tag{6.3}$$

Global and local analysis module

The load path prediction scheme discussed in chapter 5 is used in this optimization study as a loads model. The local analysis module is discussed in chapter 3.

6.3 Response surface construction

The local postbuckling analysis even with smaller number of functions $N = 4$ becomes computationally expensive when the analysis module is coupled with genetic algorithm which requires large number of evaluations. An alternative is to use an approximate/surrogate model. In this work, we used a quadratic response surface for predicting both local failure and

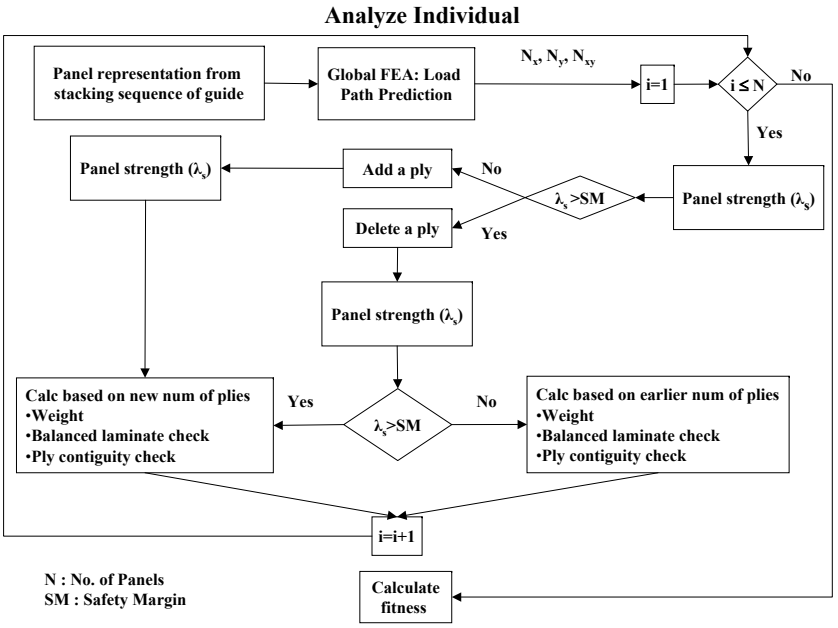

Figure 6.3: Flowchart of fitness evaluation in guide based GA.

postbuckled stiffness. Let $\bar{f}(\boldsymbol{x})$ be the true response function and $\hat{f}(\boldsymbol{x})$ its approximation using the second order polynomial in the form

$$\hat{f}(x) = \beta_0 + \sum_{i=1}^{m} \beta_i x_i + \sum_{i=1}^{m} \beta_{ii} x_i^2 + \sum_{i=1}^{m-1} \sum_{j=i+1}^{m} \beta_{ij} x_i x_j, \tag{6.4}$$

where m is the total number of design variables, x_i is the i^{th} design variable, and the βs are the unknown coefficients. For n sampling of design variables $x_{ki}\,(k = 1, 2, \ldots, n; n = 1, 2, \ldots, m)$ and the corresponding function values $\bar{f}_k\,(k = 1, 2, \ldots, n)$, 6.4 leads to n linear equations expressed as

$$\begin{aligned}
\bar{f}_1 &= \overline{\beta}_0 + \sum_{i=1}^{m} \overline{\beta}_i x_{1i} + \sum_{i=1}^{m} \overline{\beta}_{ii} x_{1i}^2 + \sum_{i=1}^{m-1} \sum_{j=i+1}^{m} \overline{\beta}_{ij} x_{1i} x_{1j}, \\
\bar{f}_2 &= \overline{\beta}_0 + \sum_{i=1}^{m} \overline{\beta}_i x_{2i} + \sum_{i=1}^{m} \overline{\beta}_{ii} x_{2i}^2 + \sum_{i=1}^{m-1} \sum_{j=i+1}^{m} \overline{\beta}_{ij} x_{2i} x_{2j}, \\
&\ldots \\
\bar{f}_n &= \overline{\beta}_0 + \sum_{i=1}^{m} \overline{\beta}_i x_{ni} + \sum_{i=1}^{m} \overline{\beta}_{ii} x_{ni}^2 + \sum_{i=1}^{m-1} \sum_{j=i+1}^{m} \overline{\beta}_{ij} x_{ni} x_{nj}.
\end{aligned}$$

The above system of equations can also be written in matrix form as

$$\bar{\boldsymbol{f}} = \boldsymbol{X}\overline{\boldsymbol{\beta}}, \tag{6.5}$$

Table 6.1: Accuracy of response surfaces in predicting postbuckled stiffness in different thickness zone

Thickness bounds (in)	A_{11}^{PB}	A_{12}^{PB}	A_{22}^{PB}
$0.05 - 0.20$	0.066	0.191	0.151
$0.20 - 0.30$	0.122	0.092	0.087
$0.30 - 0.40$	0.008	0.012	0.019
$0.40 - 0.50$	0.003	0.006	0.006
$0.50 - 0.60$	0.0006	0.0013	0.0001
$0.60 - 0.70$	0.0005	0.0012	0.0001
$0.70 - 0.80$	0.0029	0.0047	0.0065
$0.80 - 0.90$	0.0002	0.0005	0.0001
$0.90 - 1.00$	0.0004	0.0008	0.0001

where the vector of unknown coefficients $\overline{\boldsymbol{\beta}}$ is the least-square estimator of the true coefficient vector and is solved using the method of least squares as

$$\overline{\boldsymbol{\beta}} = \left(\boldsymbol{X}^T \boldsymbol{X}\right)^{-1} \left(\boldsymbol{X}^T \bar{\boldsymbol{f}}\right). \tag{6.6}$$

Statistical analysis techniques such as ANOVA can be used to check the fitness of an RS model and to identify the main defects of design variables. However, main effect analysis is not the focus of this study and will not be discussed here. The accuracy of the RS model is estimated by root mean square of error E_{RMS} calculated as,

$$E_{RMS} = \sqrt{\frac{\sum_{i=1}^{n_e} \left(\frac{\bar{f}_i(x) - \hat{f}_i(x)}{\bar{f}_i(x)}\right)^2}{n_e}} \tag{6.7}$$

In this work, following Todoroki *et al.* [68] we constructed the response surface with inplane, flexural lamination parameters, and thickness of the laminate as input variables. For the sake of simplicity and better accuracy of response model, we constructed different response surface in different thickness zone. This is particularly advantageous given the complex nature of the response we are trying to approximate via quadratic response surface. In table 6.1 and 6.2, we report the root mean square of the error for different response surfaces for 50 random points. The response surface for postbuckled stiffness, and buckling factor is constructed using $N = 9$. The response surface for failure load is constructed using $N = 4$ because of the computational cost. It is observed that the strategy of constructing multiple response surfaces in different thickness bounds actually paid off. Only for the very thin laminate (0.05-0.20 in), the root mean square of the error is around 19 percent. For all the other cases, the error is within reasonable limits.

Table 6.2: Accuracy of response surfaces in predicting buckling factor and failure load in different thickness zone

Thickness bounds (in)	λ_{cr}	N_x^F
$0.05 - 0.20$	0.076	0.121
$0.20 - 0.30$	0.020	0.111
$0.30 - 0.40$	0.018	0.074
$0.40 - 0.50$	0.020	0.047
$0.50 - 0.60$	0.014	0.107
$0.60 - 0.70$	0.009	0.041
$0.70 - 0.80$	0.011	0.033
$0.80 - 0.90$	0.009	0.027
$0.90 - 1.00$	0.010	0.025

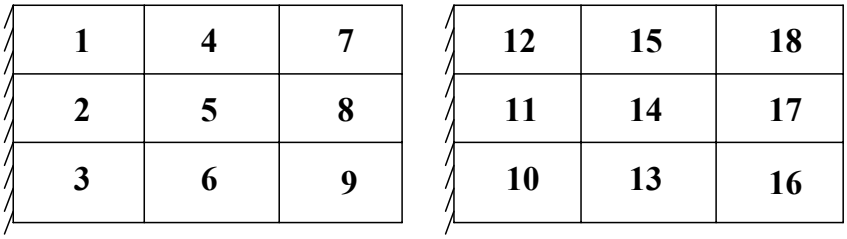

Figure 6.4: Upper (left) and lower (right) panel numberings.

6.4 Results

In this section, we present the composite wingbox design problem solved in chapter 2 with local postbuckling constraint and blending constraint. The material properties are: $E_1 = 18.5 \times 10^6 lb - in^{-2}$, $E_2 = 1.89 \times 10^6 lb - in^{-2}$, $G_{12} = 0.93 \times 10^6 lb - in^{-2}$, $\nu_{12} = 0.3$, $\rho = 0.057 lb - in^{-3}$, $\epsilon_{1,all} = 0.008$, $\epsilon_{2,all} = 0.029$, $\gamma_{12,all} = 0.015$, and $t = 0.005 in$. Two different guides, as discussed in chapter 2, are chosen to represent the top and bottom skin laminates. The GA parameters are: initial population = 200, maximum half laminate thickness for upper skin panels = 100, maximum half laminate thickness for lower skin panels = 70, probability of crossover = 1.0, probability of mutation = 0.05, number of elites retained in elitist selection = 1, penalty for unbalanced laminate, $p_u = 2.7$, and safety margin = 0.2. The panel numberings are shown in Figure 6.4. All the designs are reported after 200 GA iterations.

In Table 6.3 and 6.4, the optimal designs for outer blending and inner blending are presented. From Table 6.3 and 6.4, one can observe the thickness variation of the optimal design. As

mentioned earlier that it was found that as the solution converges, the load paths change significantly which undermines the basic assumption of local improvement operator. To avoid the numerical difficulties, a safety margin is imposed. The justification of such a safety margin can be explained from the result obtained. From Table 6.3, we observe that the constraint margin in many cases though in feasible domain has violated the safety margin and in some cases almost close to zero or failure boundary. This indicates that the load paths are changing significantly and as local improvement operator takes decision at local level without any knowledge of the effect of that decision at global level, the application of safety margin is justifiable. Another approach could have been re analysis of the global model after each ply deletion or ply addition. But even the current iterative load path prediction model becomes computationally expensive. While doing numerical experiments, we found that as GA converges toward a solution, many times GA loses the best solution found till date. This is because load redistribution is significant at this stage. And since local improvement operator is truly local in nature, the elitist selection fails to recognize a bad design while forming new child population. This happens even after applying safety margin of 20 percent. So, a re analysis of the design is performed to re evaluate the fitness of the design after all the local improvements based on the local information is done. Thus, instead of performing a re analysis after each ply deletion or addition, we perform an analysis after all the ply deletion and additions are done for the guide. This increases the computational load but it is the minimum that is required for design of such complex structures.

In chapter 2, we demonstrated a guide based design of wing structure with local buckling constraint and global blending constraint [72]. The total weight reported was 513.52 lb which is around 46 percent higher than what is obtained in the current work. The total weight of the wingbox is 351.44 lb and 358.45 for outer blending and inner blending respectively. Also in the earlier work, the bottom panels are made of only zero degree plies [72]. This was because the bottom panel was assumed to be in tension and no ply contiguity constraint was applied. Here also, we do not have any ply contiguity or buckling constraint but the bottom panel designs contains all the three type of fiber orientation layers. This suggests that the bottom panels play a very important role in the load path distribution as soon as the some of the top panels start buckling. This is also suggested by the fact the panel 10 (in bottom skin) is significantly thicker than the most of the other panels in top skin.

The thickness patterns for both outer and inner blending results are same and consistent. However, the inner blending result is on thicker side around 2 percent thicker than outer blending designs. But given the number of design variables (100+70), this could be an artifact of poorly converged solution of GA.

6.5 Summary

In this chapter, we present a methodology to design large composite structures with local postbuckled components and global blending constraint. The iterative procedure for pre-

Table 6.3: Outer blending results.

Panel no.	Stacking sequence	No. of plies			Constraint margin	Weight (lbs)
		0	45	90		
1	$[\underline{\mathbf{P8}}\ 0_2\ 90\ 0]_s$	14	08	04	0.021	10.13
2	$[\underline{\mathbf{P6}}\ 45\ 0_4\ 90\ -45\ 90\ \pm 45\ 0\ 90]_s$	48	30	54	0.156	55.33
3	$[\underline{\mathbf{P2}}]_s$	48	30	54	0.020	55.33
4	$[\underline{\mathbf{P1}}]_s$	16	00	14	0.248	10.13
5	$[\underline{\mathbf{P9}}\ 0\ 90_2\ 0_2\ 90_2\ \pm 45\ 0]_s$	26	12	14	0.125	20.26
6	$[\underline{\mathbf{P5}}\ 90_3\ \pm 45\ 0\ 90\ \pm 45\ 90_3\ 0\ 90\ 0\ 45\ 90_2\ -45\ 45\ 0\ 90\ -45\ 90\ 45\ 90\ 0_2\ 90_2\ -45\ 90_2]_s$	38	22	48	0.236	45.97
7	$[\underline{\mathbf{P7}}]_s$	04	08	00	0.126	4.675
8	$[\underline{\mathbf{P7}}\ 0_2\ 90]_s$	08	08	02	0.294	7.013
9	$[\underline{\mathbf{P1}}\ 90\ 0_2]_s$	18	08	06	0.142	12.47
P7	$0\ 45\ 0\ -45\ \pm 45$					
10	$[\underline{\mathbf{P13}}\ 90_3\ 0\ 90\ 0_5\ 90\ 0_2\ 45\ 0_2\ -45]_s$	72	16	18	0.086	41.30
11	$[\underline{\mathbf{P12}}\ 0\ \pm 45\ 0_4\ \pm 45\ 45\ 0\ -45\ 0]_s$	40	12	02	0.164	21.04
12	$[\underline{\mathbf{P14}}\ 0_3]_s$	26	00	02	0.077	10.91
13	$[\underline{\mathbf{P11}}\ 0_5\ 90_3\ 0]_s$	52	12	08	0.313	28.05
14	$[\underline{\mathbf{P15}}\ 0]_s$	20	00	02	0.115	8.572
15	$[\underline{\mathbf{P18}}\ 0_4\ 90\ 0_2]_s$	18	00	02	0.316	7.792
16	$[\underline{\mathbf{P15}}]_s$	18	00	02	0.120	7.792
17	$[\underline{\mathbf{P18}}]_s$	06	00	00	1.080	2.338
18	$[\underline{\mathbf{P18}}]_s$	06	00	00	0.728	2.338
P18	0_3					
	Total					351.44

Table 6.4: Inner blending results.

Panel no.	Stacking sequence	No. of plies 0	45	90	Constraint margin	Weight (lbs)
1	$[45\ 90_2\ 0\ -45\ 0\ \underline{\mathbf{P9}}]_s$	14	08	08	0.186	18.70
2	$[\pm 45\ (90\ 0)_2\ 45\ 0\ -45\ 90\ 0_2\ 90_2\ \underline{\mathbf{P6}}]_s$	56	20	38	0.245	52.99
3	$[0_4\ 90_2\ \underline{\mathbf{P2}}]_s$	64	20	42	0.066	57.66
4	$[45\ 90\ 0_2\ 90\ 0\ -45\ 0_2\ \underline{\mathbf{P7}}]_s$	16	08	12	0.329	13.25
5	$[0_2\ \underline{\mathbf{P1}}]_s$	18	08	08	0.119	20.26
6	$[0_2\ 90\ 0_3\ 90\ 0_4\ 90\ 0_3\ 90\ 0\ 90_3\ 0\ 45\ 90\ -45\ 90\ \pm 45\ 90\underline{\mathbf{P5}}]_s$	46	12	28	0.198	42.08
7	$[\underline{\mathbf{P7}}]_s$	08	04	04	0.232	6.23
8	$[\underline{\mathbf{P7}}]_s$	08	04	04	0.185	6.23
9	$[0\ \underline{\mathbf{P4}}]_s$	10	04	04	0.228	14.03
P7	$45\ 90\ 0_2\ 90\ 0\ -45\ 0$					
10	$[0_2\ 45\ 90\ 0_2\ -45\ 90\ 45\ 0_2\ 90_2\ -45\ 0_3\ 90_2\ 0_2\underline{\mathbf{P13}}]_s$	66	12	12	0.078	38.96
11	$[0_6\ \underline{\mathbf{P12}}]_s$	44	04	00	0.279	18.70
12	$[0_4\ \underline{\mathbf{P14}}]_s$	32	04	00	0.236	14.03
13	$[0_5\ \underline{\mathbf{P11}}]_s$	54	04	00	0.314	22.60
14	$[0_3\ \underline{\mathbf{P15}}]_s$	24	04	00	0.248	10.91
15	$[0\ \underline{\mathbf{P16}}]_s$	18	04	00	0.360	8.572
16	$[0_3\ 45\ 0\ -45\ \underline{\mathbf{P17}}]_s$	16	04	00	0.211	7.792
17	$[0\ \underline{\mathbf{P18}}]_s$	08	00	00	1.015	3.117
18	$[\underline{\mathbf{P18}}]_s$	06	00	00	0.845	2.338
P18	0_3					
	Total					358.45

dicting approximate load paths in large composite structures is integrated to the optimizer. The guide based design methodology using response surface is demonstrated via a complex composite wing structure design. The numerical difficulties and the computational aspects are discussed. The example problem solved suggests that as solution converges, the local improvement operator may create problem and a simple, intuitive but effective solution is suggested.

Chapter 7

Conclusions

7.1 Conclusions

In this research work, we developed a optimization framework for design of large composite structures with discrete stacking sequence composite laminates. The methodology is demonstrated via design of a composite wing box structure where the global local coupling is strong and cannot be neglected. As mentioned earlier, a blending constriant is imposed via a guide based methodology. The results obtained are compared to the published ones. We achieved hundred percent stacking sequence continuity for the same weight. However, it is important to note that the guide based genetic algorithm discussed here found fairly optimal designs simply because good number of blended designs exists. There may be other ways to obtain fairly decent blended solutions. But since the discrete composite laminate stacking sequence design problem is in essence a combinatorial optimization problem, it is difficult or computationally expensive to improve the quality of a decent solution to true optimal. This is true for combinatorial optimization problems like the traveling salesman problem, for example.

However, for a structure to be more weight efficient we have to allow some of the secondary load carrying members in the structure to go beyond buckling load without any structural damage. This means we need an efficient, cheap, and accurate global loads model that can predict the loads in the structure. We proposed a new methodology based on progressive buckling and compared our results with full nonlinear analysis. The proposed load path prediction model is based on discretizing the total applied load into a series of load according to the buckling progression and reducing the stiffness of the buckled components in the required iterations. To summarize this work, the reader should keep in mind that the proposed methodology is a first step to develop a loads model based on stiffness reduction by computing the analytical expression for simply supported panels.

The load path prediction methodology made it possible to do a preliminary design optimization study of large composite structures with local postbuckling constraints. We demon-

strated the design methodology via a composite wingbox design with local strength constraints, local postbuckling constraints, and blending constraints. Several modifications had to be made to the guide based GA framework built earlier to circumvent the numerical and computational difficulties faced in the investigation. Like we applied a small safety margin as we found that the load redistribution is significant near the constraint boundary and GA goes into the infeasible domain.

The dissertation work can be summarized briefly in the following,

1. A guide based genetic algorithm is developed for coupled global local problem for example wing structure configuration.
2. The developed structural optimization framework can handle local buckling, local strength, local flutter, and local postbuckling constraints.
3. The dissertation clearly shows the tradeoff between buckling, flutter, and postbuckling performance of simply supported panels. It is suggested to include all of them in the preliminary design optimization itself instead of treating them separately at the end.
4. The proposed framework gives completely blended solution at the end of the design optimization study.
5. A cheap and accurate load path prediction model is developed for global local design of large composite structures that can be used for preliminary design optimization study.

7.2 Future works

Future work includes integrating the memory framework for genetic algorithms developed by Vladmir *et al.* [9, 10], which have been found very effective in reducing the computational time by saving the computational history in a binary tree. In their work, the memory tree was built based on discrete stacking sequence which is infeasible in our case because of the large number of design variables. However, it might be possible to construct a guide based genetic algorithm with memory based on lamination parameters of the discrete stacking sequence.

The postbuckling optimization study of composite laminates done in the current work is limited by computational resources. A response surface methodology could be applied to the current formulation to do a more detailed study. Also the panel flutter constraint is not imposed in the design of wingbox and the analysis module developed will be integrated to the multilevel optimization problem.

The load path prediction scheme is being applied to a composite fuselage structure where it is expected to have a significant change in load path due to buckling of one or more panels.

One of the drawback of the guide based technique discussed in the current work is the need to do computationally expensive engineering analysis. Global/local decomposition is very effective in compartmentalizing the design optimization process but it suffered with a serious drawback in case of composite structures, stacking sequence discontinuity. As part of the ongoing research work, a guide based technique is being developed which can be very effectively used with global/local decomposition of composite structural design problem. Initial research in this respect is very encouraging.

Appendix A: Other Works

In this appendix, a brief summary of the other research work done, which may not be directly related to the PhD research work but are an offshoot of it, is presented. To keep the discussion brief, we just present a small literature survey, approach, and the scope of the work instead of techincal details. The technical details are given in the corresponding publications given at the end of each section.

Design of recurve actuators

Related works

One of the design challenges of this new generation of actuator is their relative complexity. Recently, design optimization has emerged as a design tool for smart actuators. As demonstrated in a number of other studies [88, 89, 90, 91, 92, 93] mathematical optimization techniques offer an organized and methodical way of formulating and solving the design problem. This approach allows the designer to potentially use a large number of design variables and fewer simplifications in modeling the system. Better models, in turn, may reduce the number of iterations during the hardware-testing phase. The increasing speed of computer hardware and the development of faster computational models allow optimum designs to be obtained in a relatively short time. Furthermore, the application of the optimization techniques can provide a better understanding of the tradeoffs involved in the design, and may even highlight those trends that are not obvious.In this work, we study the optimal design of Recurve arrays. An analytic model of the static response of the Recurve actuator is derived. Two optimization problems for the Recurve array are formulated with material, packaging, and performance constraints. One formulation is based on minimum weight. The second formulation is based on energy efficiency. A genetic algorithm is used to find the optimum designs. Recurve arrays designed for maximum energy conversion efficiency are compared to those designed for minimum weight. Parametric studies are conducted to investigate the effect of the stiffness of the driven structure and the maximum deliverable voltage on the optimized designs. These optimization formulations are effective design tools for a relatively complex actuator.

Approach and scope

In this work, we focus our attention on the Recurve array proposed by Ervin and Brei [94, 95]. The Recurve array is a good candidate for design optimization because it has many design variables, both continuous and discrete. Because this is a mixed optimization problem we used a genetic algorithm [52]. We formulated the objective function in two ways. First, we define the optimization problem as a weight minimization problem. This formulation is appropriate for applications where weight and/or volume specifications are critical. Second, we define the optimization problem as an efficiency maximization problem. This formulation is appropriate for applications where the power source has limited capacity.

The optimization formulation developed also allows for a numerical study of the interaction between the drive electronics and the complexity of the Recurve array. As the maximum voltage that the drive amplifier can deliver is decreased, the complexity of the Recurve array increases. Conversely, as the maximum voltage increases, the Recurve array looks more and more like a single piece of PZT. Since high voltage amplifiers are more complex than their low voltage counterparts, we see an interesting trade between the size and complexity of the mechanical part of the actuator and the size and complexity of the drive electronics.

Please refer to Seresta *et al.* [96] for detailed description of model, analysis, and optimization formulation.

Design of active truss topology

Related works

An excellent monograph on recent advances and trends in smart structures optimization is given by Frecker [93]. A number of studies seem to suggest that energy requirements of piezoelectric actuators are to be included in the design process ([91, 97, 98]). Giurgiutiu *et al.* [99] considered the design of a stack based actuator for maximum energy output. Prechtl and Hall [100] considered different energy metrics as figures of merits for actuator design. Mukherjee and Joshi [101] studied design of actuator profiles for minimum power consumption. Abdalla *et al.* [102, 96] maximized energy efficiency of a stack actuator coupled to a structure modeled by a linear spring through a compliant mechanism.

Optimal placement of actuators is very crucial in smart structures design. Much work has been done to determine optimal placement of actuators/sensors in areas such as vibration suppression ([103, 104, 105, 106, 107, 108, 109, 110, 111, 112, 113]), acoustic control ([114]), truss structures ([115, 116]), shape control ([117, 118, 119, 120, 121]), and structural health monitoring ([122]). Most commonly used methods are genetic algorithms, heuristic integer programming, simulated annealing and tabu search. Recently, Cheng and Li [123] studied optimal placement and shape of actuators on a host structure for minimum power con-

sumption. However, the approaches mentioned above generally consider optimal actuator placement on fixed topology structures.

Chattopadhyay and Seeley [124] proposed a multiobjective optimization procedure based on continuous optimization / simulated annealing to address the combined problems of the synthesis of structures/controls and actuator location problem for the design of intelligent structures. Liu *et al.* [125] investigated the simultaneous topology design and fixed numbered actuator placement for truss structures using simulated annealing. Moini [126] proposed concurrent design of structure and distributed PZT actuators. The above approaches didn't include energy in the design framework.

Compliant mechanism amplifiers are often used in conjunction with piezoelectric actuators. Generally a topology optimization scheme is used to design the compliant mechanism with a fixed actuator configuration (Frecker *et al.* [127], Du *et al.* [128], Frecker and Canfield [129], Lau *et al.* [130], Bharti and Frecker [131], Carbonari *et al.* [132], Huang and Lan [133]). Johnson and Frecker [134] also studied the optimum active material location using genetic algorithms and ground structure approach. Recently, topology optimization methods are increasingly being used for simultaneous design of active and passive material distribution for two dimensional continuum structures (Carbonari *et al.* [135], Buehler *et al.* [136]). Investigation of actuator optimization using topology optimization method is first presented by Bharti and Frecker [137], who proposed a two step optimization process. In the first step the ground structure consists of only active elements, and in the second step replacing the active elements in the ground structure that have negative strain by passive elements i.e., the coupled effect of active and passive elements is considered in second step. The resulting structure has a mix of active and passive members, but the active members all have the same degree of activation. A more general interaction between active and passive material may be obtained by removing the constraint that the elements are made up of either only active or passive material. Moreover, in the previous design formulation, the maximization of output displacement was considered with a constraint on the available volume of the active material. As demonstrated in Zhu *et al.* [138], constraining input energy is a more relevant constraint, since input energy requirements drive the design of the drive electronics and power supply (e.g., batteries).

Approach and scope

In order to allow for a more general interaction between the actuator and the structure, the present study proposes a new optimization formulation. The present formulation is similar to the work of Bharti and Frecker [137] as we use truss elements to avoid bending of the piezoelectric material. This formulation improves the interpretability of the topology results in terms of distributed stack actuators, leading to better manufacturability provided that a dense grid of truss structure is used in the design (Bharti and Frecker [137]). The truss elements are assumed to be made partly of an active piezoelectric material and partly

of a passive material. The applied electric field is allowed to vary from one member to another. The crucial ingredient of the new formulation is the parameterization of the active truss member in terms of the cross sectional area of the member, the fraction of length occupied by piezoelectric material, and the input electric field to the piezoelectric material. In this fashion, the optimization process has maximum generality in distributing structural stiffness, active material, and actuation throughout the design domain. The conventional ground structure approach is adopted in the present work. The external structure to be driven by the ground truss active structure is modeled as a set of known constant loads acting on the actuator as well as a set of known linear springs of constant stiffness. This formulation allows for the modeling of prestress in the actuator, and for multipoint outputs. The proposed formulation also seeks to maximize a combination of output displacements rather than the displacement at any given point. A constraint is placed on the maximum available active truss material volume. The maximum available input electric energy of the active truss is also considered as a constraint on the design. By varying the value of the maximum available input electric energy, the trade-off between minimizing input energy and maximizing output displacements can be studied for various parametric values of the material constraints.

Please refer to Seresta *et al.* [139] for detailed description of model, analysis, and optimization formulation.

Summary

In this appendix, we provided a very brief summary of the related research works done. Design and optimization of recurve actuators using genetic algorithms is formulated. Energy metric is introduced in the design optimization process.

A new optimization formulation for active material distribution is formulated based on topology optimization method. The formulation is based on ground structure method and method of moving asymptotes is employed for structural sizing.

Appendix B: Composite laminate analysis

Strength analysis

The strength constraint λ_s is computed with a factor of safety 1.5 as,

$$\lambda_s = \frac{1}{1.5}\min\left\{\frac{\epsilon_{1,all}}{\epsilon_1}, \frac{\epsilon_{2,all}}{\epsilon_2}, \frac{\gamma_{12,all}}{\gamma_{12}}\right\}, \tag{B-1}$$

where $\epsilon_{1,all}$, $\epsilon_{2,all}$, $\gamma_{12,all}$ are the allowable strains.

Buckling analysis

The plate is assumed to be simply supported with dimensions a and b along x and y axes subjected to inplane loads N_x, N_y, and N_{xy}. Under normal biaxial load, the critical load is given by,

$$\lambda_n = \pi^2 \frac{\left[D_{11}\left(\frac{m}{a}\right)^4 + 2\left(D_{12}+2D_{66}\right)\left(\frac{m}{a}\right)^2\left(\frac{n}{b}\right)^2 + D_{22}\left(\frac{n}{b}\right)^4\right]}{\left(\frac{m}{a}\right)^2 N_x + \left(\frac{n}{b}\right)^2 N_y}, \tag{B-2}$$

where m and n are number of half waves in the x and y directions, respectively, selected as to minimize λ_n. D_{11}, D_{12}, D_{22}, and D_{66} are flexural stiffness coefficients. The shear buckling capacity λ_{sh} of the plate is calculated from the analytical solution for an infinite plate since modeling buckling for shear loading is computationally expensive and beyond the scope of the current work.

$$\lambda_{sh} = \frac{4\beta_1\left(D_{11}D_{22}^3\right)^4}{b^2 N_{xy}} \quad \text{for} \quad 1 \le \Gamma \le \infty \tag{B-3}$$

$$\lambda_{sh} = \frac{4\beta_1\sqrt{D_{22}\left(D_{12}+2D_{66}\right)}}{b^2 N_{xy}} \quad \text{for} \quad 0 \le \Gamma \le 1, \tag{B-4}$$

where Γ is given by

$$\Gamma = \frac{\sqrt{D_{11}D_{22}}}{(D_{12} + 2D_{66})}, \tag{B-5}$$

and the values of β_1 are given in Ref. [77, 140]. The combined biaxial buckling factor λ_b is given by $\min(\lambda, \lambda_{sh})$, where λ is given by, [140]

$$\frac{1}{\lambda} = \frac{1}{\lambda_n} + \frac{1}{\lambda_{sh}^2}. \tag{B-6}$$

Appendix C: Tensors and Condensation Procedure

Full form of tensors

The full forms of the tensors appearing in system of equations in Chapter 3 and Chapter 5 are,

$$g_l^u = \int_0^{\underline{a}}\int_0^{\underline{b}} \left[A_{11}\frac{u_0}{\underline{a}} + A_{12}\frac{v_0}{\underline{b}}\right]\phi_{l,x}^u dxdy$$

$$g_l^v = \int_0^{\underline{a}}\int_0^{\underline{b}} \left[A_{12}\frac{u_0}{\underline{a}} + A_{22}\frac{v_0}{\underline{b}}\right]\phi_{l,y}^v dxdy$$

$$g_l^{ux} = \int_0^{\underline{a}}\int_0^{\underline{b}} A_{11}\phi_{l,x}^u dxdy$$

$$g_l^{uy} = \int_0^{\underline{a}}\int_0^{\underline{b}} A_{12}\phi_{l,x}^u dxdy$$

$$g_l^{uxy} = \int_0^{\underline{a}}\int_0^{\underline{b}} A_{66}\phi_{l,y}^u dxdy$$

$$
\begin{aligned}
g_l^{vx} &= \int_0^{\underline{a}}\int_0^{\underline{b}} A_{12}\phi_{l,y}^v dxdy \\
g_l^{vy} &= \int_0^{\underline{a}}\int_0^{\underline{b}} A_{22}\phi_{l,y}^v dxdy \\
g_l^{vxy} &= \int_0^{\underline{a}}\int_0^{\underline{b}} A_{66}\phi_{l,x}^v dxdy
\end{aligned}
$$

$$
\begin{aligned}
K_{il}^{ub} &= \int_0^{\underline{a}}\int_0^{\underline{b}} [A_{11}\phi_{i,x}^u\phi_{l,x}^u + A_{66}\phi_{i,y}^u\phi_{l,y}^u]dxdy \\
K_{il}^{uc} &= \int_0^{\underline{a}}\int_0^{\underline{b}} [A_{12}\phi_{i,y}^v\phi_{l,x}^u + A_{66}\phi_{i,x}^v\phi_{l,y}^u]dxdy
\end{aligned}
$$

$$
K_{ijl}^{ua} = \frac{1}{2}\int_0^{\underline{a}}\int_0^{\underline{b}} [A_{11}\phi_{i,x}^w\phi_{j,x}^w\phi_{l,x}^u + A_{12}\phi_{i,y}^w\phi_{j,y}^w\phi_{i,x}^u + A_{66}\phi_{i,x}^w\phi_{j,y}^w\phi_{l,y}^u + A_{66}\phi_{i,y}^w\phi_{j,x}^w\phi_{l,y}^u]dxdy
$$

$$
\begin{aligned}
K_{il}^{vb} &= \int_0^{\underline{a}}\int_0^{\underline{b}} [A_{12}\phi_{i,x}^u\phi_{l,y}^v + A_{66}\phi_{i,y}^u\phi_{l,x}^v]dxdy \\
K_{il}^{vc} &= \int_0^{\underline{a}}\int_0^{\underline{b}} [A_{22}\phi_{i,y}^v\phi_{l,y}^v + A_{66}\phi_{i,x}^v\phi_{l,x}^v]dxdy
\end{aligned}
$$

$$
K_{ijl}^{va} = \frac{1}{2}\int_0^{\underline{a}}\int_0^{\underline{b}} [A_{12}\phi_{i,x}^w\phi_{j,x}^w\phi_{l,y}^v + A_{22}\phi_{i,y}^w\phi_{j,y}^w\phi_{l,y}^v + A_{66}\phi_{i,x}^w\phi_{j,y}^w\phi_{l,x}^v + A_{66}\phi_{i,y}^w\phi_{j,x}^w\phi_{l,x}^v]dxdy
$$

$$
\begin{aligned}
\bar{K}_{il} &= \int_0^{\underline{a}}\int_0^{\underline{b}} [D_{11}\phi_{i,xx}^w\phi_{l,xx}^w + D_{12}\phi_{i,yy}^w\phi_{l,xx}^w + D_{12}\phi_{i,xx}^w\phi_{l,yy}^w + D_{22}\phi_{i,yy}^w\phi_{l,yy}^w + 2D_{16}\phi_{i,xy}^w\phi_{l,xx}^w + \\
&\qquad 2D_{16}\phi_{i,xx}^w\phi_{l,xy}^w + 2D_{26}\phi_{i,xy}^w\phi_{l,yy}^w + 2D_{26}\phi_{i,yy}^w\phi_{l,xy}^w + 4D_{66}\phi_{i,xy}^w\phi_{l,xy}^w]dxdy \\
\bar{K}_{il}^g &= \int_0^{\underline{a}}\int_0^{\underline{b}} \left[\left(A_{11}\frac{u_0}{\underline{a}} + A_{12}\frac{v_0}{\underline{b}}\right)\phi_{i,x}^w\phi_{l,x}^w + \left(A_{12}\frac{u_0}{\underline{a}} + A_{22}\frac{v_0}{\underline{b}}\right)\phi_{i,y}^w\phi_{l,x}^w\right]dxdy
\end{aligned}
$$

$$\bar{K}_{il}^{gx} = \int_0^{\underline{a}}\int_0^{\underline{b}} \left[A_{11}\phi_{i,x}^{w}\phi_{l,x}^{w} + A_{12}\phi_{i,y}^{w}\phi_{l,x}^{w}\right] dxdy$$

$$\bar{K}_{il}^{gy} = \int_0^{\underline{a}}\int_0^{\underline{b}} \left[A_{12}\phi_{i,x}^{w}\phi_{l,x}^{w} + A_{22}\phi_{i,y}^{w}\phi_{l,y}^{w}\right] dxdy$$

$$\bar{K}_{il}^{gxy} = \int_0^{\underline{a}}\int_0^{\underline{b}} \left[A_{66}\phi_{i,y}^{w}\phi_{l,x}^{w} + A_{66}\phi_{i,x}^{w}\phi_{l,y}^{w}\right] dxdy$$

$$K_{ikl}^{wba} = \int_0^{\underline{a}}\int_0^{\underline{b}} [A_{11}\phi_{i,x}^{u}\phi_{k,x}^{w}\phi_{l,x}^{w} + A_{12}\phi_{i,x}^{u}\phi_{k,y}^{w}\phi_{l,y}^{w} + A_{66}\phi_{i,y}^{u}\phi_{k,y}^{w}\phi_{l,x}^{w} + A_{66}\phi_{i,y}^{u}\phi_{k,x}^{w}\phi_{l,y}^{w}]dxdy$$

$$K_{ikl}^{wca} = \int_0^{\underline{a}}\int_0^{\underline{b}} [A_{12}\phi_{i,y}^{v}\phi_{k,x}^{w}\phi_{l,x}^{w} + A_{22}\phi_{i,y}^{v}\phi_{k,y}^{w}\phi_{l,y}^{w} + A_{66}\phi_{i,x}^{v}\phi_{k,y}^{w}\phi_{l,x}^{w} + A_{66}\phi_{i,x}^{v}\phi_{k,x}^{w}\phi_{l,y}^{w}]dxdy$$

$$\begin{aligned}\bar{K}_{ijkl}^{waa} = \frac{1}{2}\int_0^{\underline{a}}\int_0^{\underline{b}} [&A_{11}\phi_{i,x}^{w}\phi_{j,x}^{w}\phi_{k,x}^{w}\phi_{l,x}^{w} + A_{12}\phi_{i,y}^{w}\phi_{j,y}^{w}\phi_{k,x}^{w}\phi_{l,x}^{w} + A_{12}\phi_{i,x}^{w}\phi_{j,x}^{w}\phi_{k,y}^{w}\phi_{l,y}^{w} + \\ &A_{22}\phi_{i,y}^{w}\phi_{j,y}^{w}\phi_{k,y}^{w}\phi_{l,y}^{w} + A_{66}\phi_{i,x}^{w}\phi_{j,y}^{w}\phi_{k,y}^{w}\phi_{l,x}^{w} + A_{66}\phi_{i,x}^{w}\phi_{j,y}^{w}\phi_{k,x}^{w}\phi_{l,y}^{w} + \\ &A_{66}\phi_{i,y}^{w}\phi_{j,x}^{w}\phi_{k,y}^{w}\phi_{l,x}^{w} + A_{66}\phi_{i,y}^{w}\phi_{j,x}^{w}\phi_{k,x}^{w}\phi_{l,y}^{w}]dxdy\end{aligned}$$

Condensation procedure

The condensation procedure involves readjusting and reordering of the tensors in the following manners:

$$\{\boldsymbol{e}\} = \left\{ \begin{array}{c} \{\boldsymbol{b}\} \\ \{\boldsymbol{c}\} \end{array} \right\},$$

$$\{\boldsymbol{g}\} = \left\{ \begin{array}{c} \{\boldsymbol{g}^u\} \\ \{\boldsymbol{g}^v\} \end{array} \right\},$$

$$[\boldsymbol{K}^a] = \left[\begin{array}{cc} [\boldsymbol{K}^{ub}] & [\boldsymbol{K}^{uc}] \\ [\boldsymbol{K}^{vb}] & [\boldsymbol{K}^{vc}] \end{array} \right],$$

$$K_{ijp}^{ab} = \left\{ \begin{array}{ll} K_{ijl}^{uaa} & for \quad p = 1, 2, 3, \cdots, 2n \\ K_{ijl}^{vaa} & for \quad p = 2n+1, \cdots, 4n \end{array} \right. , \text{and}$$

$$K_{pkl}^{ba} = \begin{cases} K_{ikl}^{wba} & for \quad p = 1, 2, 3, \cdots, 2n \\ K_{ikl}^{wca} & for \quad p = 2n+1, \cdots, 4n \end{cases} .$$

Then, e_p is given as,

$$e_p = \lambda^T \left(K_{pl}^{-a} g_l \right) - K_{ps}^{-a} K_{ijs}^{ab} a_i a_j = \lambda^T h_p - K_{ps}^{-a} K_{ijs}^{ab} a_i a_j.$$

Substituting e_p in last equation of Eq. (3.8), we the get following equation,

$$K_{il} a_i - \lambda^T \bar{K}_{il}^g a_i + K_{pkl}^{ba} \left(\lambda^T h_p - K_{ps}^{-a} K_{ijs}^{ab} a_i a_j \right) a_k + K_{ijkl}^{waaa} a_i a_j a_k = 0$$

Rearranging the terms in the above equation, we get the final equation as,

$$\begin{array}{l} \left[K_{il} - \lambda^T \left(\bar{K}_{il}^g - K_{pil}^{ba} h_p \right) \right] a_i + \left(K_{ijkl}^{waaa} - K_{pkl}^{ba} K_{ps}^{-a} K_{ijs}^{ab} \right) a_i a_j a_k = 0, \text{or} \\ \left[K_{il} - \lambda^T K_{il}^g \right] a_i + K_{ijkl}^{NL} a_i a_j a_k = 0 \end{array} .$$

Appendix D: Flutter Model

Plate model for moderately large deformation

The thermal forces generated due to uniform temperature differential ΔT is given by

$$\left\{ \begin{array}{c} N_x^T \\ N_y^T \\ N_{xy}^T \end{array} \right\} = \sum_{k=1}^{N} \int_{z_{k-1}}^{z_k} \left[\begin{array}{ccc} \overline{Q}_{11} & \overline{Q}_{12} & \overline{Q}_{16} \\ \overline{Q}_{12} & \overline{Q}_{22} & \overline{Q}_{26} \\ \overline{Q}_{16} & \overline{Q}_{26} & \overline{Q}_{66} \end{array} \right]_k \left\{ \begin{array}{c} \overline{\alpha}_1 \\ \overline{\alpha}_2 \\ \overline{\alpha}_6 \end{array} \right\}_k \Delta T dz,$$

where $\left(\overline{Q}_{ij}\right)_k$ are the reduced stiffness coefficients given in terms of engineering constants of the material and the fiber orientation angle of the k^{th} layer (see Appendix A). In the above equation, N is the total number of plies. $\left(\overline{\alpha}_i\right)_k$ are the transformed material coefficients.

Assuming that the plate is thin, such that the Kirchoff hypothesis is valid, the inplane strain components are given by,

$$\epsilon_x = \epsilon_x^0 + z\kappa_x, \epsilon_y = \epsilon_y^0 + z\kappa_y, \gamma_{xy} = \gamma_{xy}^0 + z\kappa_{xy}.$$

The superscript $(^0)$ indicates the associated quantity at the mid surface. Using von Kármán equations, the mid plane strain vector in terms of mid plane displacements u, v, and w is given by,

$$\left\{ \begin{array}{c} \epsilon_x^0 \\ \epsilon_y^0 \\ \gamma_{xy}^0 \end{array} \right\} = \left\{ \begin{array}{c} u_{,x} + \frac{1}{2} w_{,x}^2 \\ v_{,y} + \frac{1}{2} w_{,y}^2 \\ u_{,y} + v_{,x} + w_{,x} w_{,y} \end{array} \right\}.$$

The bending curvature vector is given by,

$$\left\{ \begin{array}{c} \kappa_x \\ \kappa_y \\ \kappa_{xy} \end{array} \right\} = \left\{ \begin{array}{c} -w_{,xx} \\ -w_{,yy} \\ -2w_{,xy} \end{array} \right\}.$$

The subscript (“,x” or “,y”) denotes space derivative with respect to the variables x and y.

The kinetic energy T is given by,

$$T = \frac{1}{2} \int_0^{\underline{a}} \int_0^{\underline{b}} m \left(\frac{\partial w}{\partial t} \right)^2 dxdy.$$

The strain energy U of symmetric and balanced laminate is given by,

$$\begin{aligned} U &= \frac{1}{2} \int_0^{\underline{a}} \int_0^{\underline{b}} [A_{11} \left(\epsilon_x^0\right)^2 + 2A_{12}\epsilon_x^0\epsilon_y^0 + A_{22} \left(\epsilon_y^0\right)^2 + A_{66} \left(\gamma_{xy}^0\right)^2 + D_{11}\kappa_x^2 + 2D_{12}\kappa_x\kappa_y + D_{22}\kappa_y^2 + \\ &\quad 2D_{16}\kappa_x\kappa_{xy} + 2D_{26}\kappa_y\kappa_{xy} + D_{66}\kappa_{xy}^2]dxdy, \end{aligned}$$

where the inplane stiffnesses - A_{11}, A_{12}, A_{22}, and A_{66}, and the flexural stiffnesses - D_{11}, D_{12}, D_{22}, D_{16}, D_{26} and D_{66} of the laminate are given in terms of engineering constants of the material (see [77]). The work done by the aerodynamic load is given in terms of pressure distribution Δp by,

$$Q_A = \int_0^{\underline{a}} \int_0^{\underline{b}} \Delta p w(x, y, t) dxdy,$$

and the work done by the thermal load is given by,

$$\overline{W} = \int_0^{\underline{a}} \int_0^{\underline{b}} \left(N_x^T \epsilon_x^0 + N_y^T \epsilon_y^0 + N_{xy}^T \gamma_{xy}^0 \right) dxdy.$$

Thus, the total work done by external load is given by,

$$W = Q_A + \overline{W}.$$

The pressure distribution on an initially flat panel using third order piston theory is given in terms of density of air ρ_∞, speed of sound a_∞, and downwash velocity V_z as [141, 79],

$$\Delta p = \rho_\infty a_\infty^2 \left(\frac{V_z}{a_\infty} + \frac{1}{2} \frac{V_z^2}{a_\infty^2} + \frac{1}{6} \frac{V_z^3}{a_\infty^3} \right).$$

The downwash velocity V_z is given in terms of flow velocity U_∞, and lateral displacement w as

$$V_z = U_\infty \frac{\partial w}{\partial x} + \frac{\partial w}{\partial t}.$$

Full form of the tensors that appear in the model

The terms in Eqs. (4.5), (4.6), and (4.7) are given as,

$$g_l^u = \int_0^{\underline{a}}\int_0^{\underline{b}} [N_x^T \phi_{l,x}^u + N_{xy}^T \phi_{l,y}^u] dxdy$$

$$g_l^v = \int_0^{\underline{a}}\int_0^{\underline{b}} [N_y^T \phi_{l,y}^v + N_{xy}^T \phi_{l,x}^v] dxdy$$

$$K_{il}^{ub} = \int_0^{\underline{a}}\int_0^{\underline{b}} [A_{11}\phi_{i,x}^u \phi_{l,x}^u + A_{66}\phi_{i,y}^u \phi_{l,y}^u] dxdy$$

$$K_{il}^{uc} = \int_0^{\underline{a}}\int_0^{\underline{b}} [A_{12}\phi_{i,y}^v \phi_{l,x}^u + A_{66}\phi_{i,x}^v \phi_{l,y}^u] dxdy$$

$$K_{ijl}^{ua} = \frac{1}{2}\int_0^{\underline{a}}\int_0^{\underline{b}} [A_{11}\phi_{i,x}^w \phi_{j,x}^w \phi_{l,x}^u + A_{12}\phi_{i,y}^w \phi_{j,y}^w \phi_{i,x}^u + A_{66}\phi_{i,x}^w \phi_{j,y}^w \phi_{l,y}^u + A_{66}\phi_{i,y}^w \phi_{j,x}^w \phi_{l,y}^u] dxdy$$

$$K_{il}^{vb} = \int_0^{\underline{a}}\int_0^{\underline{b}} [A_{12}\phi_{i,x}^u \phi_{l,y}^v + A_{66}\phi_{i,y}^u \phi_{l,x}^v] dxdy$$

$$K_{il}^{vc} = \int_0^{\underline{a}}\int_0^{\underline{b}} [A_{22}\phi_{i,y}^v \phi_{l,y}^v + A_{66}\phi_{i,x}^v \phi_{l,x}^v] dxdy$$

$$K_{ijl}^{va} = \frac{1}{2}\int_0^{\underline{a}}\int_0^{\underline{b}} [A_{12}\phi_{i,x}^w \phi_{j,x}^w \phi_{l,y}^v + A_{22}\phi_{i,y}^w \phi_{j,y}^w \phi_{l,y}^v + A_{66}\phi_{i,x}^w \phi_{j,y}^w \phi_{l,x}^v + A_{66}\phi_{i,y}^w \phi_{j,x}^w \phi_{l,x}^v] dxdy$$

$$M_{il} = \int_0^{\underline{a}}\int_0^{\underline{b}} m\phi_i^w \phi_l^w dxdy$$

$$\bar{K}_{il}^s = \int_0^{\underline{a}}\int_0^{\underline{b}} [D_{11}\phi_{i,xx}^w \phi_{l,xx}^w + D_{12}\phi_{i,yy}^w \phi_{l,xx}^w + D_{12}\phi_{i,xx}^w \phi_{l,yy}^w + D_{22}\phi_{i,yy}^w \phi_{l,yy}^w + 2D_{16}\phi_{i,xy}^w \phi_{l,xx}^w + 2D_{16}\phi_{i,xx}^w \phi_{l,xy}^w + 2D_{26}\phi_{i,xy}^w \phi_{l,yy}^w + 2D_{26}\phi_{i,yy}^w \phi_{l,xy}^w + 4D_{66}\phi_{i,xy}^w \phi_{l,xy}^w] dxdy$$

$$\bar{K}^{g}_{il} = \int_0^{\underline{a}}\int_0^{\underline{b}} [N^T_x \phi^w_{i,x}\phi^w_{l,x} + N^T_y \phi^w_{i,y}\phi^w_{l,x} + N^T_{xy}(\phi^w_{i,y}\phi^w_{l,x} + \phi^w_{i,x}\phi^w_{l,y})]dxdy$$

$$K^{wba}_{ikl} = \int_0^{\underline{a}}\int_0^{\underline{b}} [A_{11}\phi^u_{i,x}\phi^w_{k,x}\phi^w_{l,x} + A_{12}\phi^u_{i,x}\phi^w_{k,y}\phi^w_{l,y} + A_{66}\phi^u_{i,y}\phi^w_{k,y}\phi^w_{l,x} + A_{66}\phi^u_{i,y}\phi^w_{k,x}\phi^w_{l,y}]dxdy$$

$$K^{wca}_{ikl} = \int_0^{\underline{a}}\int_0^{\underline{b}} [A_{12}\phi^v_{i,y}\phi^w_{k,x}\phi^w_{l,x} + A_{22}\phi^v_{i,y}\phi^w_{k,y}\phi^w_{l,y} + A_{66}\phi^v_{i,x}\phi^w_{k,y}\phi^w_{l,x} + A_{66}\phi^v_{i,x}\phi^w_{k,x}\phi^w_{l,y}]dxdy$$

$$\begin{aligned}\bar{K}^{waa}_{ijkl} = \frac{1}{2}\int_0^{\underline{a}}\int_0^{\underline{b}} [&A_{11}\phi^w_{i,x}\phi^w_{j,x}\phi^w_{k,x}\phi^w_{l,x} + A_{12}\phi^w_{i,y}\phi^w_{j,y}\phi^w_{k,x}\phi^w_{l,x} + A_{12}\phi^w_{i,x}\phi^w_{j,x}\phi^w_{k,y}\phi^w_{l,y} + \\ &A_{22}\phi^w_{i,y}\phi^w_{j,y}\phi^w_{k,y}\phi^w_{l,y} + A_{66}\phi^w_{i,x}\phi^w_{j,y}\phi^w_{k,y}\phi^w_{l,x} + A_{66}\phi^w_{i,x}\phi^w_{j,y}\phi^w_{k,x}\phi^w_{l,y} + \\ &A_{66}\phi^w_{i,y}\phi^w_{j,x}\phi^w_{k,y}\phi^w_{l,x} + A_{66}\phi^w_{i,y}\phi^w_{j,x}\phi^w_{k,x}\phi^w_{l,y}]dxdy\end{aligned}$$

$$K^{(1)}_{il} = \rho_\infty a^2_\infty M_\infty \int_0^{\underline{a}}\int_0^{\underline{b}} \phi^w_{i,x}\phi^w_l dxdy$$

$$K^{(2)}_{il} = \rho_\infty a_\infty \int_0^{\underline{a}}\int_0^{\underline{b}} \phi^w_i \phi^w_l dxdy$$

$$K^{(3)}_{ijl} = \frac{1}{2}\rho_\infty a^2_\infty M^2_\infty \int_0^{\underline{a}}\int_0^{\underline{b}} \phi^w_{i,x}\phi^w_{j,x}\phi^w_l dxdy$$

$$K^{(4)}_{ijl} = \rho_\infty a_\infty M_\infty \int_0^{\underline{a}}\int_0^{\underline{b}} \phi^w_{i,x}\phi^w_j \phi^w_l dxdy$$

$$K^{(5)}_{ijl} = \frac{1}{2}\rho_\infty \int_0^{\underline{a}}\int_0^{\underline{b}} \phi^w_i \phi^w_j \phi^w_l dxdy$$

$$
\begin{aligned}
K_{ijkl}^{(6)} &= \frac{\rho_\infty a_\infty^2 M_\infty^3}{6} \int_0^{\frac{a}{2}} \int_0^{\frac{b}{2}} \phi_{i,x}^w \phi_{j,x}^w \phi_{k,x}^w \phi_l^w dxdy \\
K_{ijkl}^{(7)} &= \frac{\rho_\infty a_\infty M_\infty^2}{2} \int_0^{\frac{a}{2}} \int_0^{\frac{b}{2}} \phi_{i,x}^w \phi_{j,x}^w \phi_k^w \phi_l^w dxdy \\
K_{ijkl}^{(8)} &= \frac{\rho_\infty M_\infty}{2} \int_0^{\frac{a}{2}} \int_0^{\frac{b}{2}} \phi_{i,x}^w \phi_j^w \phi_k^w \phi_l^w dxdy \\
K_{ijkl}^{(9)} &= \frac{\rho_\infty}{6a_\infty} \int_0^{\frac{a}{2}} \int_0^{\frac{b}{2}} \phi_i^w \phi_j^w \phi_k^w \phi_l^w dxdy
\end{aligned}
$$

Bibliography

[1] Liaw, D. G., "Nonlinear Supersonic Flutter of Laminated Composite Plates under Thermal Loads," *Computers and Structures*, Vol. 65, No. 5, 1997, pp. 733–740.

[2] Schmit, L. A. and Farshi, B., "Optimum Design of Laminate Fiber Composite Plates," *International Journal for Numerical Methods in Engineering*, 1977, pp. 623–640.

[3] Nagendra, S., Haftka, R. T., and Gürdal, Z., "Stacking Sequence Optimization of Simply Supported Laminates with Stability and Strain Constraints," *AIAA Journal*, Vol. 30, No. 8, 1992, pp. 2132–2137.

[4] Miki, M. and Sugiyama, Y., "Optimum Design of Laminated Composite Plates using Lamination Parameters," *AIAA Journal*, Vol. 31, No. 5, 1993, pp. 921–922.

[5] Le Riche, R. and Haftka, R. T., "Optimization of Stacking Sequence Design for Buckling Load Maximization using Genetic Algorithm," *AIAA Journal*, Vol. 31, No. 5, 1993, pp. 951–956.

[6] Kogiso, N., Watson, L. T., Gürdal, Z., and Haftka, R. T., "Genetic Algorithms with Local Improvement for Composite Laminate Design," *Structural Optimization*, Vol. 7, No. 4, 1994, pp. 207–218.

[7] Kogiso, N., Watson, L. T., Gürdal, Z., Haftka, R. T., and Nagendra, S., "Minimum Thickness Design of Composite Laminates Subject to Buckling and Strength Constraints by Genetic Algorithms," *Proceedings of the* 35^{th} *AIAA/ASME/ASCE/AHS/ ASC Structures, Structural Dynamics and Materials Conference*, New York, NY, USA, 1994, pp. 2257–2275.

[8] Soremekun, G., Gürdal, Z., Haftka, R. T., and Watson, L. T., "Composite Laminate Design Optimization by Genetic Algorithm with Generalized Elitist Selection," *Computers & Structures*, Vol. 79, No. 2, 2001, pp. 131–143.

[9] Gantovnik, V., Anderson-Cook, M. C., Gürdal, Z., and Watson, L. T., "A Genetic Algorithm with Memory for Mixed Discrete-Continuous Design Optimization," *Computers & Structures*, Vol. 81, No. 20, 2003, pp. 2003–2009.

[10] Gantovnik, V., Gürdal, Z., Watson, L. T., and Anderson-Cook, M. C., "Genetic Algorithm for Mixed Integer Nonlinear Programming Problems using Separate Constraint Approximations," *AIAA Journal*, Vol. 43, No. 8, 2005, pp. 1844–1849.

[11] Lansing, W., Dwyer, W., Emerton, R., and Ranalli, E., "Application of Fully Stressed Design Procedures to Wing and Empennage Structures," *Journal of Aircraft*, Vol. 8, No. 9, 1971, pp. 683–688.

[12] Giles, G. L., "Procedure for Automating Aircraft Wing Structural Design," *Journal of Structural Division, ASCE*, Vol. 97, 1971, pp. 99–113.

[13] Sobieszczanski-Sobieski, J. and Loendorf, D., "A Mixed Optimization Method for Automated Design of Fuselage Structures," *Journal of Aircraft*, Vol. 9, No. 12, 1972, pp. 805–811.

[14] Schmit, L. A. and Ramanathan, R. K., "Multilevel Approach to Minimum Weight Design including Buckling Constraints," *AIAA Journal*, Vol. 16, No. 2, 1978, pp. 97–104.

[15] Schmit, L. A. and Mehrinfar, M., "Multilevel Optimum Design of Structures with Fiber Composite Stiffened Panel Components," *AIAA Journal*, Vol. 20, No. 1, 1982, pp. 138–147.

[16] Sobieszczanski-Sobieski, J., James, B. B., and Dovi, A., "Structural Optimization by Multilevel Decomposition," *AIAA Journal*, Vol. 23, No. 11, 1985, pp. 1775–1782.

[17] Sobieszczanski-Sobieski, J., James, B. B., and Riley, M. F., "Structural Sizing by Generalized Multilevel Optimization," *AIAA Journal*, Vol. 25, No. 1, 1987, pp. 139–145.

[18] Thareja, R. and Haftka, R. T., "Numerical Difficulties Asscoiated with using Equality Constraints to achieve Multilevel Decomposition in Structural Optimization," *Proceedings of the* 27^{th} *AIAA/ASME/ASCE/AHS/ASC Structures, Structural Dynamics and Materials Conference*, San Antonio, TX, USA, 1986, pp. 21–28.

[19] Ragon, S. A., Gürdal, Z., Haftka, R. T., and Tzong, T. J., "Bilevel Design of Wing Structure using Response Surfaces," *Journal of Aircraft*, Vol. 40, No. 5, 2003, pp. 985–992.

[20] Liu, B., Haftka, R. T., and Akgün, M. A., "Two Level Composite Wing Structure Optimization using Response Surfaces," *Structural and Multidisciplinary Optimization*, Vol. 20, 2000, pp. 87–96.

[21] Sobieszczanski-Sobieski, J., "Optimization by Decomposition: A Step from Hierarchic to Non-Hierarchic Systems," *Proceedings of the* 2^{nd} *NASA/USAF Symposium on Recent Advances in Multidisciplinary Analysis and Optimization*, 1989, pp. 51–78.

[22] Renaud, J. E. and Gabriele, G. A., "Improved Coordination in Non Hierarchic System Optimization," *AIAA Journal*, Vol. 31, No. 12, 1993, pp. 2367–2373.

[23] Renaud, J. E. and Gabriele, G. A., "Approximation in Non Hierarchic System Optimization," *AIAA Journal*, Vol. 32, No. 1, 1994, pp. 198–205.

[24] Braun, R. D. and Kroo, I., "Development and Application of the Collaborative Optimization Architecture in a Multidisciplinary Design Environment," *Multidisciplinary Design Optimization, State of the Art, edited by N. Alexandrov and M. Y. Hussaini*, Society of Industrial and Applied Mathematics, Philadelphia, 1987.

[25] Braun, R. D. and Kroo, I., "Collaborative Optimization using Response Surfaces Estimation," *AIAA Journal*, Vol. 38, No. 10, 1998, pp. 1931–1938.

[26] Cramer, E. J., Dennis, J. E., Frank, P. D., Lewis, R. M., and Shubin, G. R., "Problem Formulation for Multidisciplinary Design Optimization," *SIAM Journal on Optimization*, Vol. 4, No. 4, 1994, pp. 754–776.

[27] Sobieszczanski-Sobieski, J., Agte, J., and Jr, R. S., "Bi-Level Integrated System Synthesis (BLISS)," *Proceedings of the AIAA/USAF/NASA/ISSMO* 7^{th} *Symposium on Multidisciplinary Analysis and Optimization, AIAA, Reston, VA*, 1998, pp. 1543–1557.

[28] Kodiyalam, S. and Sobieszczanski-Sobieski, J., "Bilevel Integrated System Synthesis with Response Surfaces," *AIAA Journal*, Vol. 38, No. 8, 2000, pp. 1479–1485.

[29] Liu, B. and Haftka, R. T., "Composite Wing Structural Design Optimization with Continuity Constraints," *Proceedings of the* 42^{nd} *AIAA/ASME/ASCE/AHS/ASC Structures, Structural Dynamics and Materials Conference, Arpil 16-19*, Seattle, WA, USA, 2001, pp. 1–12.

[30] Soremekun, G., Gürdal, Z., Kassapoglou, C., and Toni, D., "Stacking Sequence Blending of Multiple Composite Laminates using Genetic Algorithm," *Composite Structures*, Vol. 56, No. 1, 2002, pp. 53–62.

[31] Adams, D. B., Watson, L. T., and Gürdal, Z., "Optimization and Blending of Composite Laminates using Genetic Algorithms with Migration," *Mechanics of Advanced Materials and Structures*, Vol. 10, No. 3, 2003, pp. 183–203.

[32] Adams, D. B., Watson, L. T., Gürdal, Z., and Anderson-Cook, C. M., "Genetic Algorithm Optimization and Blending of Composite Laminates by Locally Reducing Laminate Thickness," *Advances in Engineering Software*, Vol. 35, No. 1, 2004, pp. 35–45.

[33] Shin, D. K., Gürdal, Z., and Griffin, O. H., "Minimum Weight Design of Laminated Composite Plates for Postbuckling Performance," *Proceedings of the* 32^{nd} *AIAA/ASME/ASCE/AHS/ASC Structures, Structural Dynamics and Materials Conference, April 8-10*, Baltimore, MD, USA, 1991, pp. 257–266.

[34] Starnes, J. H. and Rouse, M., "Postbuckling and Failure Characteristics of Selected Flat Rectangular Graphite-Eposxy Panels Loaded in Compression," *Proceedings of the* 22^{nd} *AIAA/ASME/ASCE/AHS/ASC Structures, Structural Dynamics and Materials Conference, April*, Atlanta, GA, USA, 1981, pp. 423–434.

[35] Perry, A. C., Gürdal, Z., and Starnes Jr., J. H., "Minimum-Weight Design of Compressively Loaded Stiffened Panels for Postbuckling Response," *Engineering Optimization*, Vol. 28, 1997, pp. 175–197.

[36] Adali, S., Walker, M., and Verijenko, V. E., "Multiobjective Optimization of Laminated Plates for Maximum Prebuckling, Buckling and Postbuckling Strength using Continuous and Discrete Ply Angles," *Composite Structures*, Vol. 35, No. 1, 1996, pp. 117–130.

[37] Diaconu, C. G. and Weaver, P. M., "Approximate Solution and Optimum Design of Compression Loaded, Postbuckled Laminated Composite Plates," *AIAA Journal*, Vol. 43, No. 4, 2005, pp. 906–914.

[38] Dowell, E. H., "Nonlinear Oscillations of a Fluttering Plate," *AIAA Journal*, Vol. 4, No. 7, 1966, pp. 1267–1275.

[39] Dowell, E. H., "Nonlinear Oscillations of a Fluttering Plate II," *AIAA Journal*, Vol. 5, No. 10, 1967, pp. 1856–1862.

[40] Librescu, L., *Elastostatics and Kinetics of Anisotropic and Heterogenous Shell-type Structures*, Noordhoff International, Leyden, 1975.

[41] Librescu, L., "Aeroelastic Stability of Orthotropic Heterogeneous Thin Panels in the Vicinity of the Flutter Critical Boundary, Part One: Simply Supported Panels," *Journal de Mécanique*, Vol. 4, No. 1, 1965, pp. 51–76.

[42] Librescu, L., "Aeroelastic Stability of Orthotropic Heterogeneous Thin Panels in the Vicinity of the Flutter Critical Boundary, Part Two," *Journal de Mécanique*, Vol. 6, No. 1, 1967, pp. 133–152.

[43] Chatterjee, S. N. and Kulkarni, S. V., "Effects of Environment, Damping and Shear Deformations on Flutter of Laminated Composite Panels," *International Journal of Solids and Structures*, Vol. 15, No. 6, 1979, pp. 479–491.

[44] Oyibo, G. A., "Flutter of Orthotropic Panels in Supersonic Flow using Affine Transformations," *AIAA Journal*, Vol. 21, No. 2, 1983, pp. 283–289.

[45] Birman, V. and Librescu, L., "Supersonic Flutter of Shear Deformable Laminated Composite Flat Panels," *Journal of Sound and Vibration*, Vol. 139, No. 2, 1990, pp. 265–275.

[46] Dixon, I. R. and Mei, C., "Finite Element Analysis of Large-Amplitude Panel Flutter of Thin laminates," *AIAA Journal*, Vol. 31, No. 4, 1993, pp. 701–707.

[47] Marzocca, P., Lazzaro, R., and Librescu, L., "Flutter/Aeroelastic response of Panels via a Combined Galerkin-Volterra Approach," *Proceeding of the* 45^{th} *AIAA/ASME/ ASCE/AHS/ASC Structures, Structural Dynamics, and Materials Conference, April 19-22*, Palm Springs, CA, USA, 2004, pp. 1–12.

[48] Lee, I., Lee, D. M., and Oh, I. K., "Supersonic Flutter Analysis of Stiffened Laminated Plates Subject to Thermal Load," *Journal of Sound and Vibration*, Vol. 224, No. 1, 1999, pp. 49–67.

[49] Liaw, D. G., "Supersonic Flutter of Laminated Thin Plates with Thermal Effects," *AIAA Journal of Aircraft*, Vol. 30, No. 1, 1993, pp. 105–111.

[50] Cheng, G. and Mei, C., "Finite Element Modal Formulation for Hypersonic Panel Flutter Analysis with Thermal Effects," *AIAA Journal*, Vol. 42, No. 4, 2004, pp. 687–695.

[51] Bolotin, V. V., *Nonconservative Problems of the Theory of Elasticity (translated from Russian)*, New York, Macmillan, 1963.

[52] McMahon, M. T., Watson, L. T., Soremekun, G., Gürdal, Z., and Haftka, R. T., "A Fortran 90 Genetic Algorithm Module for Composite Laminate Structure Design," *Engineering Computers*, Vol. 14, 1998, pp. 260–273.

[53] Soremekun, G., Gürdal, Z., Haftka, R. T., and Watson, L. T., "Composite Laminate Design Optimization by Genetic Algorithm with Generalized Elitist Selection," *Computers and Structures*, Vol. 79, No. 2, 2001, pp. 131–143.

[54] Venkataraman, S. and Haftka, R. T., "Structural Optimization Complexity: What has Moore's Law done for us?" *Structural and Multidisciplinary Optimization*, Vol. 28, No. 6, 2004, pp. 375–387.

[55] Beiner, L. and Librescu, L., "Minimum-Weight Design of an Orthotropic Shear Panel with Fixed Flutter speed," *AIAA Journal*, Vol. 21, No. 7, 1983, pp. 1015–1016.

[56] Haftka, R. T., "Structural Optimization with Aeroelastic Constraints - A Survey of US Applications," *International Journal of Vehicle Design*, Vol. 7, 1986, pp. 381–392.

[57] Seresta, O., Abdalla, M. M., and Gürdal, Z., "Optimal Design of Laminated Composite Plates for Maximum Postbuckling Strength," *Proceedings of the* 46^{th} *AIAA/ASME/ ASCE/AHS/ASC Structures, Structural Dynamics and Materials Conference, April 18-21*, Austin, TX, USA, 2005.

[58] Grisham, O. F., "A Method for Including Postbuckling of Plate Elements in the Internal Load Analysis of Any Complex Structure Idealized Using Finite Element Analysis Methods," *Proceedings of the* 19^{th} *Structural Dynamics and Materials Conference, April 3-5, Bethesda, MD, USA*, 1978, pp. 359–369.

[59] Anderson, M. S., "Design of Panels having Postbuckling Strength," *Proceedings of the* 38^{th} *AIAA/ASME/ASCE/AHS/ASC Structures, Structural Dynamics and Materials Conference, April 7-10, Kissimmee, FL, USA*, 1997, pp. 2407–2413.

[60] Williams, F. W., Kennedy, D., Butler, R., and Anderson, M. S., "VICONOPT: Program for Exact Vibration and Buckling Analysis or Design of Prismatic Plate Assemblies," *AIAA Journal*, Vol. 29, No. 11, 1991, pp. 1927–1928.

[61] Viljoen, A., Visser, A. G., and Groenwold, A. A., "Computationally Efficient Analysis and Optimization of Stiffened Thin-Walled Panels in Shear," *Journal of Aircraft*, Vol. 42, No. 3, 2005, pp. 743–747.

[62] Collier, C., Yarrington, P., and West, B. V., "Composite, Grid-Stiffened Panel Design for Post Buckling using Hypersizer," *Proceedings of the* 43^{rd} *AIAA/ASME/ASCE/AHS/ASC Structures, Structural Dynamics and Materials Conference, April 22-25, Denver, CO, USA*, 2002, pp. 1–16.

[63] Rikards, R., Abramovich, H., Kalnins, K., and Auzins, J., "Surrogate Modeling in Design Optimization of Stiffened Composite Shells," *Composite Structures*, Vol. 63, No. 2, 2004, pp. 243–251.

[64] Lanzi, L. and Giavotto, V., "Postbuckling Optimization of Composite Stiffened Panels: Computations and Experiments," *Composite Structures*, Vol. 73, No. 2, 2006, pp. 208–220.

[65] Murphy, A., Price, M., Gibson, A., and Armstrong, C. G., "Efficient Nonlinear Idealisations of Aircraft Fuselage Panels in Compression," *Finite Elements in Analysis and Design*, Vol. 40, 2004, pp. 1977–1993.

[66] Kling, A., Degenhardt, R., and Zimmermann, R., "A Hybrid Subspace Analysis Procedure for Non-linear Postbuckling Calculation," *Composite Structures*, Vol. 73, No. 2, 2005, pp. 162–170.

[67] Myers, R. H. and Montgomery, D. C., *Response Surface Methodology: Process and Product Optimization using Designed Experiments*, John Wiley & Sons, Inc., New York, NY, 1995.

[68] Todoroki, A. and Ishikawa, T., "Design of Experiments for Stacking Sequence Optimizations with Genetic Algorithms using Response Surface Approximations," *Composite Structures*, Vol. 64, 2004, pp. 349–357.

[69] Callahan, K. J. and Weeks, G. E., "Optimal Design of Composite Laminates Using Genetic Algorithms," *Composite Engineering*, Vol. 2, No. 3, 1992, pp. 149–160.

[70] McMahon, M. T. and Watson, L. T., "A Distributed Genetic Algorithm with Migration for the Design of Composite Laminate Structures," *Parallel Algorithms and Applications*, Vol. 14, 2000, pp. 329–362.

[71] Goldberg, D. E., *Genetic Algorithms in Search, Optimization, and Machine Learning*, Addison-Wesley Longman Publishing Co., Inc., Boston, MA, USA, 1989.

[72] Seresta, O., Gürdal, Z., Adams, D. B., and Watson, L. T., "Optimal Design of Composite Wing Structures with Blended Laminates," *Composites Part B. Engineering*, submitted.

[73] Inc., V. R. . D., *Genesis Manual*, Vanderplaats R & D Inc., 1767, S. 8th St., Ste., 100, Colorado Springs, CO 80906.

[74] Liu, B. and Haftka, R. T., "Single Level Composite Wing Optimization based on Flexural Lamination Parameters," *Structural and Multidisciplinary Optimization*, Vol. 26, No. 1-2, 2000, pp. 111–120.

[75] Ragon, S. A., Gürdal, Z., and Watson, L. T., "Comparison of Three Algorithms for Tracing Nonlinear Equilibrium Path of Structural Systems," *Proceedings of the* 41^{st} *AIAA/ASME/ASCE/AHS/ASC Structures, Structural Dynamics and Materials Conference, Vol. 1, No. 2*, Reston, VA, USA, 2000, pp. 850–860.

[76] Shin, D. K., Jr., O. H. G., and Gürdal, Z., "Postbuckling Response of Laminated Plates Under Uniaxial Compression," *International Journal for Non-linear Mechanics*, Vol. 28, No. 1, 1993, pp. 95–115.

[77] Whitney, J. M., *Structural Analysis of Laminated Anisotropic Plates*, Technomic Publishing AG, 1987.

[78] Turvey, G. J. and Marshall, I. H., *Buckling and Postbuckling of Composite Plates*, Chapman and Hall, 1995.

[79] Librescu, L., Marzocca, P., and Silva, W. A., "Supersonic/Hypersonic Flutter and Postflutter of Geometrically Imperfect Circular Cylindrical Panels," *Journal of Spacecraft and Rockets*, Vol. 39, No. 5, 2002, pp. 802–812.

[80] Dowell, E. H., *Aeroelasticity of Plates and Shells*, Noordhoff International Publishing, Leyden, The Netherlands, 1975.

[81] Kuznetsov, Y. A., *Elements Of Applied Bifurcation Theory (Applied Mathematical Sciences)*, Springer, 1998.

[82] Nayfeh, A. H. and Mook, D. T., *Nonlinear Oscillations*, Wiley-IEEE, 1995.

[83] Osyczka, A., *Evolutionary Algorithms for Single and Multicriteria Design Optimization*, Physica-Verlag, 2002.

[84] Kilroy, K., *MSC/NASTRAN Quick Reference Guide*, The MacNeal-Schwendler Corporation, 815 Colorado, Boulevard, Los Angeles, CA, 90041-1777, USA, 1997.

[85] Stein, M., "Postbuckling of Orthotropic Composite Plates Loaded in Compression," *AIAA Journal*, Vol. 21, No. 12, 1983, pp. 1729–1735.

[86] Johnson, E. R. and Haftka, R. T., "Initial Postbuckling Response of Anisotropic Laminated Rectangular Plates," *Proceedings of the* 33^{rd} *AIAA/ASME/ASCE/AHS/ASC Structures, Structural Dynamics and Materials Conference, Arpil 13-15*, Washington D.C., USA, 1992, pp. 241–263.

[87] Meyers, C. A. and Hyer, M. W., "Thermally Induced, Geometrically Nonlinear Response of Symmetrically Laminated Composite Plates," *Proceedings of the* 33^{rd} *AIAA/ ASME/ASCE/AHS/ASC Structures, Structural Dynamics and Materials Conference, Arpil 13-15*, Washington D.C., USA, 1992, pp. 1027–1037.

[88] Abdalla, M. M., Song, C., Lindner, D. K., and Gürdal, Z., "Combined Optimization of a Recurve Actuator and its Driving Circuit," *Journal of Intelligent Material Systems and Structures*, Vol. 14, 2003, pp. 275–286.

[89] Busquets-Monge, S., Soremekun, G., Hertz, E., Crebier, C., Ragon, S., Boroyevich, D., Gürdal, Z., Arpilliere, M., and Lindner, D. K., "Power Converter Design Optimization: A GA Based Design Approach to Optimization of Power Electronic Circuits," *IEEE, Industrial Applications*, Vol. 10, 2004, pp. 32–39.

[90] Chandrasekaran, S., Lindner, D. K., and Smith, R. C., "Optimized Design of Switching Amplifiers for Piezoelectric Actuators," *Journal of Intelligent Materials Systems and Structures*, Vol. 11, 2000, pp. 887–901.

[91] Chandrasekaran, S. and Lindner, D. K., "Power Flow through Controlled Piezoelectric Actuators," *Journal of Intelligent Material Systems and Structures*, Vol. 11, 2000, pp. 469–481.

[92] Lindner, D. K., Vujic, N., and Leo, D. J., "Comparison of Drive Amplifer for Piezoelectric Actuators," *Proceeding of SPIE- The International Society of Opt. Engg.*, Vol. 4332, 2001, pp. 281–291.

[93] Frecker, M., "A Review of Current Research Activities in Optimization of Smart Structures and Actuators," *Proceeding SPIE's 2002 North American Symp. on Smart Structures and Materials, Modeling, and Signal Processing*, Vol. 4693, San Diego, CA, USA, 2002, pp. 112–123.

[94] Ervin, J. D. and Brei, D., "Recurve Piezoelectric Strain Amplifying Actuator Architecture," *IEEE/ASME Trans. Mechatron.*, Vol. 3, 1998, pp. 293–301.

[95] Ervin, J. D. and Brei, D., "Parallel and Serial Connections for Piezoceramic Recurve Actuator Arrays," *Proceeding SPIE's- Smart Structures and Materials, Modeling, and Signal Processing: Mathematics and Control in Smart Structures*, Vol. 3323, San Diego, CA, USA, 1998, pp. 732–742.

[96] Seresta, O., Ragon, S., Abdalla, M. M., Gürdal, Z., and Lindner, D. K., "Design of Recurve Actuator for Maximum Energy Efficiency," *Smart Materials and Structures*, Vol. 15, No. 6, 2006, pp. 1919–1926.

[97] Lockyer, A. J., Martin, C. A., Lindner, D. K., Walia, P. S., and Carpenter, B. F., "Power Systems and Requirements for Integration of Smart Structures into Aircrafts," *Journal of Intelligent Material Systems and Structures*, Vol. 15, No. 4, 2004, pp. 305–315.

[98] Joo, J. J., Sanders, B., and Washington, G., "Energy Based Efficiency of Adaptive Structure Systems," *Smart Materials and Structures*, Vol. 15, No. 1, 2006, pp. 171–181.

[99] Giurgiutiu, V., Rogers, C. A., and Chaudry, Z., "Design of Displacement Amplified Induced Strain Actuators for Maximum Energy Output," *Journal of Mechanical Design, Trans. of ASME*, Vol. 119, No. 4, 1997, pp. 511–517.

[100] Prechtl, E. and Hall, S., "Design of High Efficiency, Large Stroke, Electromechanical Actuator," *Smart Materials and Structures*, Vol. 8, No. 1, 1999, pp. 13–30.

[101] Mukherjee, A. and Joshi, S. P., "Design of Actuator Profiles for Minimum Power Consumption," *Smart Materials and Structures*, Vol. 10, No. 2, 2001, pp. 305–313.

[102] Abdalla, M. M., Frecker, M., Gürdal, Z., Johnson, T., and Lindner, D. K., "Design of Piezoelectric Actuator and Compliant Mechanism Combination for Maximum Energy Efficiency," *Smart Materials and Structures*, Vol. 14, No. 6, 2005, pp. 1421–1430.

[103] Nam, C., Kim, Y., and Weisshaar, T. A., "Optimal Sizing and Placement of Piezoelectric Actuators for Active Flutter Suppression," *Smart Materials and Structures*, Vol. 5, No. 2, 1996, pp. 216–224.

[104] Fahroo, F. and Yun, W., "Optimal Location of Piezoceramic Actuators for Vibration Suppression of a Flexible Structure," *Proceedings of the* 36^{th} *IEEE Conference on Decision and Control*, Vol. 2, 1997, pp. 1966–1971.

[105] Barbaroni, R., Mannini, A., Fantini, E., and Gaudenzi, P., "Optimal Placement of PZT Actuators for Control of Beam Dynamics," *Smart Materials and Structures*, Vol. 9, No. 1, 2000, pp. 110–120.

[106] Zhu, Y., Qiu, J., Du, H., and Tani, J., "Simultaneous Optimal Design of Structural Topology, Actuator Locations, and Control Parameters for a Plate Structure," *Computational Mechanics*, Vol. 29, No. 2, 2002, pp. 89–97.

[107] Damaren, C. J., "Optimal Location of Collocated Piezo-Actuator/Sensor Combination in Spacecraft Box Structures," *Smart Materials and Structures*, Vol. 12, No. 3, 2003, pp. 494–499.

[108] Jha, A. K. and Inman, D. J., "Optimal Sizes and Placements of Piezoelectric Actuators and Sensors for an Inflated Torus," *Journal of Intelligent Material Systems and Structures*, Vol. 14, No. 9, 2003, pp. 563–576.

[109] Maxwell, N. D. and Asokanthan, S. F., "Optimally Distributed Actuator Placement and Control for a Slewing Single Link Flexible Manipulator," *Smart Materials and Structures*, Vol. 12, No. 2, 2003, pp. 287–296.

[110] Quek, S. T., Wang, S. Y., and Ang, K. K., "Vibration Control of Composite Plates via Optimal Placement of Piezoelectric Patches," *Journal of Intelligent Material Systems and Structures*, Vol. 14, No. 4-5, 2004, pp. 229–245.

[111] Jin, Z., Yang, Y., and Soh, C. K., "Application of Fuzzy GA for Optimal Vibration Control of Smart Cylindrical Systems," *Smart Materials and Structures*, Vol. 14, No. 6, 2005, pp. 1250–1264.

[112] Bruant, I. and Proslier, L., "Optimal Location of Actuators and Sensors in Active Vibration Control," *Journal of Intelligent Material Systems and Structures*, Vol. 16, No. 3, 2005, pp. 197–206.

[113] Peng, F., NG, A., and Hu, Y. R., "Actuator Placement Optimization and Adaptive Vibration Control of Plate Smart Structures," *Journal of Intelligent Material Systems and Structures*, Vol. 16, No. 3, 2005, pp. 263–271.

[114] Padula, S. and Palumbo, D. L., "Optimal Sensor/Actuator Locations for Active Acoustic Control," *Proceeding of the* 39^{th} *AIAA/ASME/ASCE/AHS/ASC Structures, Structural Dynamics, and Materials Conference*, Long Beach, CA, USA, 1998.

[115] Chen, G., Bruno, R. J., and Salama, M., "Optimal Placement of Active/Passive Members in Truss Structure using Simulated Annealing," *AIAA Journal*, Vol. 29, No. 8, 1991, pp. 1327–1334.

[116] Yan, Y. J. and Yam, L. H., "Optimal Design of Number and Locations of Actuators in Active Vibration Control of a Space Truss," *Smart Materials and Structures*, Vol. 11, No. 4, 2002, pp. 496–503.

[117] Baier, H. and Locatelli, G., "Optimization of Actuator Placement and Structural Parameters in Smart Structures," *Proceeding of SPIE Conference on Smart Structures and Materials- Mathematics and Control in Smart Structures*, Vol. 3667, Newport Beach, CA, USA, 1999, pp. 267–276.

[118] Bruch Jr, J. C., Sloss, J. M., Adali, S., and Sadek, I. S., "Optimal Piezo-actuator Locations/Lengths and Applied Voltage for Shape Control of Beams," *Smart Materials and Structures*, Vol. 9, No. 2, 2000, pp. 205–211.

[119] Andoh, F., Washington, G., Yoon, H. S., and Utkin, V., "Efficient Shape Control of Distributed Reflectors with Discrete Piezoelectric Actuators," *Journal of Intelligent Material Systems and Structures*, Vol. 15, No. 1, 2004, pp. 3–15.

[120] Lucato, S. L. D. S., McMeeking, R. M., and Evans, E. G., "Actuator Placement Optimization in a Kagome Based High Authority Shape Morphing Structure," *Smart Materials and Structures*, Vol. 14, No. 4, 2005, pp. 869–875.

[121] Sun, D. and Tong, L., "Design Optimization of Piezoelectric Actuator Patterns for Static Shape Control of Smart Plates," *Smart Materials and Structures*, Vol. 14, No. 6, 2005, pp. 1353–1362.

[122] Guo, H. Y., Zhang, L., Zhang, L. L., and Zhou, J. X., "Optimal Placement of Sensors for Structural Health Monitoring using Improved Genetic Algorithms," *Smart Materials and Structures*, Vol. 13, No. 3, 2004, pp. 528–534.

[123] Cheng, C. C. and Lin, C. C., "An Impedance Approach for Determining Optimal Locations and Shapes of Multiple Induced Strain Actuators," *Smart Materials and Structures*, Vol. 14, No. 6, 2005, pp. 1120–1126.

[124] Chattopadhyay, A. and Seeley, C. E., "A Simulated Annealing Technique for Multiobjective Optimization of Intelligent Structures," *Smart Materials and Structures*, Vol. 3, No. 2, 1994, pp. 98–106.

[125] Liu, X., Begg, D. W., and Matravers, D. R., "Optimal Topology/Actuator Placement Design of Structures Using SA," *Journal of Aerospace Engineering*, Vol. 10, No. 3, 1997, pp. 119–125.

[126] Moini, H., "Concurrent Design of a Structure and its Distributed Piezoelectric Actuators," *Smart Materials and Structures*, Vol. 6, No. 1, 1997, pp. 62–66.

[127] Frecker, M., Kota, S., and Kikuchi, N., "Optimal Design of Compliant Mechanisms for Smart Structures Applications," *Proceeding of SPIE Conference on Smart Structures and Materials- Mathematics and Control in Smart Structures*, Vol. 3323, San Diego, CA, USA, 1998, pp. 234–242.

[128] Du, H., Lau, G. K., Lim, M. K., and Qui, J., "Topological Optimization of Mechanical Amplifiers for Piezoelectric Actuators under Dynamic Motion," *Smart Materials and Structures*, Vol. 9, No. 6, 2000, pp. 788–800.

[129] Frecker, M. and Canfield, S., "Optimal Design and Experimental Validation of Compliant Mechanism Amplifiers for Piezoceramic Stack Actuators," *Journal of Intelligent Material Systems and Structures*, Vol. 11, No. 5, 2000, pp. 360–369.

[130] Lau, G. K., Du, H., Guo, N., and Lim, M. K., "Systematic Design of Displacement Amplifying Mechanisms for Piezoelectric Stacked Actuators Using Topology Optimization," *Journal of Intelligent Material Systems and Structures*, Vol. 11, No. 9, 2000, pp. 685–695.

[131] Bharti, S. and Frecker, M., "Optimal Design and Experimental Characterization of a Compliant Mechanism Piezoelectric Actuator for Inertially Stabilized Rifle," *Journal of Intelligent Material Systems and Structures*, Vol. 15, No. 2, 2004, pp. 93–106.

[132] Carbonari, R. C., Nishiwaki, S., and Silva, E. C. N., "Design of Piezoelectric Multiactuated Microtools Using Topology Optimization," *Smart Materials and Structures*, Vol. 14, No. 6, 2005, pp. 1431–1447.

[133] Huang, S. C. and Lan, G. J., "Design and Fabrication of a Micro-Compliant Amplifier with a Topology Optimal Compliant Mechanism Integrated with a Piezoelectric Mircoactuator," *Journal of Micromechanics and Microengineering*, Vol. 16, No. 3, 2006, pp. 531–538.

[134] Johnson, T. and Frecker, M., "Optimal Placement of Active Material Actuators Using Genetic Algorithm," *Proceeding of SPIE Conference on Smart Materials and Structures- Modeling, Signal Processing and Control*, Vol. 5383, Wellingham, WA, USA, 2004, pp. 221–231.

[135] Carbonari, R. C., Nishiwaki, S., and Silva, E. C. N., "Optimal Placement of Piezoelectric Material in the Piezoactuator Design," *Proceeding of SPIE Conference on Smart Materials and Structures- Modeling, Signal Processing and Control*, Vol. 6166, San Diego, CA, USA, 2006.

[136] Buehler, M. J., Bettig, B., and Parker, G. G., "Topology Optimization of Smart Structures Using a Homogenization Approach," *Journal of Intelligent Material Systems and Structures*, Vol. 15, No. 8, 2004, pp. 655–667.

[137] Bharti, S. and Frecker, M., "Compliant Mechanical Amplifier Design Using Multiple Optimally Placed Actuators," *Proceeding of IMECE'03, International Mechanical Engineering Congress and R&D Expo*, Washington DC, USA, 2003.

[138] Zhu, H., Ragon, S., Lindner, D. K., Abdalla, M. M., Seresta, O., and Gürdal, Z., "Optimization of Driving Amplifiers for Smart Structures Using Genetic Algorithms," *Proceeding of 29th Annual Conference of the IEEE Industrial Electronic Society*, Roanoke, VA, USA, 2003, pp. 2951–2956.

[139] Seresta, O., Abdalla, M. M., Gürdal, Z., and Lindner, D. K., "Topology Design of Active Truss for Maximum Energy Efficiency," *Proceedings of* 45^{th} *AIAA/ASME/ ASC/AHS, Structures, Structural Dynamics and Materials Conference, April 19-22*, Pasadena, CA, USA, 2004.

[140] Lekhintskii, S. G., *Anisotropic Plates Translated by S. W. Tsai and Cheron T. Gordon*, Breach Science Publ. Inc., 1968.

[141] Dowell, E. H. and Llgamov, M., *Studies in Non Linear Aeroelasticity*, Springer-Verlag, 1988.

Curriculum Vitae

Omprakash Seresta was born on December 1978 in Calcutta, India. He obtained his bachelor of civil engineering degree in spring 2000 from Jadavpur University, Calcutta. After graduating in 2000, he joined Indian Institute of Technology, Kanpur in fall 2000 for his Masters degree. In his M. Tech, he applied generalized finite element method to predict quasistatic crack growth in isotropic materials. In fall 2002, he joined Virginia Tech for his doctoral degree in Aerospace Engineering and graduated in spring 2007. His Ph.D. work focussed on developing a computational framework for design of composite wing structures with blended laminates.